THE EFFECT OF HOT DEFORMATION ON THE STRENGTH OF PRECIPITATION HARDENED STEELS

IAN ROBERT MCDONALD

THESIS SUBMITTED FOR THE DEGREE

OF

DOCTOR OF PHILOSOPHY

THE UNIVERSITY OF ASTON

IN BIRMINGHAM

JANUARY 1983

THE UNIVERSITY OF ASTON IN BIRMINGHAM

THE EFFECT OF HOT DEFORMATION ON THE STRENGTH OF PRECIPITATION HARDENED STEELS

IAN ROBERT MCDONALD

THESIS SUBMITTED FOR THE DEGREE OF
DOCTOR OF PHILOSOPHY, 1982

SUMMARY

The chemistry of precipitation hardened micro-alloyed steels has received considerable attention over the past 20 years. In parallel with this study, the process of controlled rolling has been developed and used to optimise the properties of this type of steel.

In many applications, the plate or strip product produced by controlled rolling is not suitable without further thermo-mechanical treatment. The effect that reheating and deforming micro-alloyed steels has on the structure and properties has, however, received little attention. The sensitivity of some simple steels to processing variables in the warm-forming regime, and the structure - properties relationships that determine the properties of warm-formed steels have been the subject of this thesis.

The effect of warm deformation on plain carbon, vanadium and niobium steels was studied, using rolling and torsion as the mode of deformation.

The microstructure was observed, using the Scanning Electron Microscope in the Back Scattered Electron Mode. This relatively new technique enabled the development of sub-structure within grains to be observed.

For the air-cooled materials, the proof stress increases with deformation up to a strain of 0.5 with little temperature dependence. For higher strains, the proof stress increases with a decrease in deformation temperature. The proof stress of the steels deformed by a true strain of 1.8 can be predicted with reference to the initial grain size, and sub-grain size of the deformed ferrite. Both vanadium and niobium micro-alloying additions reduce the sensitivity of the as warm-worked strength to strain for true strains greater than 0.5, although the temperature sensitivity is still quite strong.

Keywords

Warm Deformation
Micro-Alloyed Steels
Proof Stress
Grain Size

CONTENTS

Contd/....

CONTENTS

Contd.

Contd/....

CONTENTS

Contd.

Contd/....

CONTENTS

Contd.

LIST OF TABLES

LIST OF FIGURES

LIST OF FIGURES

Page

LITERATURE SURVEY (Contd)

LIST OF FIGURES

LIST OF FIGURES

LIST OF FIGURES

LIST OF FIGURES

LIST OF FIGURES

Page

RESULTS (Contd)

DISCUSSION

Page

DISCUSSION (Contd)

LIST OF FIGURES

LIST OF PHOTOGRAPHS

Page

RESULTS (Contd)

ACKNOWLEDGEMENTS

My thanks are due to my supervisor, Dr I L Dillamore, formerly Head of the Department of Metallurgy and Materials Engineering, for his guidance during the progress of my research work, and helpful discussions on the preparation of this thesis. My thanks are also due to the following members of staff in the Department of Metallurgy and Materials Engineering at the University of Aston in Birmingham:

- Mr D Whyley and his colleagues for their help with the electrical control equipment used with the torsion apparatus;

- The staff in the Workshop for their work in machining the torsion specimens.

My thanks are also due to Dr P Williams and Mr B Jefferies of Design Audit Limited, for their assistance in the preparation of my thesis. In particular, I gratefully acknowledge the work that Mrs E Hammonds has done in typing this thesis.

1. INTRODUCTION

In many applications a steel is required which has all of the following properties:

- high yield strength
- low brittle-to-ductile transition temperature
- ductility
- weldability

In general, improving one of these properties has an adverse effect on another. Thus improving strength by increasing the carbon content, decreases ductility and toughness, and impairs weldability. Lowering the carbon equivalent by reducing the alloy content may improve weldability but can decrease strength.

Over the past 20 years the chemistry of high strength low alloy steels has developed. In parallel with this development, the process known as controlled rolling has been used to optimise the properties of high strength low alloy steels. This is done by careful control of the temperature and deformation throughout the rolling schedule.

The successful application of controlled rolling depends on the power of the mill to roll steels at lower than normal temperatures, and the configuration of the mill. The product is invariably plate or strip. In warm forming operations however, the process is limited by the shape of the product being manufactured. It is therefore not possible to control the temperature and degree of deformation as it is in a rolling operation.

This study was initiated by the British Gas Corporation, who posed the general question about the properties of steels of simple compositions, in the warm-formed condition. Their interest derived from the fact that many pipe fittings are warm-formed, and in the subsequently normalised condition, have strength levels that are lower than those of the line-pipe materials in current use. If steels became available that had good properties as warm-formed, this would present some opportunities for future development.

The experimental work was a first attempt to ascertain the structure - properties relationships that determine the properties of warm-formed steels, and to investigate the sensitivity of some simple steels to processing variables in the warm-forming regime.

2. LITERATURE SURVEY

2.1 STRENGTH AND TOUGHNESS

The yield strength and toughness (impact transition temperature) of high strength low alloy (HSLA) steels are governed by the following inter-related factors:-

- grain size
- precipitation
- dislocation substructure
- solid solution effects

The relative effect of these factors on the yield strength and toughness of an HSLA steel is shown schematically in figure 2.1[1]. The most desirable effect arises from those factors which give the largest negative ratio, that is from low carbon, high manganese, aluminium grain refined steels.

The effect of these various factors on yield strength and toughness has been systematically quantified over the last 25 years. In the early 1950's, Hall[2] and Petch[3,6], demonstrated that for a plain carbon steel the following relationship held:-

$$\sigma_y = \sigma_i + K_y(d^{-\frac{1}{2}}) \qquad (2.1)$$

where, σ_y = yield strength

σ_i = a stress constant including the effects of lattice friction and solute atoms

K_y = the grain size coefficient is related to the stress concentration required to activate slip dislocation sources

d = grain size in mm

Using multiple regression techniques, the effect of solute atoms in a plain carbon-manganese steel can be assessed. Equation 2.1 is then modified to the following form[4]:

$$\sigma_y = \left\{K_o + 37(\%Mn) + 83(\%Si) + 2918(\%N_f)\right\} + 15.1(d^{-\frac{1}{2}}) \qquad (2.2)$$

where

K_o = $88MNm^{-2}$ for air-cooled material and $62MNm^{-2}$ for furnace cooled material. This variation is due to the effect of cooling rate on the distribution of cementite.

d = grain size (mean linear intercept) in mm

N_f = weight precent of free nitrogen in the steel

This equation predicts the yield stress with a 95% confidence limit of $\pm 31MNm^{-2}$ for a steel containing a pearlite volume fraction of less than 0.3. The relative influence that various factors given in equation 2.2 have on yield strength is shown graphically in figure 2.2. The pearlite volume fraction is not significant with respect to yield strength when it is less than 0.3. For higher pearlite volume fractions (greater than 0.5), the influence of pearlite is significant. For a pearlite fraction in the range 0 - 0.9 the following relationship between yield stress and microstructure has been reported[5]:

$$\sigma_y = 54\, f_\alpha + \left[380 + 94(\%Mn) \right] f_p + 72(\%Si) + 26\, f_\alpha (d^{-\frac{1}{2}}) \qquad (2.3)$$

where,

f_α = volume fraction of ferrite

f_p = volume fraction of pearlite

Equations 2.2 and 2.3 do not differ significantly for a pearlite volume fraction in the region of 0.2 and a grain size given by $d^{-\frac{1}{2}} = 12mm^{-\frac{1}{2}}$. The difference is more pronounced when the pearlite fraction is increased, equation 2.3 predicting the higher value.

The factors which affect toughness (impact transition temperature) were first quantified by Petch[7], who formulated the following relationship.

$$\beta . T_c = \ln\beta - \ln C - \ln(d^{-\frac{1}{2}}) \qquad (2.4)$$

where β = material constant, a measure of the resistance of the lattice to distortion

C = measure of the difficulty of propagation of a crack.

T_c = Charpy V-notch impact transition temperature

The effect of microstructural and compositional features on the impact transition temperature (I.T.T.) was determined by Irani[8] (equation 2.5) and Gladman[4] (equation 2.6).

$$\text{I.T.T.}(^{o}C) = 36 + \frac{690 - 190 d^{-\frac{1}{2}}}{3.5 + \%\ \text{Pearlite}} \qquad (2.5)$$

$$I.T.T.\,(^{o}C) = 19 + 44(\%Si) + 700(\%N_f)^{\frac{1}{2}} + 2.2(\%\ Pearlite) - 11.5(d^{-\frac{1}{2}}) \qquad (2.6)$$

where, N_f = weight percent of free nitrogen in the steel

In high carbon steels (> 0.4% carbon), refining the pearlite colony size reduces the adverse effect of pearlite.

The predictions of yield stress from equation 2.2 apply only to steels which are strengthened by the direct effects of lattice friction, solute elements, and grain boundaries. In steels containing micro-alloying additions, which strenthen the ferrite matrix by forming fine precipitates, the yield stress predictions fall short of experimentally observed values.

In precipitation strengthened alloys, the stress required to move dislocations appreciable distances in the slip plane is assumed to be higher than the stress needed to generate dislocations from a source. Hence, in theories attempting to explain the yield behaviour of these alloys, the yield strength is associated with the stress required for dislocations to sweep out areas in the slip planes which are large compared with dispersion spacing. Precipitation-strengthening models predict the following general relationship[10].

$$\sigma_y \simeq \frac{AD}{L} + B \qquad (2.7)$$

where, A,B = material constants for the dispersed and matrix phases respectively

D = the diameter of the dispersed particles

L = the mean spacing between the dispersed particles on the slip plane.

Several models have been proposed to predict the strengthening increment due to precipitation, of which the Ashby-Orowan model has been widely accepted. According to this model, the precipitation strengthening increment σ_p is given by:

$$\sigma_p = \frac{5.9\sqrt{f}}{\bar{x}} \ln\left(\frac{\bar{x}}{2.5 \times 10^{-4}}\right) \qquad (2.8)$$

where, f = volume fraction of particles

$\bar{x}$ = the mean planar-intercept diameter of a precipitate

Since $\frac{1}{\bar{x}}$ is the predominant function of $\bar{x}$, the stress increment due to fine precipitates increases with the reduction in precipitate size and the increase in fine precipitate fraction (figure 2.3).

The value for precipitation strengthening given by equation 2.8 is in reasonable agreement with the difference between the observed yield stress and that predicted by equation 2.2.

2.1.1 Grain Size

In general an increase in the yield strength of a steel is achieved at the expense of some loss in toughness. As a result, a compromise is often necessary to obtain acceptable mechanical properties. Refining the grain size is the one way in which the yield strength can be increased, and the impact transition

temperature reduced simultaneously. For this reason, grain size, and the factors which affect it have received considerable attention.

The degree of grain refinement varies with the product and production route. Table 2.1[4] shows the range of grain sizes which can be obtained.

The ferrite grain size depends on:-

a) the austenite grain size prior to transformation

b) the nucleation and growth rate of ferrite.

a) Austenite Grain Size

The austenite grain size prior to transformation depends on a number of factors which control the processes of recovery, recrystallisation and grain growth.

Recovery

Of the three processes, (recovery, recrystallisation and grain growth), recovery is the least important. Recovery following hot deformation is virtually a spontaneous process in steels micro-alloyed with vanadium and niobium[12].

Recrystallisation

Control of the rate of recrystallisation has been shown to be a very important factor in the development of a fine austenite grain size, and hence a fine ferrite grain size after transformation. During recrystallisation new grains nucleate at grain boundaries or within the deformed grains around precipitates or deformation bands. Due to the high aspect ratio (length to thickness ratio) of the deformed austenite, the recrystallised grains are unable to grow much before they impinge on each other. Under carefully controlled conditions a homogeneous fine-grained equiaxed structure is produced.

In plain carbon-manganese steels, the rate of recrystallisation is quite rapid, but varies with the temperature and extent of deformation. Figure 2.4 illustrates the effect of deformation. Figure 2.4 illustrates the effect of deformation temperature on the rate of recrystallisation in a carbon-manganese steel. Grain refinement in these steels is achieved by using either a low rolling temperature or high hot rolling deformations[13].

Recrystallisation kinetics are significantly retarded by micro- alloying additions, notably niobium micro-alloying addition on austenite recrystallisation has been extensively studied. The influence of niobium is complicated by the number of variables which interact - the processing variables of strain, strain rate and temperature and the distribution of niobium (i.e. in solid solution or as a precipitate).

The effect of precipitation on the static recrystallisation kinetics of a niobium-bearing steel is shown in figure 2.5[14] for various deformation temperatures in the range 850 - 1000°C. The steel was austenitised at 1200°C for 30 minutes and furnace cooled to the deformation temperature. The deformation given was 30% in tension at a true strain rate of 5 s^{-1}. These results show that recrystallisation is substantially retarded below 925°C and totally blocked at 850°C. At temperatures above 950°C, static recrystallisation is complete. At lower temperatures recrystallisation never reaches 100% due to the strain induced precipitation of fine carbo-nitride particles which has occurred in austenite during deformation. The static recrystallisation and strain-induced precipitation kinetics for a solution treated niobium steel after a torsional deformation at 900°C are shown in figure 2.6[15]. The precipitate formed in the 10 second incubation period contained about 50% of the 0.04 wt% niobium content. After 10 seconds, recrystallisation and precipitation proceeeded simultaneously and the rate of recrystallisation is relatively slow. When the holding time is increased beyond 100 seconds, the recrystallisation rate accelerates. At this point most of the niobium is in the form of precipitates which become less effective in preventing recrystallisation.

The amount of deformation significantly affects the kinetics, size and distribution of precipitates, and hence the recrystallisation kinetics. The influence of deformation on precipitation kinetics of a niobium steel is shown in figure 2.7. Figure 2.8 indicates that after a surface shear

strain of 2.26, static recrystallisation is complete after holding at 900°C for 1000 seconds. After a shear strain of 0.75 static recrystallisation can be totally inhibited for 1000 seconds.

Precipitates formed following deformation have a mean size in the range 30 - 50 Å in contrast to 1000 - 3000 Å for precipitates obtained during isothermal holding of an unstrained specimen.

Precipitates need to be extremely small to affect recrystallisation kinetics. Precipitates of niobium carbo-nitride 40-50 Å in size do not retard recrystallisation kinetics when present before the beginning of deformation performed at 900°C.

The effect of niobium on recrystallisation is not only due to precipitation. The influence of niobium in solid solution on recrystallisation has also been reported[12,15,16]. During high strain rate deformation ($\approx 6s^{-1}$), the actual amount of precipitation which can occur is negligible, and yet dynamic recrystallisation is retarded in comparison with a niobium free steel. In a set of experiments undertaken by J N Cordea[12], a niobium and vanadium steel were austenitised at either 1315°C or 1095°C. On testing at 870°C in the case of the niobium steel and 815°C for the vanadium steel, recrystallisation was retarded in the case of the lower austenitising temperature. A difference in austenite grain size does not wholly account for this, and it was therefore reported that the effect is due to the greater amount of

solute in solid solution at the higher temperature. It is suggested that niobium in solid solution in austenite enables more deformation energy to be stored as lattice defects before the onset of dynamic recrystallisation. A mechanism involving the interaction of niobium atoms in solid solution with lattice defects.

Grain Growth

Grain growth is significantly affected by the presence of second phase particles, due to the interaction between particles and grain boundaries. This interaction results from the elimination of grain boundary area (energy) when the boundary intersects a second phase particle[17]. Any movement of the grain boundary away from the second phase particle would result in a local increase in energy and a drag effect on migrating boundaries is frequently observed (Zener drag effect). The binding force between second phase particles and grain boundaries is greater than that which could be supplied by thermal activation[18], and therefore the energy required for separation must be supplied from some other source, e.g. the energy release which occurs during grain growth.

Mathematically it has been shown[19] that the energy released during grain growth E, is given very approximately by,

$$E = \frac{\gamma}{R_o}\left[\frac{2}{Z} - \frac{3}{2}\right] \qquad (2.9)$$

where, E = the energy released per unit area of the advancing grain boundary

γ = the grain boundary energy

R_o = matrix grain radius

Z = the ratio of the radii of the growing grain and the matrix grains

Clearly energy is only released when $Z > \frac{4}{3}$ and therefore the large grains grow at the expense of the smaller grains. Experimental observations confirm that this is the case.

The pinning force P, of the individual particle varies with the geometric distortion of the grain boundary and the mode of separation. Its value does not vary much for the various models which have been proposed [18],[19], and is of the order of,

$$P = 4r\gamma \qquad (2.10)$$

where, r = pinning radius

The maximum radius r_{crit} of a particle which will effectively counteract the driving force for grain boundary migration is given by the following equation,

$$r_{crit} = \frac{6R_o f}{\pi}\left(\frac{3}{2} - \frac{2}{Z}\right)^{-1} \qquad (2.11)$$

where, r_{crit} = the maximum size of particle that will effectively counteract the driving force for grain growth

f = the volume fraction of particles in the microstructure

Equation 2.11 implies that the critical particle radius is increased when,

i) the volume fraction of particles increases

ii) the matrix grain size increases.

Two further points are also significant,

i) fine particles are more effective than coarse particles in restricting grain growth.

ii) Ostwald ripening is an important phenomenon in connection with grain growth, and particle dissolution is not a necessary requirement for grain growth.

In practice, two forms of grain growth are apparent [21] - "normal" (or continuous) grain growth and "abnormal" (or discontinuous) grain growth. During normal grain growth, the size of individual grains is relatively uniform whereas in abnormal grain growth grain sizes vary owing to the rapid growth of some grains. The type of grain growth observed varies with the average grain size expressed in terms of the grain size heterogeneity Z (figure 2.9).

Abnormal grain growth can develop if the following three conditions are simultaneously fulfilled.

i) normal grain growth cannot take place due to the presence of second phase particles

ii) the average grain size has a value below the limit $\frac{1}{2Z}$

iii) there is at least one grain which is much larger than the average.

Micro-alloying additions commonly used to inhibit grain growth are vanadium and aluminium which form a nitride of limited solubility, niobium which forms a carbo-nitride, and titanium which forms both a carbide and nitride. The alloy addition is selected to give fine particles, thus prolonging the time interval between particle formation and the attainment of the critical particle size which will permit grain growth.

Aluminium is commonly used as a grain refining addition, in HSLA steels, and is considered further in order to illustrate the factors which affect grain refinement. Studies on the solubility of various carbides and nitrides have been made, and the solubility limits determined[22]. In the case of aluminium nitride, the solubility limit is given by the following equation,

$$\log_{10}[Al][N] = \frac{-7400}{T} + 1.95 \qquad (2.12)$$

Where $[X]$ is the concentration of the alumium and nitrogen in the alloy and T, is the absolute temperature. The solubility curves for aluminium nitride at 1200°C and 900°C are shown in figure 2.10, together with the line indicating stoichiometric concentration of aluminium nitride. An aluminium grain refined steel soaked at 1200°C as is often the case for hot rolling will give rise to coarse particles of aluminium nitride. Subsequent normalising of the material by the 900°C causes further precipitation to occur as indicated by the 900°C solubility curve. The proportions of coarse and fine particles are indicated for

two alloy compositions A and B. Stoichiometric alloys give the maximum fraction of fine particles when the alloy composition exceeds the upper limit of solubility. The effect on grain refinement of a decreased fraction of fine particles at high aluminium contents is shown in figure 2.11. Although this steel contains 0.15% vanadium, adequate grain refinement took place in the absence of aluminium because of fine vanadium-nitride particles, so that the behaviour described in figure 2.11 still applies. With increasing aluminium additions, the solubility limit for aluminium nitride precipitation at the soaking temperature is exceeded, and a progressively larger fraction of coarse aluminium nitride is formed, which is unsuitable for grain refinement. As a result, during subsequent normalising at 900°C, the fraction of fine nitride becomes progressively smaller, and the austenite grains become coarser, as indicated by the increase in ferrite grain size. At higher aluminium levels, the grain size is only marginally finer than that of the plain-carbon base material.

For a given alloy in the stable fine grained condition, the effects of matrix grain size and grain size heterogeneity are invariant, and the critical particle size is therefore a function of the volume fraction of particles, which, although virtually constant at a given temperature, will decrease with increasing temperature in accordance with the appropriate solubility relationship. This concept is summarised in figure 2.12, where the critical particle size is shown as a function of temperature. The criterion for grain growth is not only dependent upon the critical particle size, however, but is also dependent upon the particle coarsening characteristics as shown in figure 2.12.

Particle coarsening has been the subject of theoretical work by Lifshitz and Slyozov[23], and by Wagner[24]. According to Wagner's diffusion-controlled model, particle growth under conditions of Ostwold ripening (i.e. the growth of large particles at the expense of small particles for a given fraction of particles) is expressed by,

$$(F_t)^3 - (F_o)^3 = \frac{8.\gamma.D.C_o.V_m.t}{9RT} \qquad (2.13)$$

where,

F_t = the average particle radius after time t

F_o = the average particle radius at the onset of coarsening

D = the diffusivity of the particle species in the matrix

C_o = the concentration of the particle species

V_m = the particle molar volume

γ = the surface energy between particle and matrix

R = gas constant

T = the absolute temperature

b) Nucleation and Growth of Ferrite

Ferrite nucleates at austenite grain boundaries or within austenite grains at nucleation sites such as deformation bands or precipitates. The nucleation rate is increased by lowering the austenite/ferrite transformation temperature, which can be done in two ways - either by rapid cooling (not practical in thick sections) or by alloying additions such as manganese.

2.1.2 Precipitation

Introduction

This is the second most important means of improving the yield strength. However, it does have some adverse effect on toughness (figure 2.1). The impact transition temperature is increased by about 0.5°C for every 1 Nmm^{-2} increase in yield strength. Fine precipitates have an effect on the yield strength which is over and above that which is produced by any change in the grain size. An example of this is shown in figure 2.13 for an air-cooled carbon-manganese-niobium steel. As the austenitising temperature increased from 950°C to 1250°C, progressively more niobium dissolved, and was thus available for precipitation as fine carbide upon subsequent cooling. The strength increment above that predicted for plain carbon base steel increased accordingly. The small solubility of niobium carbide at 950°C gave insignificant strengthening. However, treatment at 1250°C produced a substantial improvement of about 200 MNm^{-2}.

The micro-alloying additions commonly used to achieve some precipitation hardening are niobium, vanadium and titanium, which form a carbide, nitride or carbo-nitride precipitate. The strengthening effect depends on the size and distribution of precipitates in ferrite. The maximum strengthening effect is achieved when the precipitate size and interparticle spacing are minimised (figure 2.3).

Factors Controlling Precipitate Size

The precipitate size and interparticle spacing are controlled by the following,

a) thermodynamic considerations which control the solubility and nucleation of precipitates in austenite and ferrite;

b) temperature and kinetics of precipitation;

c) $\alpha - \gamma$ transformation temperature;

d) effect of time/temperature on precipitate ageing.

a) Precipitation of a carbide or nitride from austenite or ferrite can only take place at supersaturation, that is, when the equilibrium solubility at a particular temperature is exceeded. Preferential formation of one precipitate over another depends on the affinity of the elements (vanadium, niobium, titanium) for carbon, nitrogen, oxygen and sulphur. The formation of a nitride as against a carbide of vanadium

or niobium under similar conditions of supersaturation depends upon the stability of nitrides. Although niobium has a higher affinity for nitrogen than vanadium, the stability of the nitride, as compared to the carbide increases more rapidly with vanadium than with niobium. Niobium therefore forms a carbonitride containing 60-90% carbon whereas vanadium can form carbonitrides containing nearly 100% nitrogen.

The solubility limits for some of the more common precipitates which strengthen the ferrite matrix are expressed in the following equations:-

$$\log_{10}[V][N] = \frac{-8,330}{T} + 3.46 \qquad (2.14)$$

$$\log_{10}[Nb][C] = \frac{-6,770}{T} + 2.26 \qquad (2.15)$$

$$\log_{10}[Ti][C] = \frac{-7,000}{T} + 2.75 \qquad (2.16)$$

$$\log_{10}[V]^{\frac{4}{3}}[C] = \frac{-10,800}{T} + 7.05 \qquad (2.17)$$

where $[X]$ is the concentration of dissolved solute and $[C]$ and $[N]$ are the concentration of dissolved carbon and nitrogen in atomic percent.

The fraction of fine precipitates formed on cooling from the austenite range depends on the alloy composition and the solubility and stoichiometry of the precipitating system. The effect of these factors on precipitation is illustrated in figure 2.14 for a steel containing 0.10% niobium or

0.10% titanium cooled from 1200°C. For carbon contents between the stoichiometric composition and the maximum for complete solubility, the full potential fraction of precipitate forms on cooling. At higher carbon contents the solubility limit is exceeded, and progressively more of the micro-alloying element is precipitated as coarse carbide, reducing the amount available for fine carbide precipitation on cooling. It is therefore important to operate as near as possible to the stoichiometric composition.

The solution treatment temperature for niobium (1100 - 1250°C) is much higher than that required for vanadium steels (900 - 950°C). Vanadium steels can therefore be effectively precipitation hardened after normalising since re-precipitation of vanadium nitride will occur.

(b) When the equilibrium solubility is exceeded, precipitation will begin depending on kinetic factors - temperature, time and deformation.

As the temperature increases, the rate of particle coarsening increases in accordance with Wagners diffusion equation. Ostwald ripening takes place, and the precipitates become less effective as a strengthening phase in the ferrite matrix. The effect of annealing temperature on the size of precipitates in niobium and titanium steels is illustrated in figure 2.15[25], and are of the same order as those obtained by Gray[26]. The effect of particle dispersion and the amount of precipitation on the yield

strength is shown in figure 2.16 for niobium, titanium and vanadium low-carbon steels which were annealed at different solution temperatures after solution heat treatment. In all three alloying systems, there is a reverse relationship between the amount of precipitate and the yield strength. The lowest strength was found at 900°C, which corresponds to maximum precipitation. As the temperature decreases, the volume of precipitate diminishes although supersaturation continues to increase. At the same time the particle size decreases until it reaches an extremely fine dispersion giving strong precipitation strengthening in the ferrite phase.

The results obtained by Le Bon[15] (figure 2.7) indicate that the static precipitation of niobium carbonitride at 900°C proceeds very slowly producing large precipitates.

Deformation has a very important effect on precipitation, through the mechanism of strain induced precipitation. Deformation markedly increases the rate of precipitation by comparison with an unstrained material[27], and reduces the size of precipitates formed, at least in the early stages of deformation[27]. The precipitates nucleating on deformation bands and lattice defects, are coherent with the matrix. The temperature significantly influences the effect of strain induced precipitation. A niobium steel rolled at about 1000°C yielded insignificant precipitation strengthening whereas the same deformation at about 750°C resulted in substantial strengthening[28].

(c) A substantial amount of precipitation occurs during the transformation from austenite to ferrite. The precipitate formed during the transformation is in the form of rows of regularly spaced fine precipitates[25]. Lowering the transformation temperature results in smaller precipitates and a finer distribution. The time for precipitates to grow is also reduced.

The transformation temperature is influenced by the cooling rate and alloying additions. The effect of cooling rate on precipitation strengthening in vanadium and niobium micro-alloyed steels is shown in figure 2.17[29]. As a result of the opposing effects of cooling rate on precipitate size and precipitate fraction there is an intermediate cooling rate which optimises the precipitation strengthening effect. Very rapid cooling of niobium steels can completely suppress precipitation producing a fine grained ferrite structure.

Micro-alloying additions of niobium, vanadium and titanium affect the transformation temperature[25]. Niobium and titanium have a much greater effect than vanadium provided the concentrations are identical. At lower austenitising temperatures niobium and titanium additions tend to accelerate and intensify ferrite formation due to the effect of carbide precipitation in austenite. Not only is some of the existing carbon chemically tied up, but the carbides also act as nuclei during transformation. Both effects promote ferrite formation.

After the carbides have dissolved during austenitising, the transformation behaviour changes considerably. The micro-alloying elements dissolved in austenite strongly retard ferrite formation, and over a wide range of cooling rates, results in martensitic and bainitic structures.

Alloying elements such as titanium or niobium may either accelerate or retard the start of a transformation depending on the temperature of austenitisation. Figure 2.18 shows this effect for a niobium steel. At low austenitising temperatures, an increase in niobium accelerates the start of the transformation. However, the start of the ferrite-pearlite formation slows down considerably as the austenitising temperature is increased and more niobium is dissolved.

Above 0.04% niobium, no further retardation is observed because no more niobium is permitted in solution due to the solubility product being exceeded. At very high niobium levels, undissolved carbonitrides also seem to accelerate the transformation. This effect becomes particularly evident at an austenitising temperature of 1100^{o}C and high niobium contents.

(d) Figure 2.19 illustrates the effect that tempering has on the strength of a niobium and vanadium steel. The loss in strength occurs as a result of Ostwald ripening. At temperatures greater than 700^{o}C niobium steels have a much greater resistance to ageing than vanadium steels.

2.1.3 Dislocation Substructure

When steels are deformed in the two phase ($\alpha + \gamma$), or ferrite regions, recrystallisation often does not occur. Dislocations formed during deformation will therefore still be present in the structure.

By the process of recovery these dislocations form dislocation walls which delineate strain-free regions or subgrains. The formation of subgrains in ferrite substantially increases the yield strength (figure 2.20)[28]. The development of a sub-structure also reduces the impact transition temperature although at the expense of the energy absorbed[30].

2.1.4 Solid Solution Effects

Figure 2.1 indicates that some elements which form a solid solution with ferrite can have a substantial effect on yield strength, at the expense of toughness. Interstitial alloying elements are theoretically the most effective. The use of these elements (e.g. carbon, nitrogen) is limited by their low solubility in ferrite, and their detrimental effect on toughness. Phosphorus too has a marked effect on yield strength, but is detrimental to ductility and toughness. Silicon is quite effective as a solid solution strengthening element. Its use is limited because it raises the transformation temperature, thus producing coarse ferrite grains, and subsequently lowering toughness.

Several elements which form a substitutional solid solution are added, not because of their effect as a strengthener, but for some other beneficial effect which they have on the structure. Manganese and molybdenum are two cases in point. Manganese has a marked effect in reducing the austenite to ferrite transformation temperature. The advantages of this have already been mentioned. Molybdenum suppresses the formation of polygonal ferrite and pearlite in favour of an acicular ferrite matrix. The highly deformed substructure gives the steel high strength and toughness.

2.2 DUCTILITY

2.2.1 Introduction

Formability of HSLA steels is an important property since many structural components have to be cold formed. The primary factors used to measure formability are flow stress, work-hardening rate, maximum uniform ductility prior to plastic instability, and the total ductility at fracture. The quantitative relationships between structure, composition and plastic deformation characteristics for ferrite-pearlite structures have been determined[31], and are given below.

$$\text{Flow stress } (MN/m^2) \text{ at strain, } \varepsilon = 0.2$$
$$= 15.4\Big[16 + 29(\%Mn) + 9(\%Si) + 60(\%P) + 11(\%Sn) + 244(\%N_f) + 0.27(\%\text{Pearlite}) + 0.97(d^{-\frac{1}{2}})\Big] \qquad (2.18)$$

Work-hardening rate (MN/m^2) at strain, $\varepsilon = 0.2$

$$= 15.4\left[25 + 7.2(\%Si) + 30(\%P) + 9.9(\%Sn) + 89(\%N_f) + 0.09(\%Pearlite) + 1.0(d^{-\frac{1}{2}})\right] \quad (2.19)$$

Maximum uniform strain, ε_μ

$$= 0.27 - 0.016(\%Pearlite) - 0.015(\%Mn) - 0.040(\%Sn) - 0.040(\%Si) - 1.1(N_f) \quad (2.20)$$

Total ductility at fracture, ε_T

$$= 1.3 - 0.20(\%Pearlite) + 0.30(\%Mn) + 0.20(\%Si) - 3.4(\%S) - 4.4(\%P) + 0.29(\%Sn) + 0.015(d^{-\frac{1}{2}}) \quad (2.21)$$

These relationships indicate the detrimental effect that pearlite has on ductility (although it increases both the flow stress and the work-hardening rate) and the effect of sulphur and phosphorous.

2.2.2 The Influence of Pearlite on Ductility

Carbon is generally detrimental to good ductility. Its effect varies with the morphology of the carbon, that is, as part of a lamellar pearlite structure or in a spheroidised form. Spheroidising increases the maximum uniform elongation (figure 2.21). Pearlite and refining the inter-lamellar spacing of the pearlite each increase the work-hardening rate, and will reduce the value of the maximum uniform strain.

2.2.3 The Influence of Inclusions on Ductility

The effect of second-phase particles, such as manganese sulphide and oxide inclusions is to decrease the total ductility. However, the effect is not linear as implied by the preceding equation, but is an exponential decrease with increasing volume fraction of second-phase particles (figure 2.22).

Ductile fracture processes involve the formation of voids in a material which nucleate as a result of either cracking in second-phase particles or by decohesion of the particle-matrix interface. Irrespective of the precise mechanism of void formation and coalescence however, total ductility depends on the shape of the particles which create the voids. Increasing the length-width ratio of the second phase particles gives a higher tensile ductility when the long axis of inclusions is parallel to the tensile axis, compared with plate-like inclusions tested parallel to their minor axis. This produces ductility anisotropy in which ductility is much lower in the transverse direction than in the longitudinal direction, for a given volume fraction of second-phase particles.

The control of inclusions in steel is therefore of particular importance with respect to improving ductility. Inclusion control may involve one or more of the following:-

a) inclusion shape control with the aim of reducing the length-to-width ratio and hence ductility anisotropy.

b) control of the inclusion distribution. Large local concentrations of inclusion significantly influence ductility[31], and should be avoided.

c) reducing the volume fraction of inclusions by precipitation out of the melt into the slag phase.

a) Inclusion Shape Control

This is an important factor in the control of inclusions[32]. Such control aims to produce inclusions which are as near spherical as possible, even under conditions of hot deformation. Spherical inclusions make it more difficult for ductile crack propagation. A drawback of this approach is that the modified inclusions are hard and may crack, thereby raising the impact transition temperature as much as 50°C[33].

Elements commonly used for shape control are zirconium, titanium, rare earth metals and calcium. Zirconium was the first element to be used successfully[34], but also forms a nitride and is therefore unsuitable for steel where nitride precipitation is important. Titanium is similar to zirconium, being a strong nitride and carbide former as well as combining with sulphide. Rare earth metal additions are mixtures of approximately 50% cerium, 25% lanthanum, 16% neodymium and 9% other lanthanides. Their chemical properties are all similar, and they do not react strongly with carbon or nitrogen. They can therefore be used in steels which rely on nitride or carbide precipitates for strength. Calcium, like the rare earth metals is a strong oxide

and sulphide former but has no strong tendency to form a nitride or sulphide.

b) Inclusion Distribution

A variation in the distribution of inclusion is well known in the case of manganese sulphide, commonly found in steel. The distribution varies with the morphology of the manganese sulphide of which three have been observed[35]. Two of these are particularly important (types I and II), the degree of de-oxidation determining which will form. Type I, manganese sulphide, occurs when the oxygen content is greater than 0.02wt%, and forms a globular inclusion. Type II forms when the oxygen content is less than 0.01wt%, and precipitates out in the form of parallel rods, giving rise to a high local concentration. Type I inclusions have a relatively low plasticity and become no worse than egg shaped during hot rolling.

c) Reducing the Volume Fraction of Precipitates

The volume fraction of sulphides can be reduced by careful control of the steel making process. This will generally involve de-sulphurisation of the blast furnace iron as well as secondary vessel steel making, in which heating and stirring allow high melting point sulphides and oxides to float out of the melt. This is done using a rare earth metal or calcium treatment.

2.3 CONTROLLED ROLLING

2.3.1 Introduction

Controlled rolling practice has developed in parallel with the development of HSLA steels, as a means of obtaining the best possible mechanical properties (high yield strength and excellent toughness) in a low alloy, and therefore relatively cheap steel. In a controlled rolling schedule, the important processing parameters are:-

(1) the reheating temperature prior to rolling;

(2) control of deformation and temperature;

(3) control of cooling rate after deformation.

2.3.2 Reheating Temperature

Varying the initial reheating temperature within the range 1050°C - 1200°C has little effect on the yield strength and toughness of a plain carbon-manganese steel, but is important when micro-alloying elements (commonly niobium and vanadium) are added (figure 2.23).

Alloying with vanadium increases the sensitivity of the yield and tensile strengths to the reheating temperature. An increase in the reheating temperature of 150°C increases the yield strength of a 0.03% vanadium steel by about 20 MNm^{-2}. A much larger increase in yield strength has been observed in niobium and niobium plus vanadium micro-alloyed steels. In the case of

0.04% niobium 0.06% vanadium steel, an increase in yield strength of over 100 MNm^{-2} has been observed.

The higher strengths resulting from the increase in reheating temperature are associated with the more complete solution of vanadium and niobium carbonitrides in austenite at the higher temperatures within the range 1050 - 1200°C.

The increase in reheating temperature slightly lowers the percentage elongation, although this is not significant since the steels have an elongation in excess of 25%.

The impact transition temperature rises as the reheating temperature is raised from 1050°C to 1200°C in the case of niobium and niobium plus vanadium steels. The effect of reheating temperature on the impact transition temperature is due to the smaller grain size which is produced at the lower reheating temperatures. The reheating temperature has little effect on the impact transition temperature of plain carbon-manganese steel.

2.3.3 Control of Deformation and Temperature

The process of controlled rolling can be divided into the following three stages[29].

a) Simultaneous deformation and recrystallisation which occurs at temperatures above about 1000°C.

b) Low temperature austenite deformation in the temperature range 950°C down to the Ar_3 temperature.

c) Deformation in the two phase austenite/ferrite region.

The temperature range in which deformation occurs markedly affects the properties of the steel, and this is most notably the case when deformation occurs in the two phase region.

a) Simultaneous Deformation and Recrystallisation

The relation between the deformation temperature and the critical amount of deformation required for the completion of dynamic recrystallisation is shown in figure 2.24. In plain carbon steels, the critical amount of deformation is small and so too is it's dependence on temperature. In the niobium steel, the critical amount of deformation is much larger and its variation with temperature substantially higher.

Figure 2.25 shows the effect of deformation temperature and initial grain size on the critical amount of deformation. In the plain carbon steel, the influence of the initial grain size and the temperature is small. In the niobium steel, the effect of grain size on the critical amount of deformation is very large and increases rapidly with decreasing deformation temperature. In practice, recrystallisation is suppressed below 950°C.

Figure 2.26 shows the influence of the amount of deformation on the recrystallised austenite grain size. In both plain carbon and niobium steel, the recrystallised grain size decreased rapidly as the amount of reduction increased. Beyond 50% reduction, however, the rate of decrease diminishes, and the grain size reaches a limiting value of about 20 μm in the niobium steel. A lower deformation temperature produces only a marginally finer grain size.

During this stage of deformation, the limiting grain size is attained by repeated recrystallisation. This is achieved by deforming the steel just sufficient to allow complete re-crystallisation to take place.

Below the critical amount of deformation, partial recrystallisation and strain induced grain boundary migration take place. In particular, deformation below 8% causes strain-induced grain boundary migration, resulting in the formation of giant grains locally[29]. In consequence, a small amount of deformation is apt to cause grain coarsening instead of grain refining.

b) Low Temperature Austenite Deformation

Figure 2.27 shows the influence of temperature and the amount of deformation on the yield and tensile strength. These results demonstrate the substantial effect that deformation in the temperature range 950 - Ar_3 has on the yield strength, and the relatively small influence of temperature.

Increasing deformation in this temperature range also reduces the impact transition temperature (figure 2.28).

During this stage, deformation produces elongated grains, deformation bands, and strain-induced precipitation of niobium carbonitride. Austenite grain boundaries are the preferred nucleation sites for the austenite-to-ferrite transformation. The elongation of the austenite grains therefore inhibits ferrite grain growth. Increasing the amount of deformation, increases the number of deformation bands, and their distribution becomes uniform, giving rise to fine uniform ferrite grains.

c) Deformation in the Two Phase Region

Deformation in the two phase austenite - ferrite region has a much larger influence upon mechanical properties than deformation in the second stage, and contributes to an abrupt increase in yield and tensile strengths and a rapid decrease in the impact transition temperature (figure 2.29).

Deformation in this temperature range produces regions of high dislocation density, cell structure and substructure, as well as equiaxed grains. With increasing deformation, the volume fraction of grains containing substructure steadily increases. This general trend applies to the plain carbon steels as well as niobium micro-alloyed steels.

The yield strength can be expressed by the following form of the Hall-Petch equation.

$$\sigma_y = \sigma_{lh} + \sigma_{sh} + \sigma_{dh} + \sigma_{ph} + \sigma_{th} + \sigma_{ssh} + K_y d^{-\frac{1}{2}} \qquad (2.22)$$

where,

σ_{lh} = intrinsic lattice hardening

σ_{sh} = solid solution hardening

σ_{dh} = dislocation hardening

σ_{ph} = precipitation hardening

σ_{th} = texture hardening

σ_{ssh} = substructure hardening

$K_y d^{-\frac{1}{2}}$ = hardening due to grain refinement

The increase in yield strength $\Delta\sigma_y$ due to deformation in the two phase region is given by,

$$\Delta\sigma_y = \Delta\sigma_{dh} + \Delta\sigma_{ph} + \Delta\sigma_{th} + \Delta\sigma_{ssh} + \Delta(K_y d^{-\frac{1}{2}}) \qquad (2.23)$$

Since σ_{lh} and σ_{sh} are independent of deformation, they are not included in the equation.

The effect of 10% deformation in the two phase region on each of these factors in equation 2.22 has been studied.

Dislocation Hardening

When deformation is completed in the austenite region, the dislocation density in ferrite is relatively low. When

deformation is extended to the austenite/ferrite two phase region, however, the dislocation density in the deformed ferrite grains is fairly high. Annealing treatment in the temperature range 550 - 650°C on both a niobium steel and a plain carbon steel did not affect the yield strength of the steel, suggesting that 10% reduction does not produce appreciable dislocation hardening.

Precipitation Hardening

The increase in yield strength for identical thermo-mechanical treatments is different for niobium and plain carbon steel. Assuming that $\Delta\sigma_y$ in niobium steel results from deformation and precipitation hardening while $\Delta\sigma_y$ in plain carbon steel is due only to the effect of deformation, then the difference in $\Delta\sigma_y$ values must be due to precipitation.

Texture Hardening

During deformation in the two phase region both austenite and ferrite are deformed. The latter recovers and/or recrystallises resulting in the development of a (100) texture. A 10% reduction in the two phase region however, produces a weak (100) texture and therefore no texture hardening occurs.

Grain Refinement

Optical metallographic observations reveal that the grain size after 10% reduction in the two phase region is the same as that obtained when there is no deformation in this region. The term $\Delta(K_y d^{-\frac{1}{2}})$ is therefore zero.

Since there is no decrease in grain size, the increase in yield strength must be interpreted in terms of some other structural features. According to electron microscopic observation, the structure associated with no deformation in the two phase region consists of polygonal grains with a low density of dislocations. After 10% deformation, the microstructure is duplex, consisting of polygonal grains interspersed with patches of substructure. The volume fraction of substructure increases with an increase in deformation.

The subgrains are produced by the formation of dislocation walls within the deformed ferrite grain. Areas bounded by the dislocation walls are relatively free from dislocations. Subgrain strengthening depends on the size and volume fraction of ferrite grains with subgrains, both of which depend on the temperature of deformation. The strengthening effect of subgrains as a function of their size (corrected for the volume fraction of ferrite grains containing subgrains) is shown in figure 2.20.

2.3.4 Control of Cooling Rate after Deformation

The cooling rate following controlled rolling can significantly affect the final microstructure, and hence the mechanical properties. The effect that the finish rolling temperature has on the impact transition temperature for three different cooling schedules is shown in figure 2.30[37]. Water spraying produces a ferrite - bainite structure and therefore the steel has a relatively high impact transition temperature. The air-cooled

plate produces a heterogeneous ferrite - pearlite structure. The difference in impact transition temperature between air-cooled and coiled material increases as the finish rolling temperature drops. This is due to the increased hardenability of austenite deformed at low temperatures. The simulated coiling schedule involved water cooling to about 550^{o}C followed by slow cooling. This produces a material with an impact transition temperature between that of water cooled and air-cooled material.

In the case of coiled strip, the coiling temperature is the important parameter. The effect of coiling temperature on the yield strength and impact transition temperature for three steels is shown in figure 2.31. In the case of the low carbon niobium steel, that improvement in impact properties with a decrease in simulated cooling temperature is thought to be due to the formation of an acicular ferrite structure as opposed to a bainite/ferrite structure.

2.4 CONTINUUM ROLLING

The continuum rolling process consists essentially of a thermo-mechanical treatment of austenite, austenite and ferrite, and ferrite in a continuous rolling sequence. The rolling schedule is therefore completed at lower temperatures than those normally used in controlled rolling. Plate produced by continuum rolling generally has a higher yield strength and notch toughness than are found in conventional hot rolled and controlled rolled steels.

The effects of finish rolling temperature on the yield strength and toughness of a vacuum-melted low sulphur (0.004%), very low carbon (<0.002%) 1% Mn steel are shown in figures 2.32 and 2.33[38]. As the finishing rolling temperatures decreased from 815°C to 150°C, the cumulative percent reduction below the Ar_1 temperature increased from 36.7% to 146.9%.

The yield strength for this steel cannot be predicted using the classic Hall-Petch criterion, since this applies only to exclusively re-crystallised structures. Account must therefore be taken of the fact that the micro-structure of steels deformed in the temperature range 150 - 815°C contains both grains and sub-grains or cells. In order to take account of a mixed micro-structure, Bramfitt and Marder proposed the following equation[38], which related yield strength to micro-structure, by modifying the Hall-Petch equation.

$$\sigma_y = \sigma_o + k\left[d_g^{-\frac{1}{2}}(f_r) + d_c^{-\frac{1}{2}} \frac{(1 - f_r) K_{cell}}{k} \right] \qquad (2.24)$$

where, σ_y = predicted yield strength

σ_o = stress constant

k = constant

K_{cell} = slope of Hall-Petch line for fully cellular structures

d_g = grain size

d_c = cell size

f_r = fraction of recrystallised grains

Close agreement between experimental data and the above equation indicates that the increase in yield strength at low finishing temperatures can be attributed primarily to,

(i) grain refinement of both austenite and ferrite by repeated deformation;

(ii) dynamic recovery that produces a fine polygonal substructure.

The improvement in the notch toughness with decreasing finishing temperature is due to grain refinement, and the crystallographic texture that results from the deformation process. The impact transition temperature varies linearly with the crystallographic texture parameter C, obtained by multiplying the relative intensities of the $\{111\}$ of the rolling plane and the $\{110\}$ of the transverse plane as follows:

$$C = (I_{111})_{RP}.(I_{110})_{TP} - 1 \qquad (2.25)$$

TABLE 2.1 SMALLEST FERRITIC GRAIN SIZE AVAILABLE IN VARIOUS PRODUCTS

Product	dμm	$d^{-\frac{1}{2}}$, $mm^{-\frac{1}{2}}$
Thick Plate	8-10	10-12
Thin Plate	5	14
Normalized Plate and Bar	5	14
Strip	3-4	16-18
Best Laboratory Normalized, 1975	3-4	16-18
Best Laboratory Controlled Rolled, 1975	1-2	25

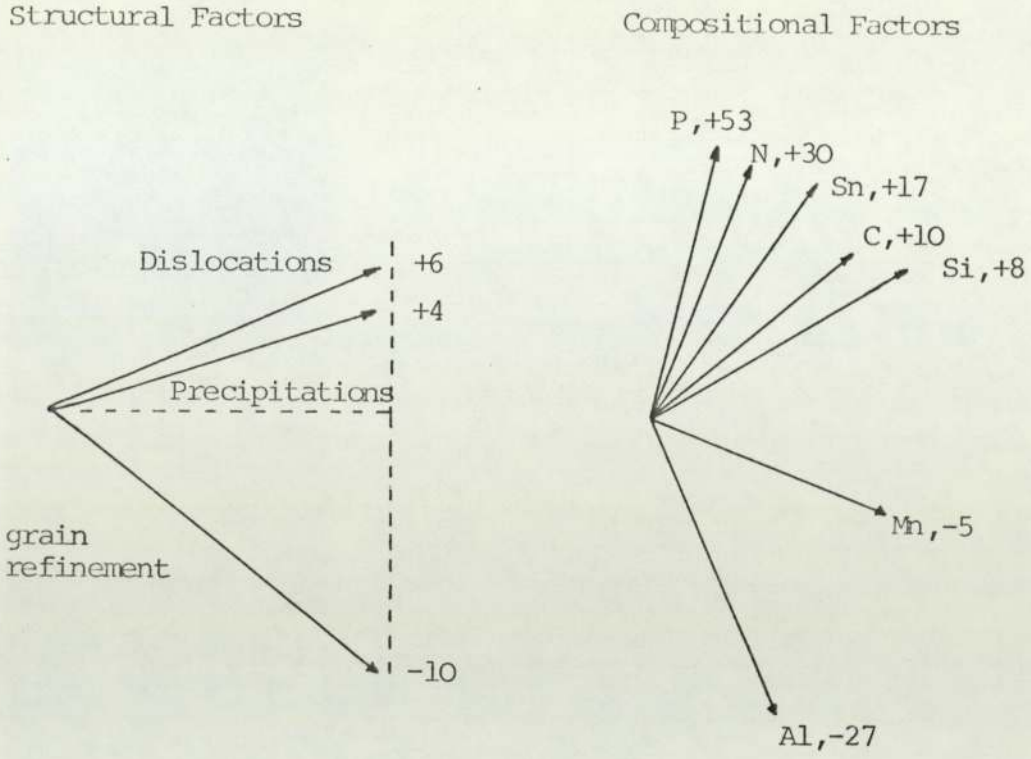

Ratios indicate change in transition temperature per 15 MNm^{-2} increase in yield strength

FIGURE 2.1 FACTORS AFFECTING YIELD STRENGTH AND IMPACT TRANSITION TEMPERATURE

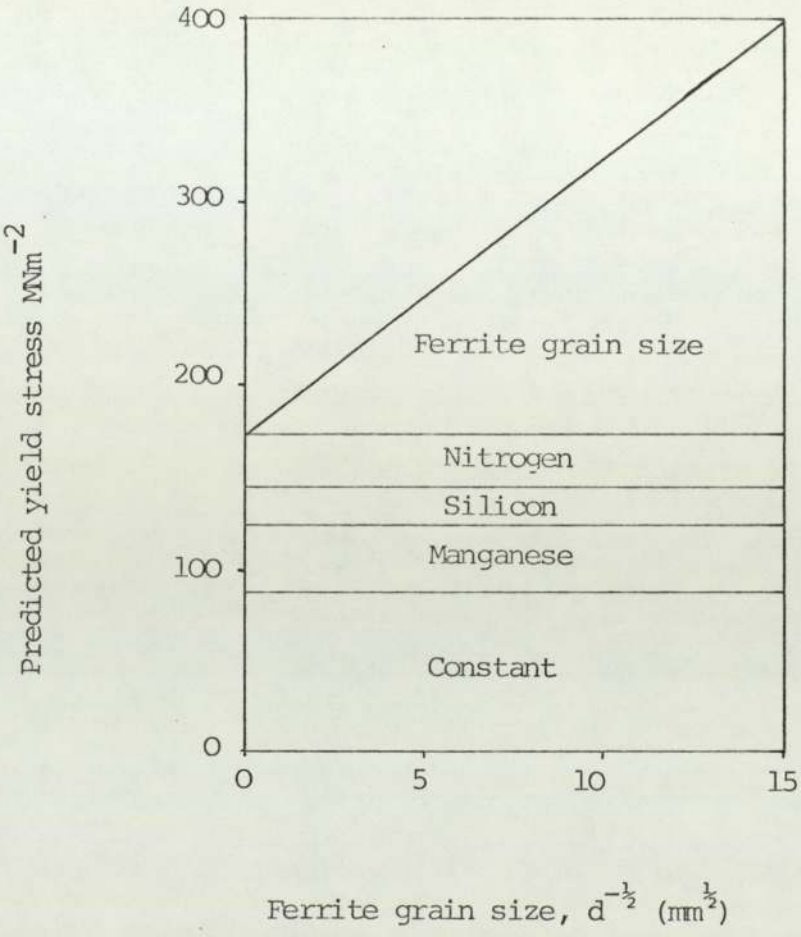

Steel Composition 1.0% Mn

0.25% Si

0.01% N

FIGURE 2.2 THE COMPONENTS OF THE YIELD STRESS PREDICTED BY EQUATION 2.2 FOR AN AIR-COOLED STEEL

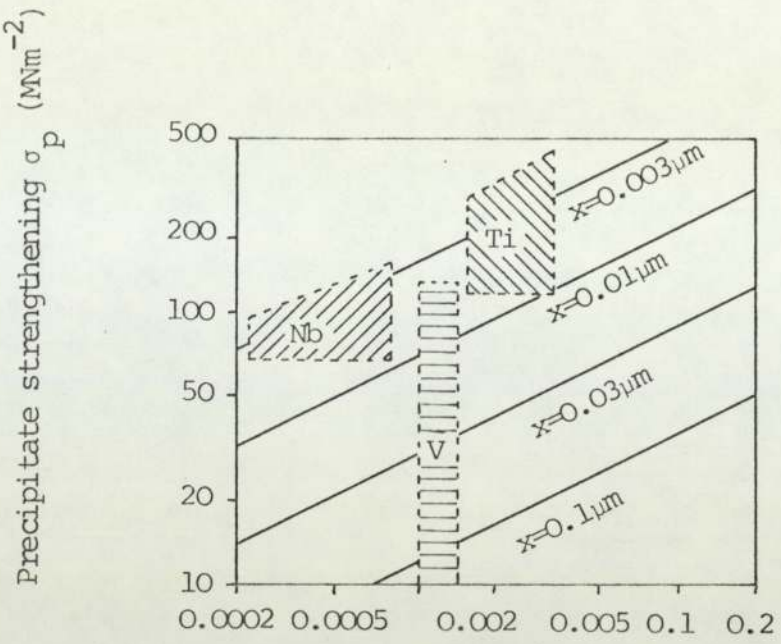

Shaded areas show experimental results

FIGURE 2.3 THE DEPENDENCE OF PRECIPITATION STRENGTHENING ON PRECIPITATE SIZE (x) AND FRACTION

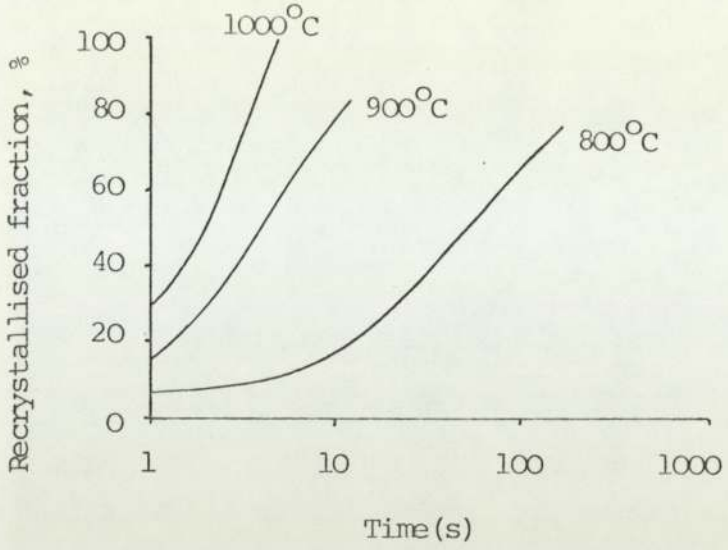

FIGURE 2.4 STATIC RECRYSTALLISATION KINETICS FOR C-Mn STEEL

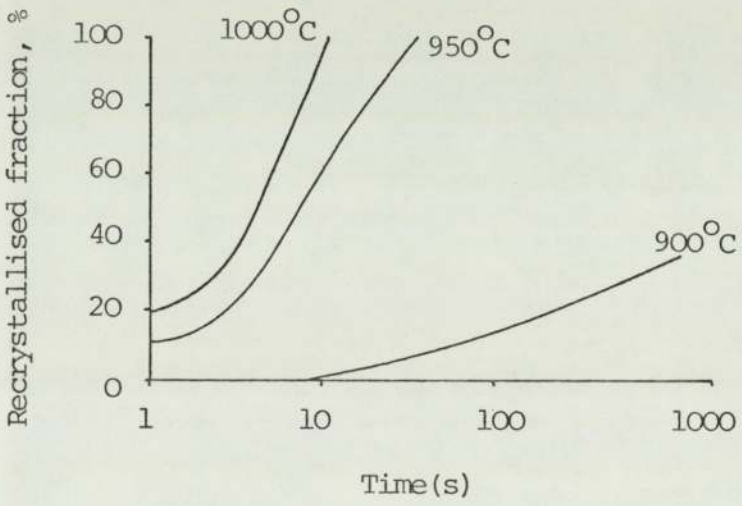

FIGURE 2.5 STATIC RECRYSTALLISATION KINETICS FOR C-Mn-Nb STEEL

	Steel Compositions(wt%)							
	C	Mn	Si	S	P	Al	Nb	N
Figure 2.4	0.150	1.198	0.333	0.006	0.009	0.039	-	0.0088
Figure 2.5	0.165	1.320	0.345	0.014	0.025	0.034	0.029	0.0063

Each steel was austenitized at 1200°C for 30 minutes and furnace cooled to the deformation temperature. Deformation was 30% in tension with a true-strain rate of 5 s^{-1}.

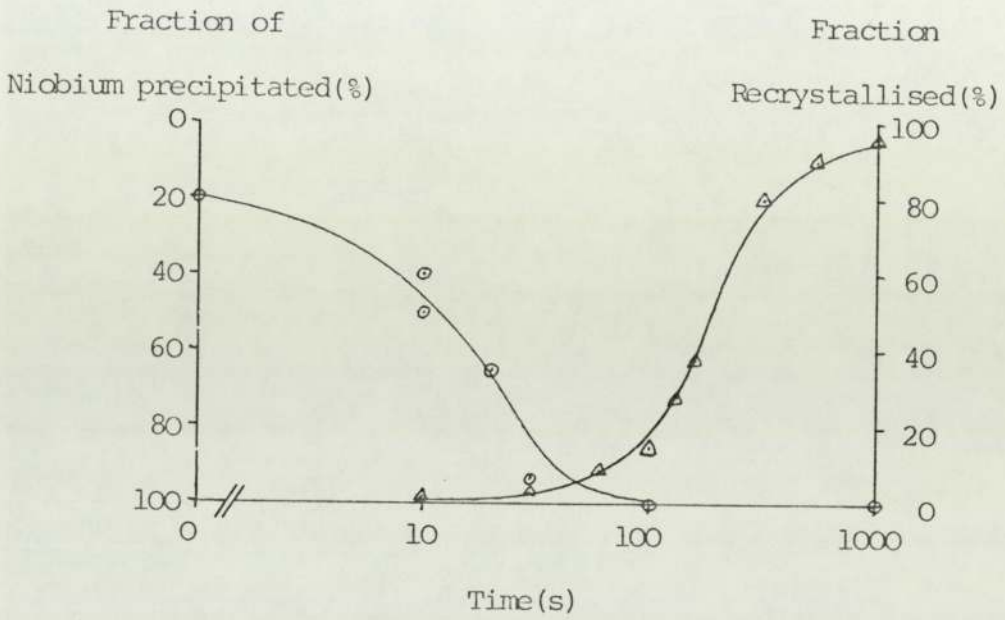

△ Fraction of structure recrystallised

⊙ Fraction of niobium precipitated

Steel Composition(wt%)

C	Mn	Si	S	P	Al	N	Nb
0.17	1.35	0.31	0.021	0.014	0.017	0.011	0.040

Thermo-mechanical treatment - solution treatment at 1260°C, furnace cool to 900°C and deform by torsion, and hold specimen at 900°C. Surface shear strain = 2.26 and strain rate = 6.3 s^{-1}

FIGURE 2.6 STATIC RECRYSTALLISATION AND STRAIN INDUCED PRECIPITATION KINETICS FOR A NIOBIUM STEEL

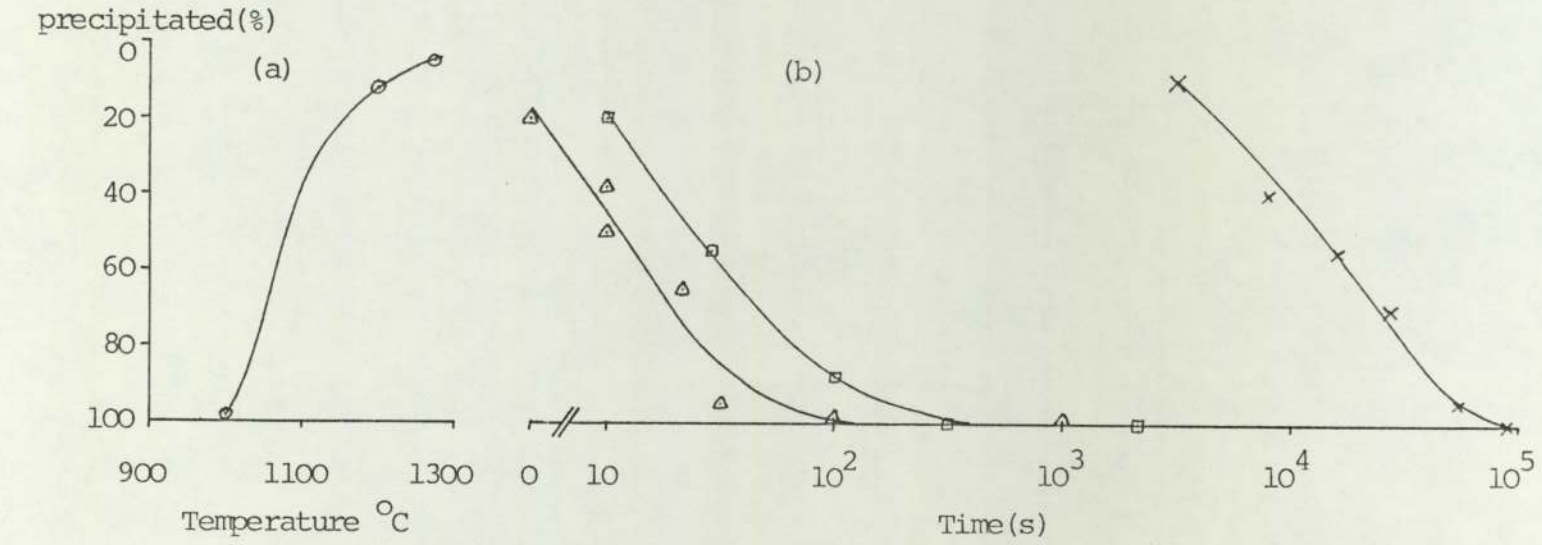

Steel composition as per figure 2.6

⊙, × unstrained austenite; ▫ surface shear strain 0.75; △ surface shear strain 2.26 (strain rate = 6.3 s^{-1})

FIGURE 2.7 DISSOLUTION AND PRECIPITATION OF NIOBIUM CARBONITRIDE

(a) Dissolution as a function of temperature

(b) Precipitation at 900°C for different amounts of deformation after solution treatment at 1260°C

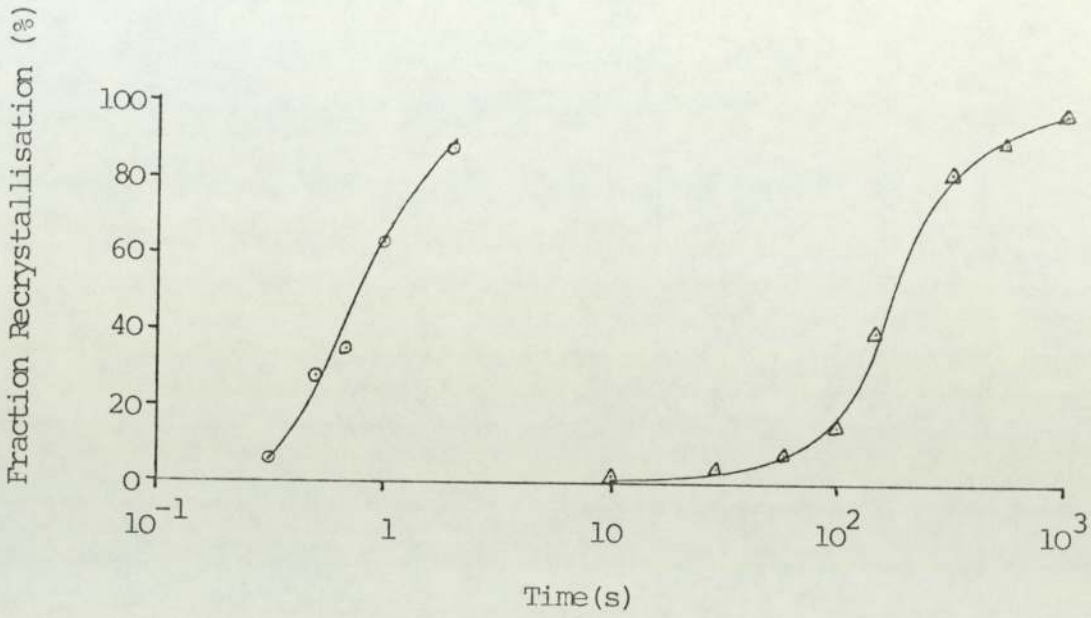

○ plain carbon steel (composition as per figure 2.6 without niobium present)

△ niobium steel (composition as per figure 2.6)

FIGURE 2.8 STATIC RECRYSTALLISATION KINETICS OF AUSTENITE AFTER A SHEAR STRAIN OF 2.26 AT 900°C IN THE ABSENCE OF ANY DYNAMIC RECRYSTALLISATION

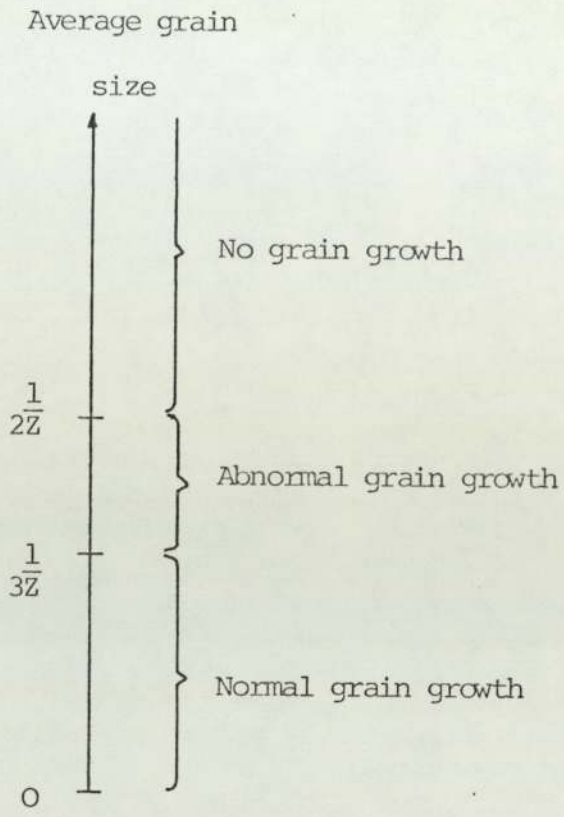

FIGURE 2.9 THE RELATIONSHIP BETWEEN TYPES OF GRAIN GROWTH AND AVERAGE GRAIN SIZE

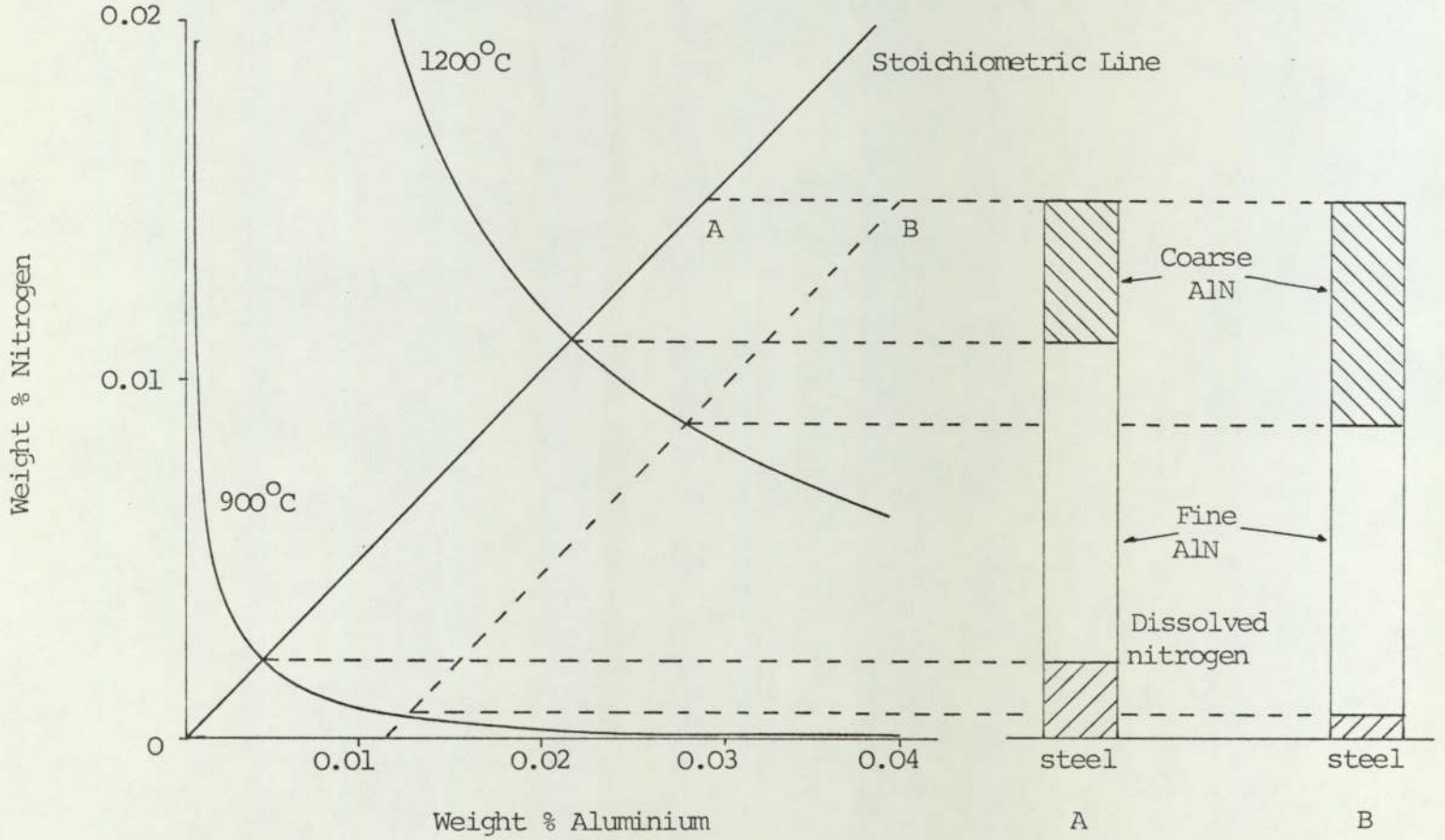

FIGURE 2.10 THE RELATIONSHIP BETWEEN THE SOLUBILITY OF AN ALUMINIUM NITRIDE GRAIN REFINING CONSTITUENT, COMPOSITION, AND THE FORMATION OF A PARTICLE DISPERSION

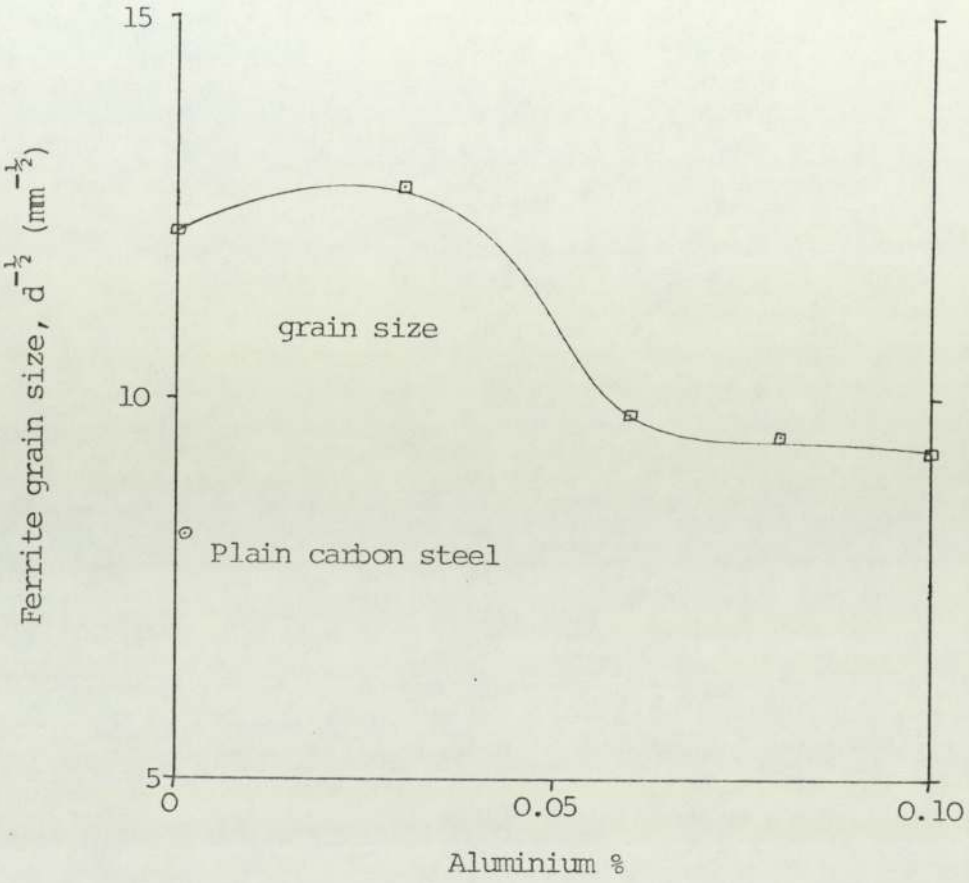

Steel Composition (wt%)

0.15% C, 1.6% Mn, 0.15% V, 0.008% N

FIGURE 2.11 THE EFFECT OF INCREASING ALUMINIUM CONTENT ON GRAIN REFINEMENT

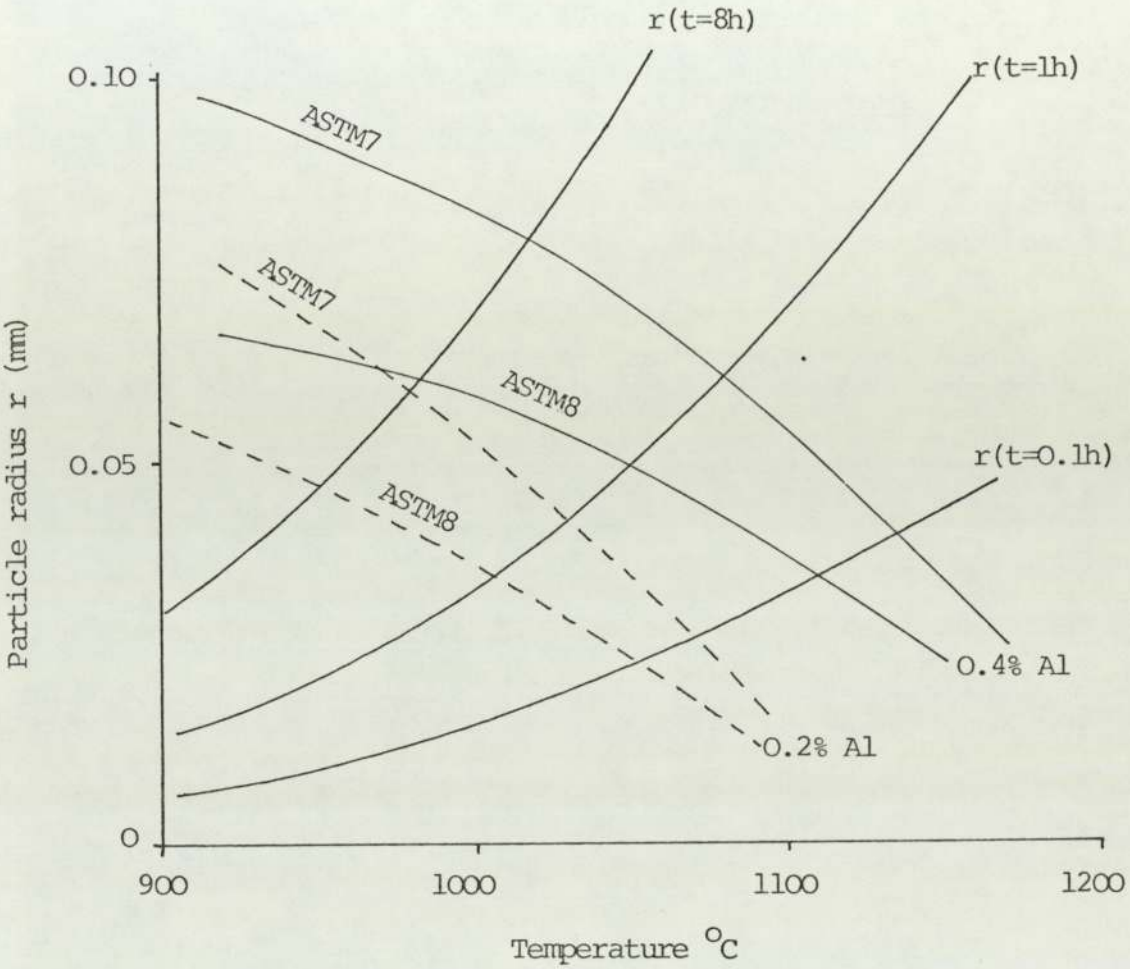

FIGURE 2.12 PARTICLE COARSENING AND DISSOLUTION

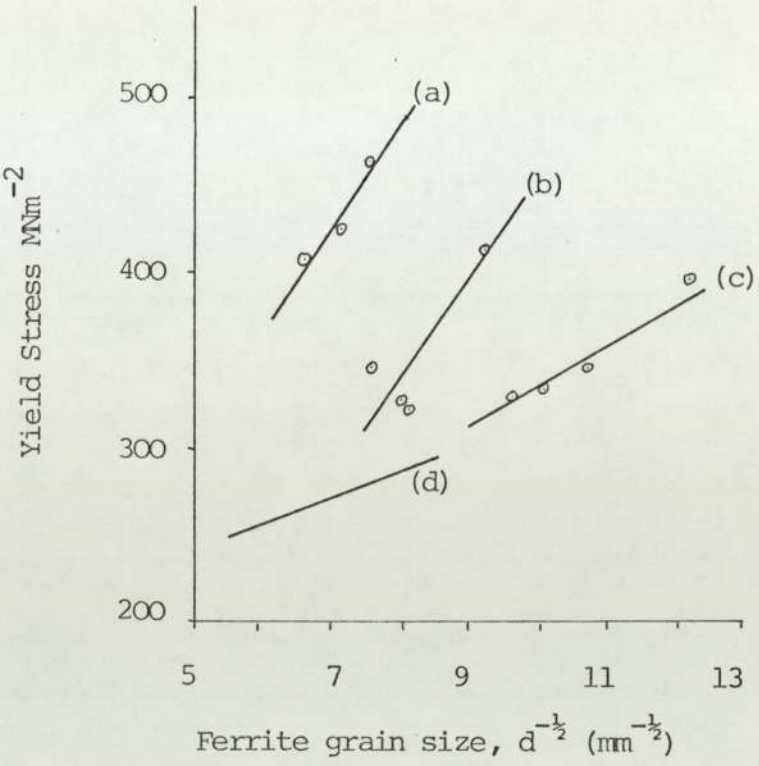

Steel Composition (wt%)
0.10% C, 0.06% Mn, 0.09% Nb

(a) Niobium steel air-cooled from 1250°C

(b) Niobium steel air-cooled from 1100°C

(c) Niobium steel air-cooled from 950°C

(d) Plain carbon steel air-cooled. Similar composition to niobium steel.

FIGURE 2.13 THE EFFECT OF AUSTENITISING TEMPERATURE ON THE RELATIONSHIP BETWEEN STRENGTH AND GRAIN SIZE

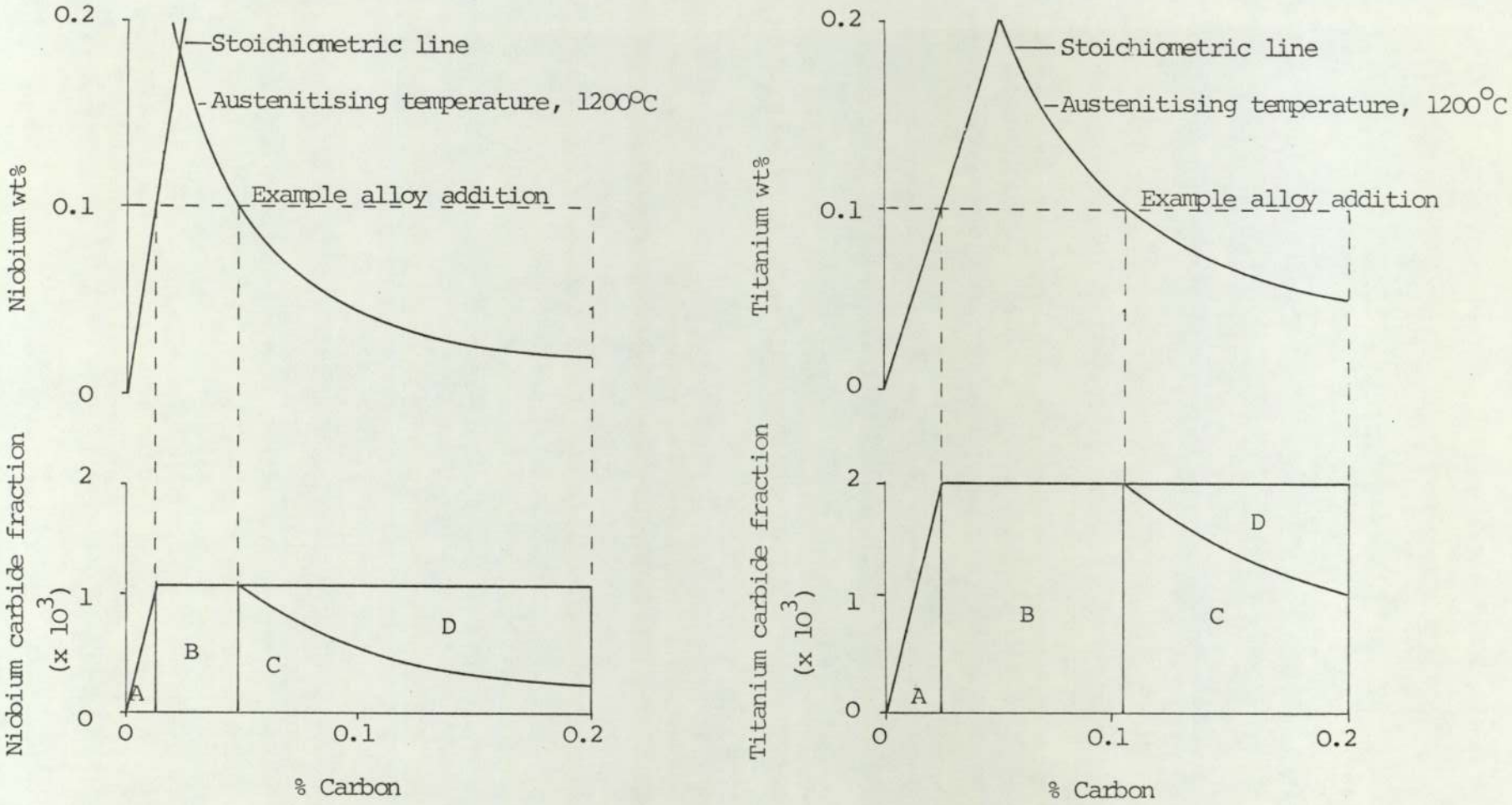

A - Precipitation limited by stoichiometry B - Maximum fine carbide precipitate

C - Precipitation limited by solubility D - Undissolved coarse carbide

FIGURE 2.14 THE EFFECT OF AN ALLOY COMPOSITION AND PRECIPITATE STOICHIOMETRY ON THE FINE CARBIDE FRACTION PRODUCED ON COOLING FROM 1200°C

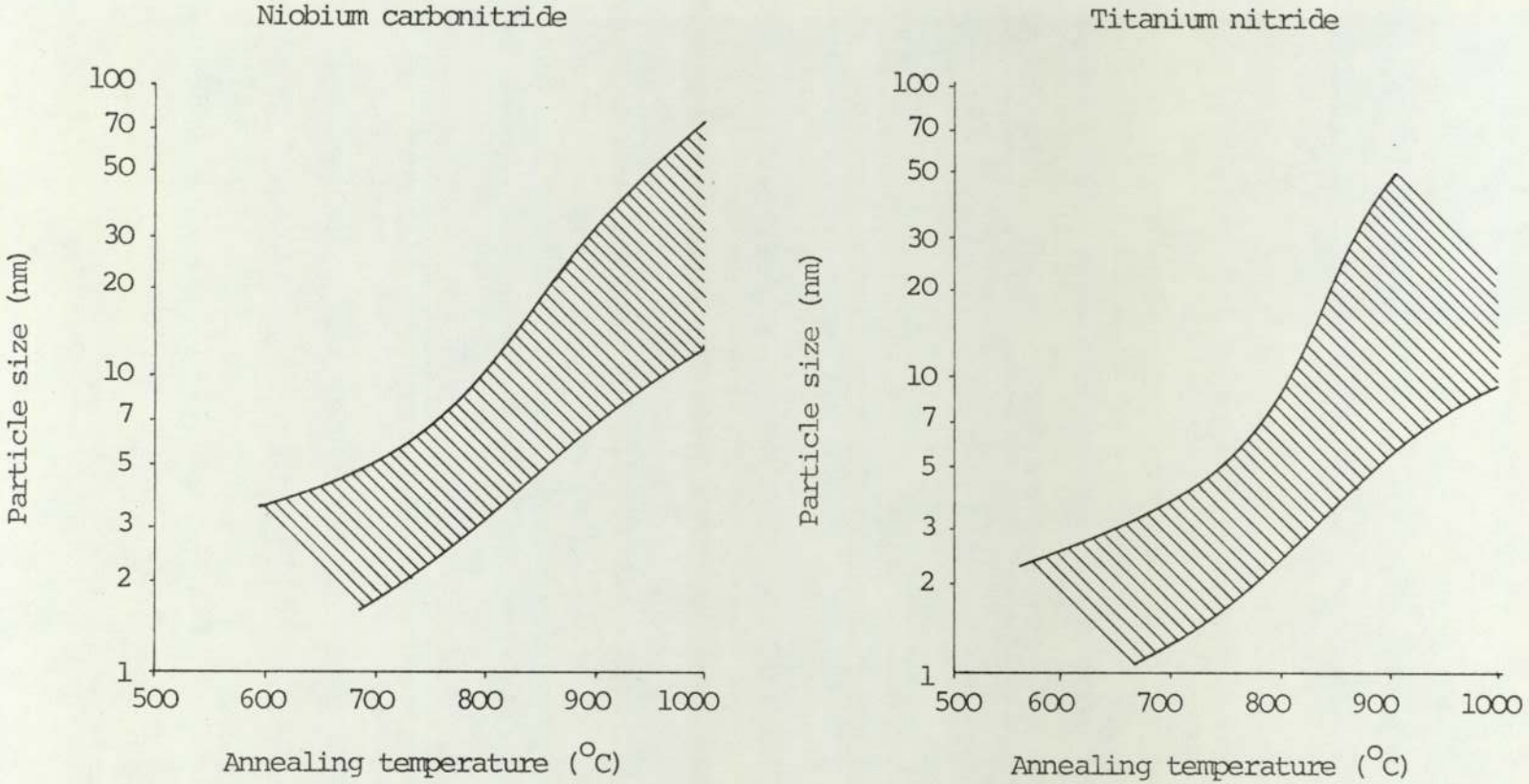

FIGURE 2.15 EFFECT OF ANNEALING TEMPERATURE ON THE SIZE OF PRECIPITATES

The steels were heated to 1300°C for 30 minutes, cooled to room temperature, and then annealed for 1 hour.

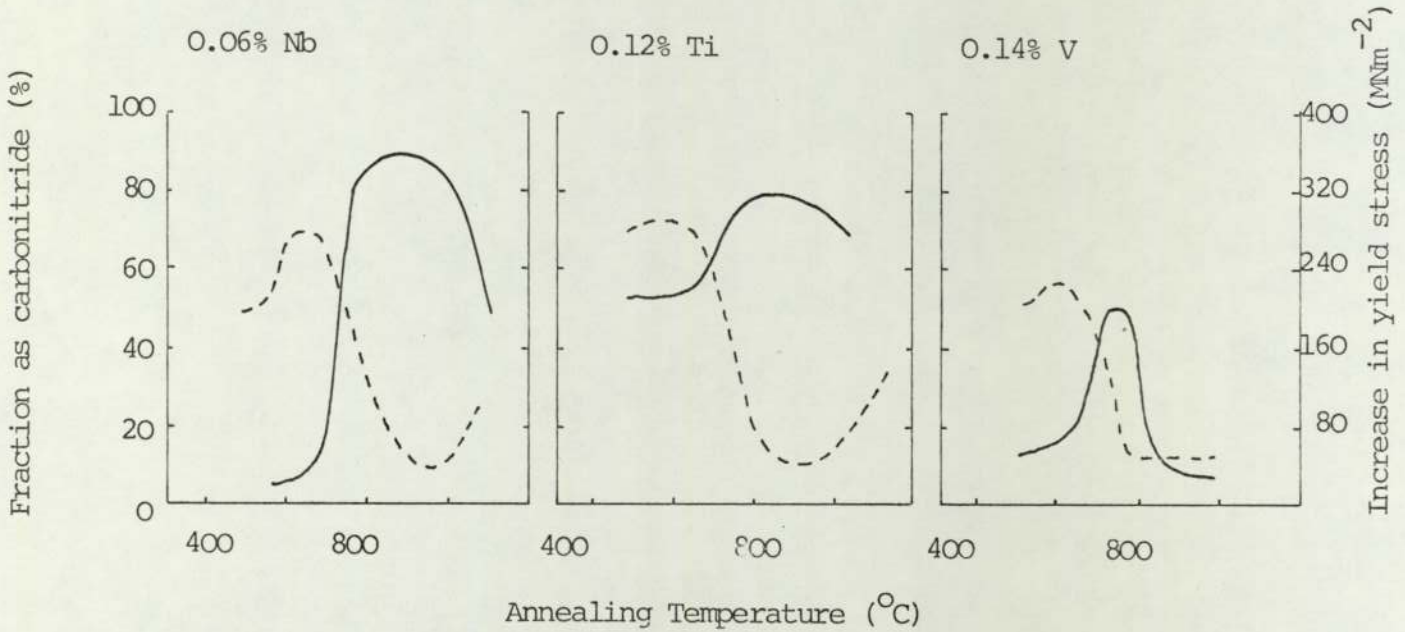

FIGURE 2.16 FRACTION OF NIOBIUM, TITANIUM OR VANADIUM PRECIPITATED AS CARBONITRIDE, AND INCREASE IN YIELD STRESS FOR A LOW CARBON STEEL AFTER SOLUTION TREATMENT AND PRECIPITATION ANNEAL FOR 1 HOUR

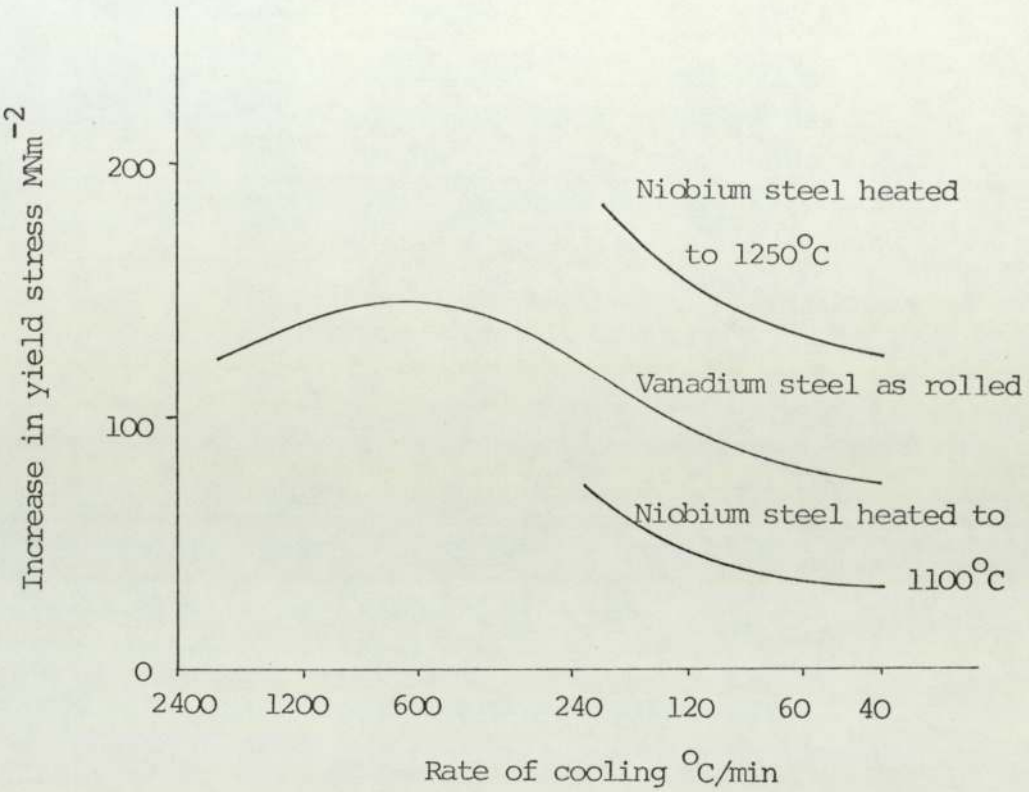

FIGURE 2.17 EFFECT OF COOLING RATE ON PRECIPITATION STRENGTHENING

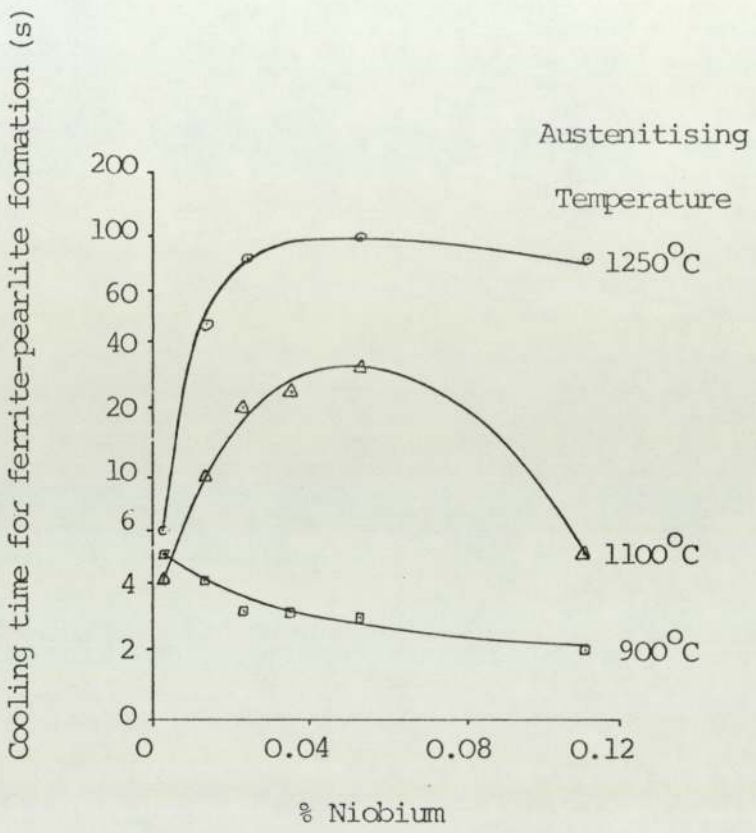

FIGURE 2.18 COOLING TIME BETWEEN 800°C AND 500°C FOR THE START OF FERRITE-PEARLITE FORMATION IN NIOBIUM STEELS AFTER AUSTENITISING AT DIFFERENT TEMPERATURES. THE STEEL CONTAINED 0.2% C AND 1.2% Mn

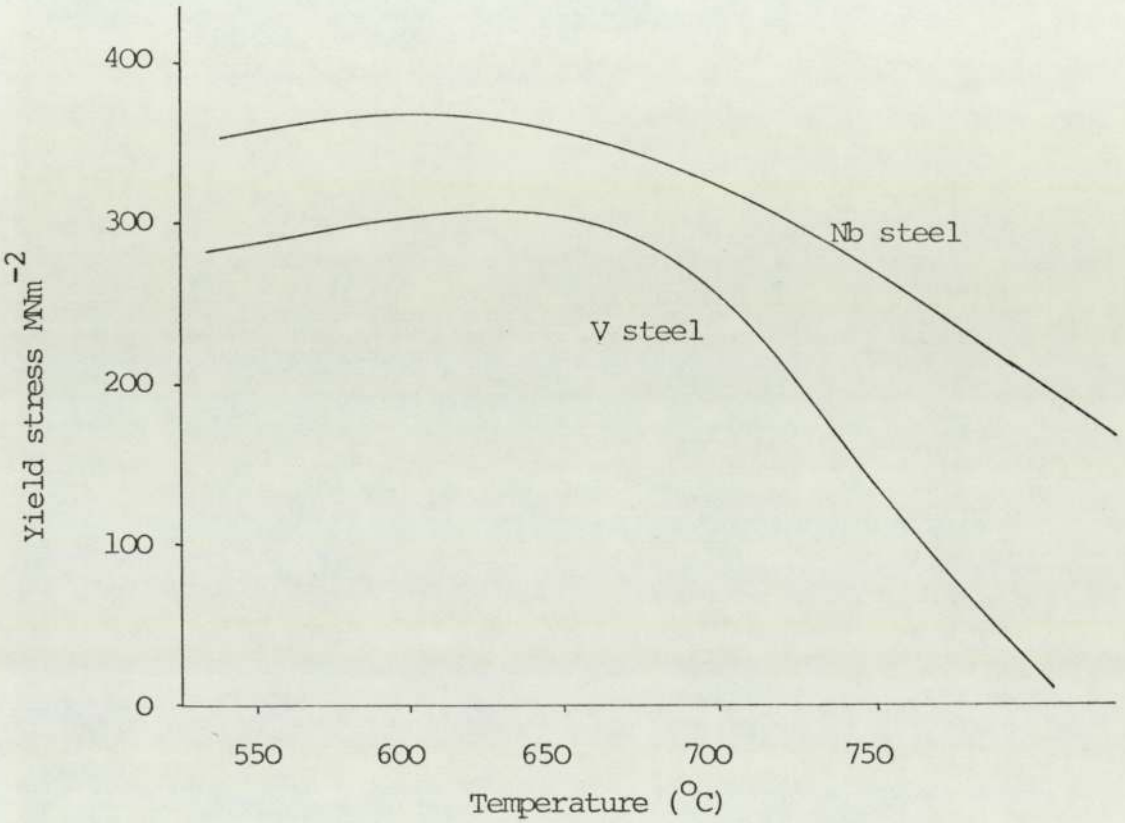

FIGURE 2.19 TEMPERING CHARACTERISTICS OF NIOBIUM AND VANADIUM STEELS

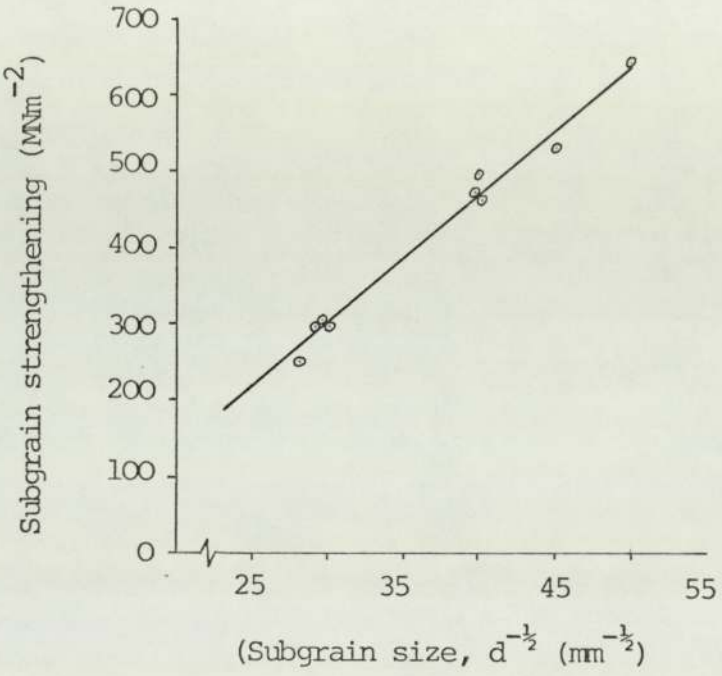

FIGURE 2.20 REGRESSION LINE BETWEEN SUBGRAIN SIZE AND ITS STRENGTHENING EFFECT

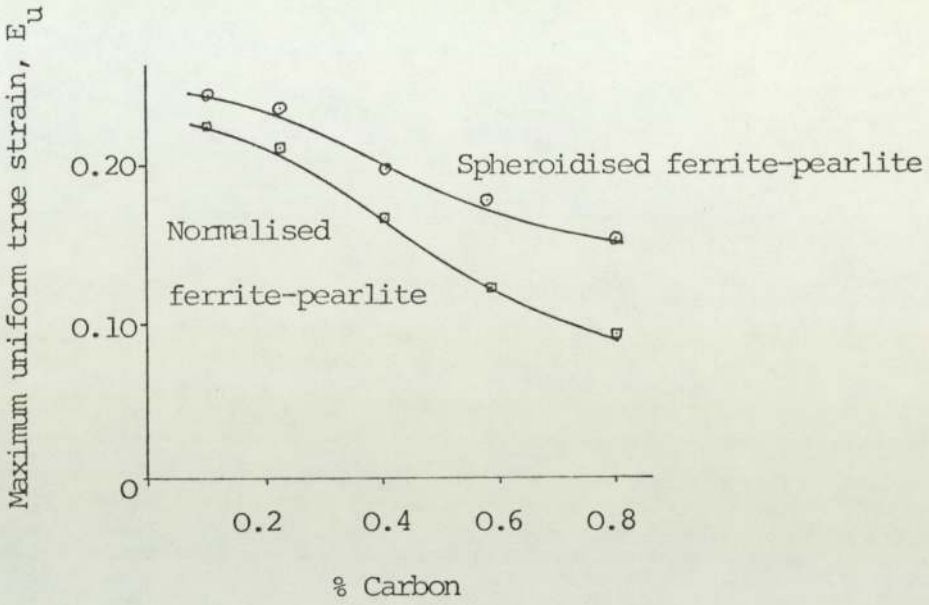

FIGURE 2.21 EFFECT OF CARBON ON MAXIMUM UNIFORM DUCTILITY

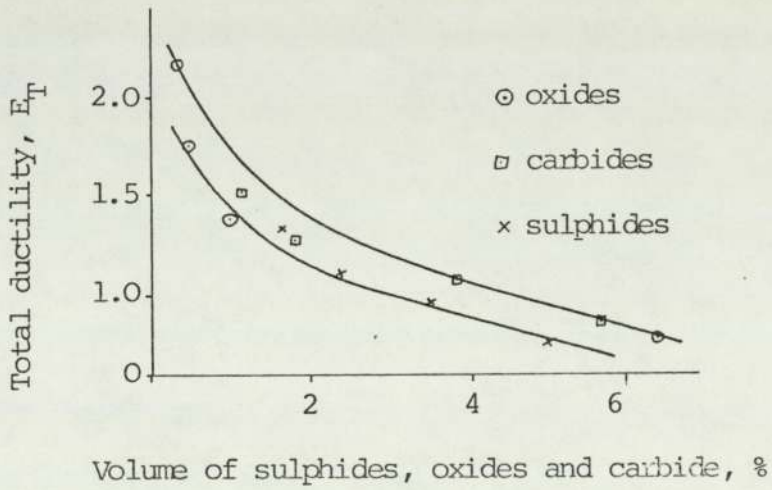

FIGURE 2.22 EFFECT OF SECOND PHASE PARTICLES ON TOTAL DUCTILITY

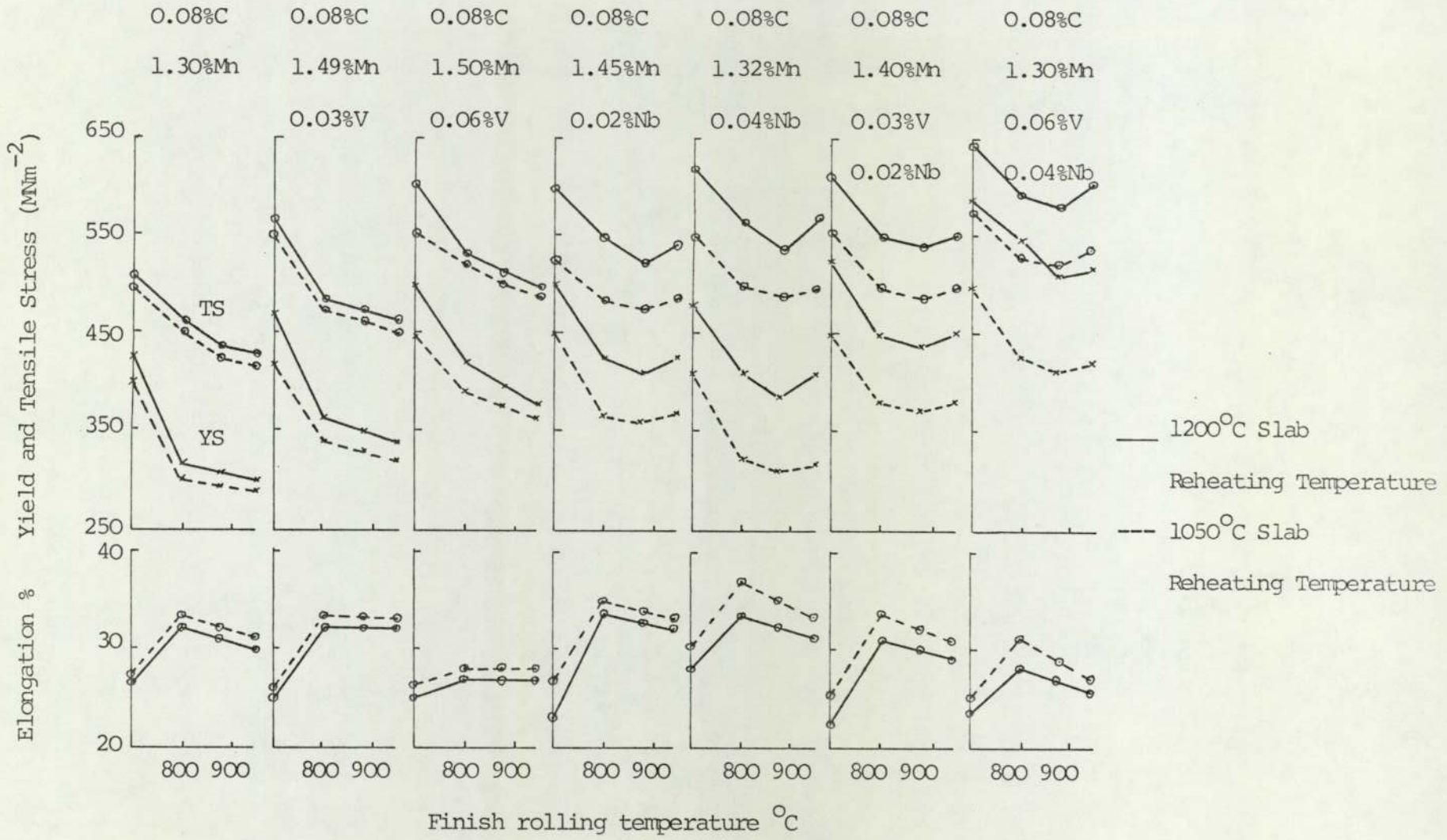

FIGURE 2.23 EFFECT OF CONTROLLED ROLLING CONDITIONS ON MECHANICAL PROPERTIES OF LABORATORY PEARLITE REDUCED STEEL

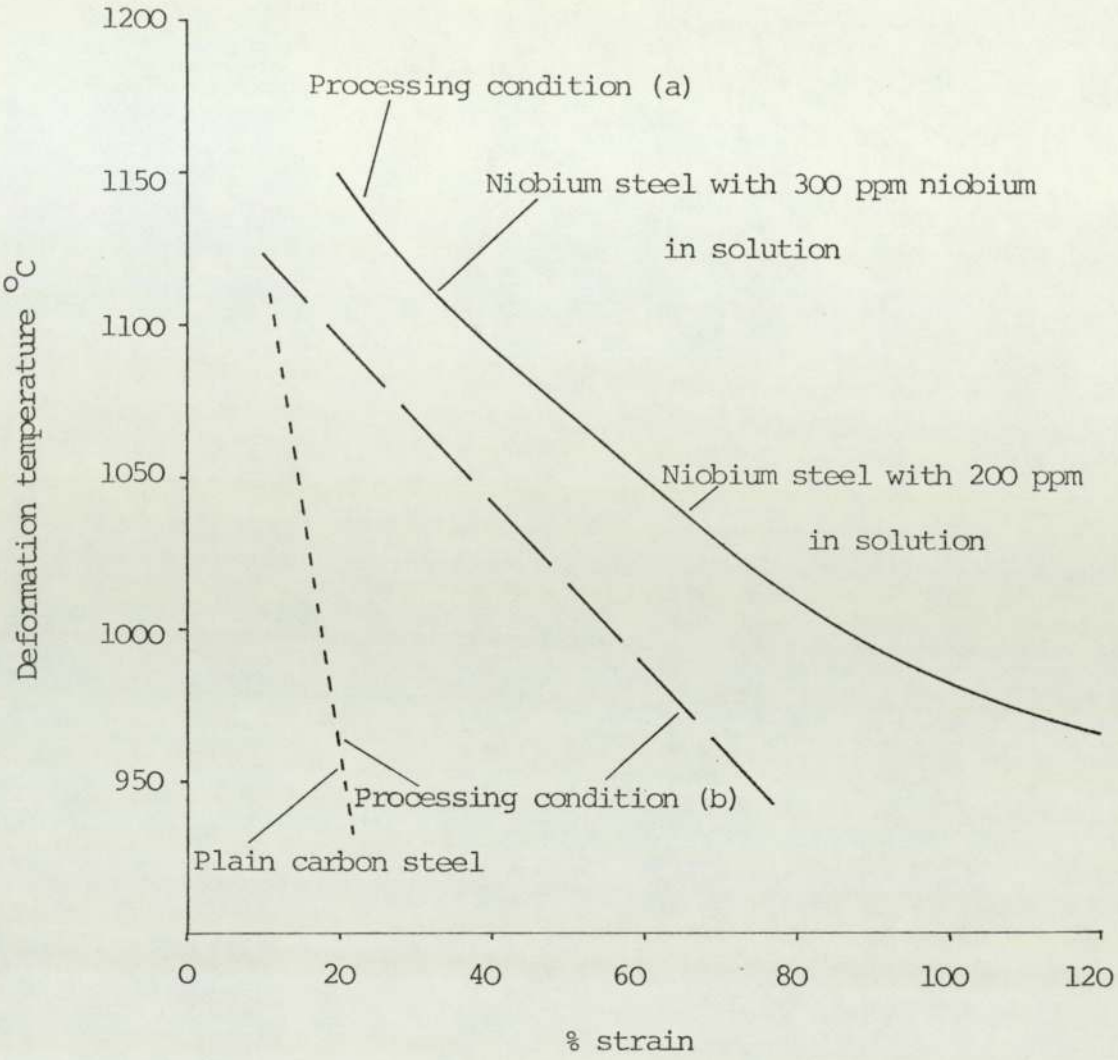

Processing conditions

(a) solution treated for 60 minutes at 115°C, air-cooled to deformation temperatures and rolled by the amount indicated and water quenched.

(b) same as (a) but held at the deformation temperature for 30 minutes prior to rolling.

FIGURE 2.24 EFFECT OF DISSOLVED NIOBIUM AND DEFORMATION TEMPERATURE ON THE CRITICAL AMOUNT OF DEFORMATION REQUIRED FOR COMPLETION OF RECRYSTALLISATION

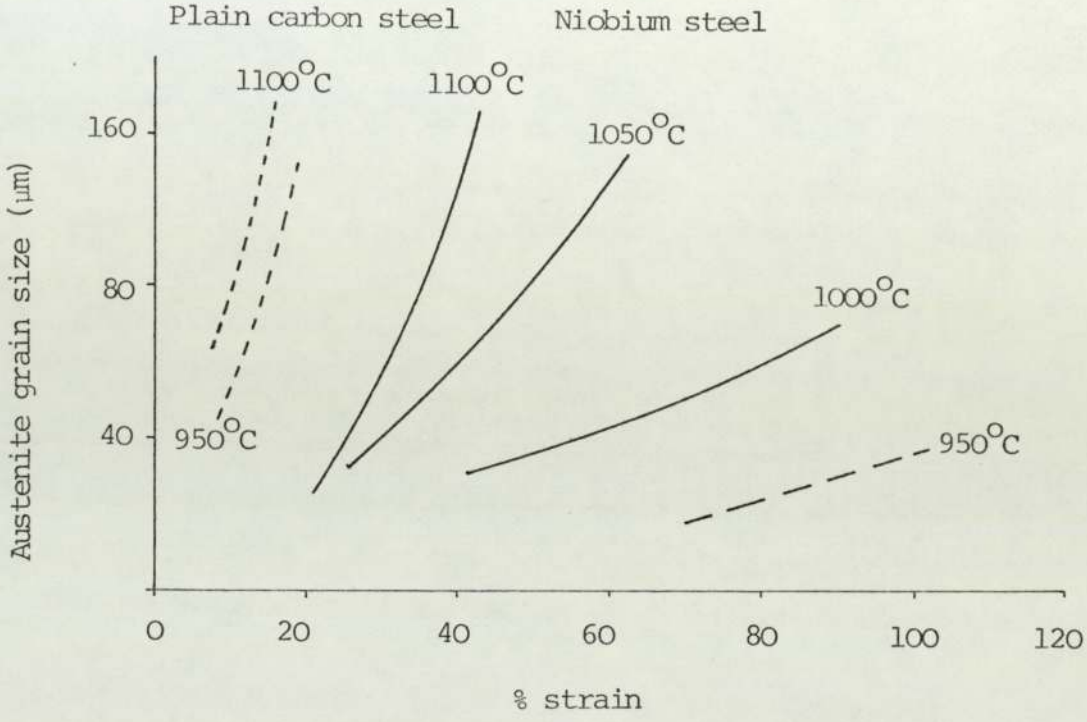

FIGURE 2.25 EFFECT OF DEFORMATION TEMPERATURE AND INITIAL GRAIN SIZE ON THE CRITICAL AMOUNT OF DEFORMATION REQUIRED FOR COMPLETION OF RECRYSTALLISATION IN THE PLAIN-CARBON AND NIOBIUM STEELS

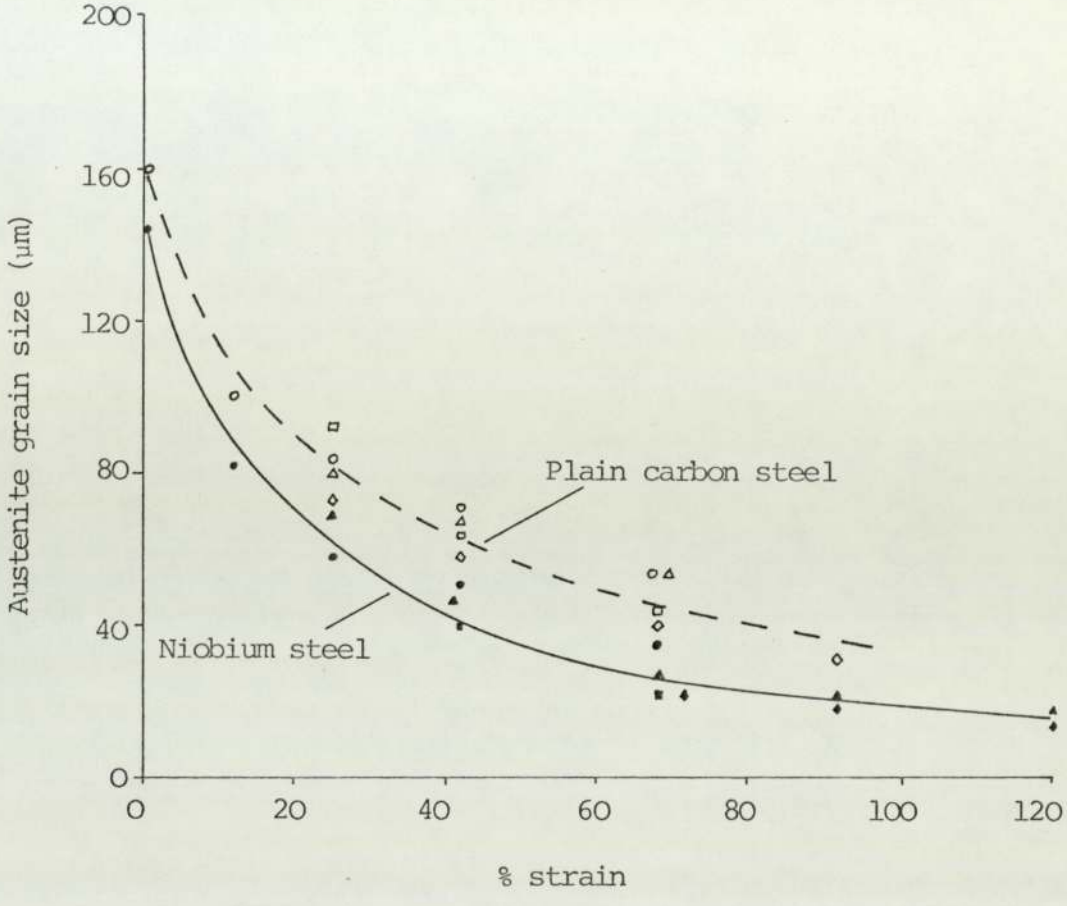

Plain carbon	Niobium steel	Deformation temperature
○	●	1150°C
△	▲	1100°C
□	■	1050°C
◇	◆	1000°C

FIGURE 2.26 INFLUENCE OF THE AMOUNT OF SINGLE PASS DEFORMATION AND THE DEFORMATION TEMPERATURE ON RECRYSTALLISED AUSTENITE GRAIN SIZE IN PLAIN CARBON AND NIOBIUM STEELS

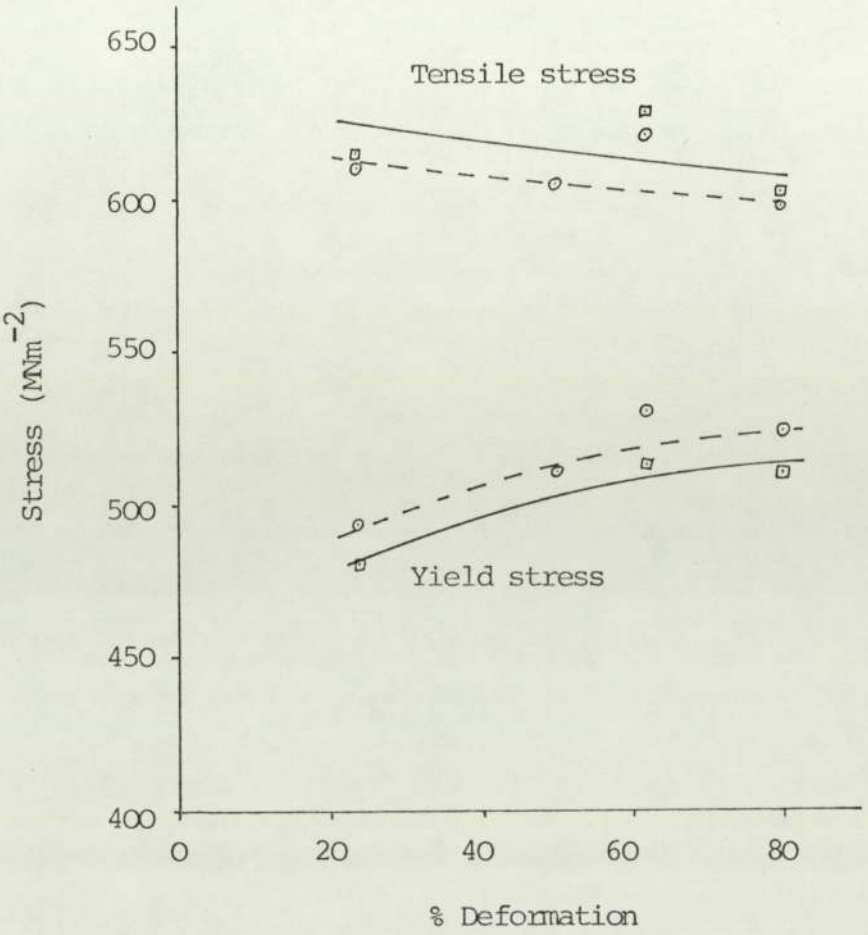

Deformation temperature

o --- 800°C

□ —— 900°C

Steel Composition

0.12%C, 0.24%Si, 1.43%Mn, 0.36%Nb

FIGURE 2.27 THE EFFECT OF AMOUNT OF DEFORMATION AND DEFORMATION TEMPERATURE IN THE SECOND STAGE ON YIELD STRESS AND TENSILE STRESS OF A NIOBIUM STEEL. THE STEEL WAS ROLLED 61.3% AT 1020°C, COOLED TO THE DEFORMATION TEMPERATURE AND REDUCED BY THE AMOUNT INDICATED

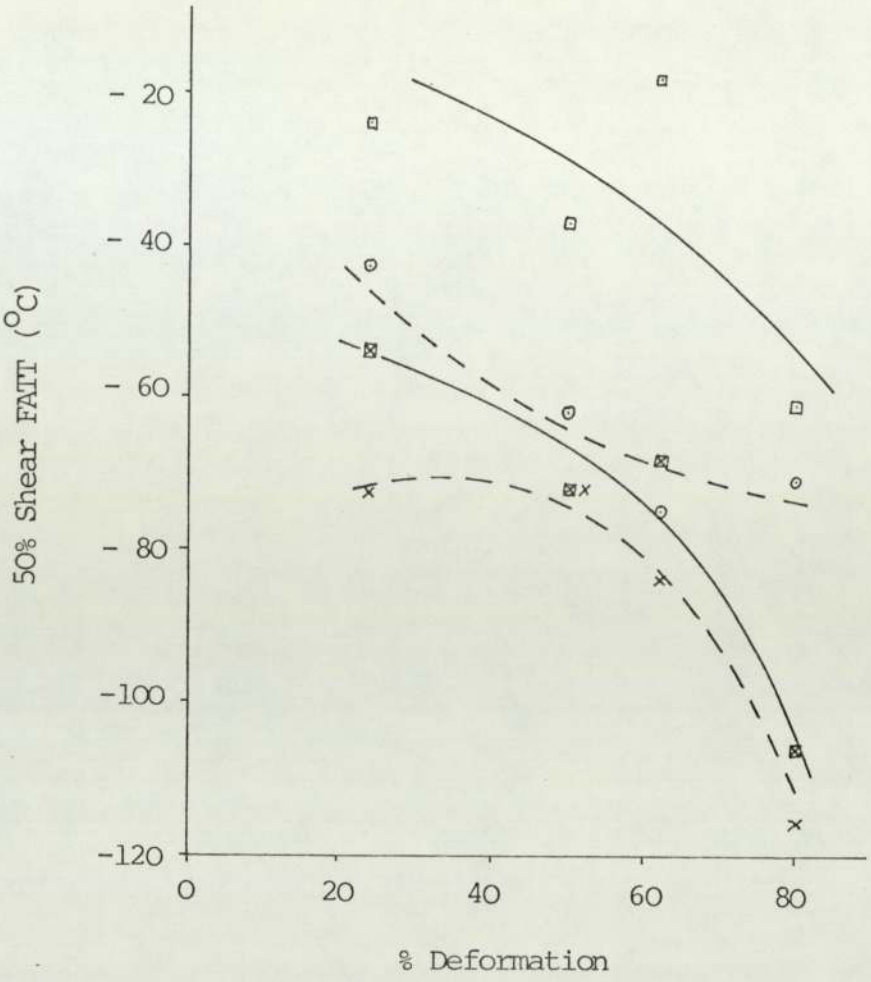

Steel Composition

Plain carbon (⊙,⊡) 0.12%C, 0.24%Si, 1.43%Mn, 0.035%Nb

Niobium steel (×,⊠) 0.18%C, 0.40%Si, 1.40%Mn

FIGURE 2.28 EFFECT OF THE AMOUNT OF DEFORMATION AND DEFORMATION TEMPERATURE IN THE SECOND STAGE ON CHARPY IMPACT PROPERTIES OF NIOBIUM AND PLAIN CARBON STEELS. THERMO-MECHANICAL TREATMENT AS PER FIGURE 2.27

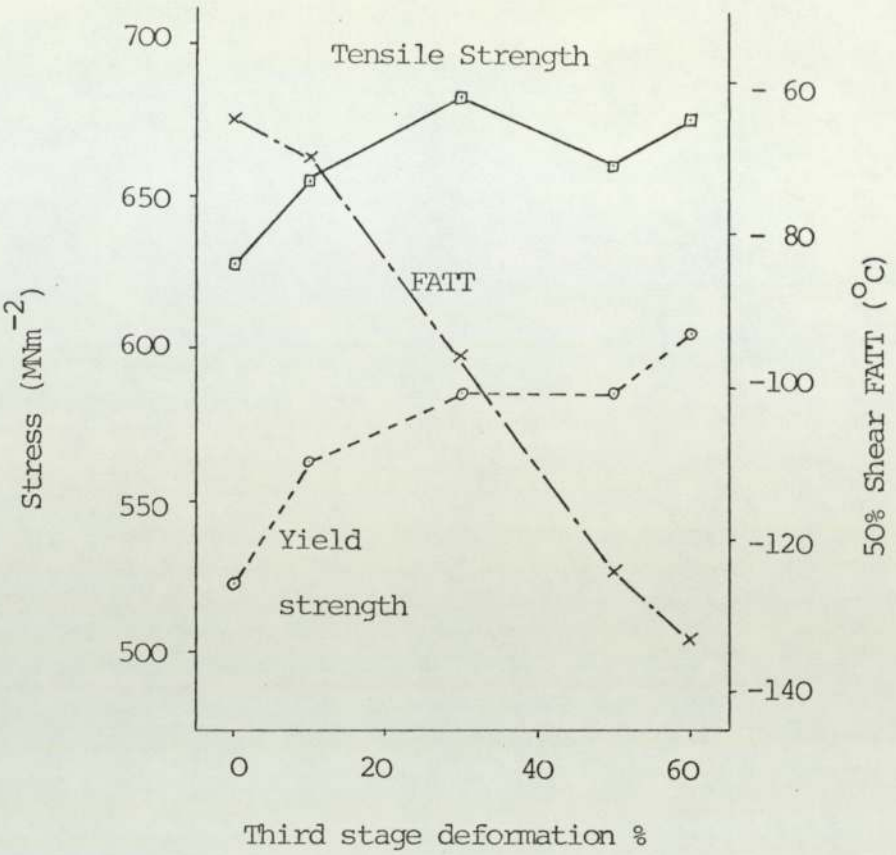

Steel Composition

0.12%C, 0.24%Si, 1.43%Mn, 0.36%Nb

Thermomechanical treatment

- rolled 62.5% in two passes at 1070 and 1020^{o}C
- cooled to 850^{o}C and reduced by 50%
- cooled to 710^{o}C and reduced by the amount indicated

FIGURE 2.29 TENSILE PROPERTIES AND CHARPY IMPACT PROPERTIES PLOTTED AGAINST THE AMOUNT OF DEFORMATION

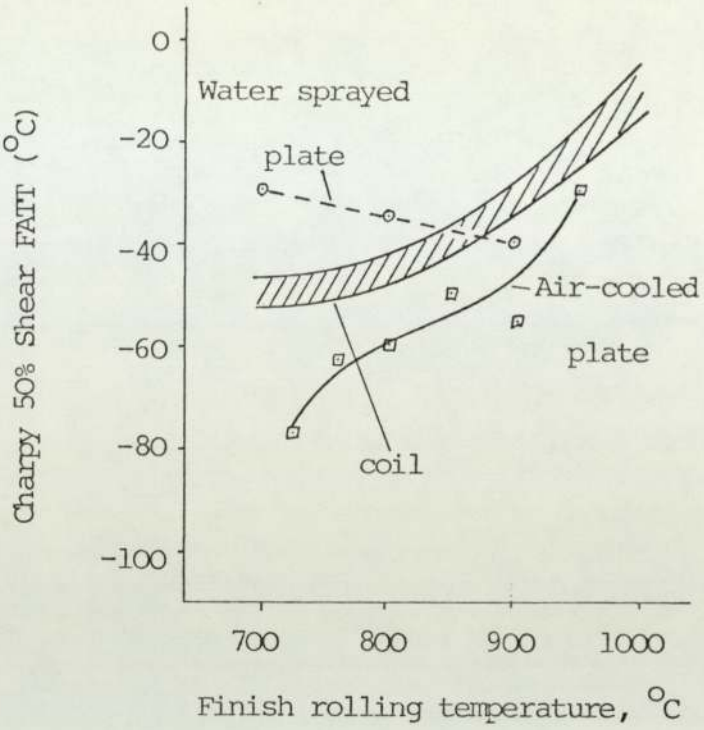

Steel Composition

0.12%C, 0.3%Si, 1.3%Mn, 0.02%Nb

FIGURE 2.30 EFFECT OF FINISHING TEMPERATURE ON THE FRACTURE APPEARANCE TRANSITION TEMPERATURE (FATT) OF AIR COOLED PLATES, WATER SPRAYED PLATES AND SIMULATED COILS

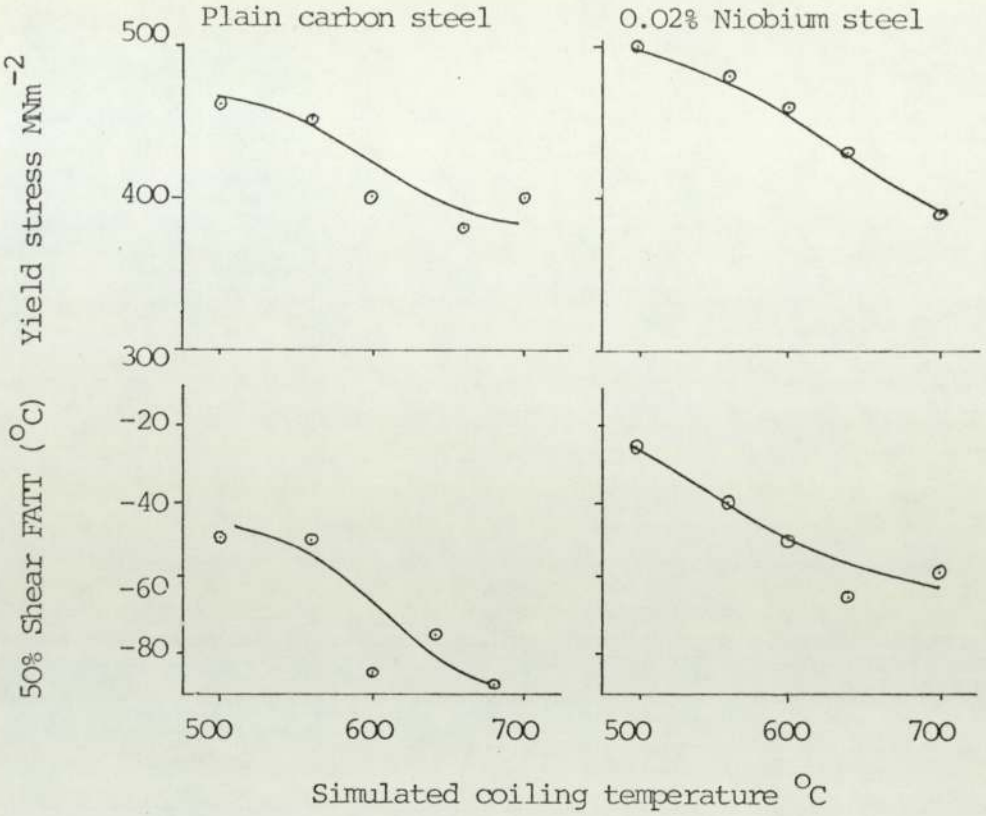

Base composition of steel

0.12%C, 1.3%Mn

FIGURE 2.31 EFFECT OF SIMULATED COILING TEMPERATURE ON YIELD STRESS AND FRACTURE APPEARANCE TRANSITION TEMPERATURE. STEELS FINISH ROLLED AT 800^{o}C

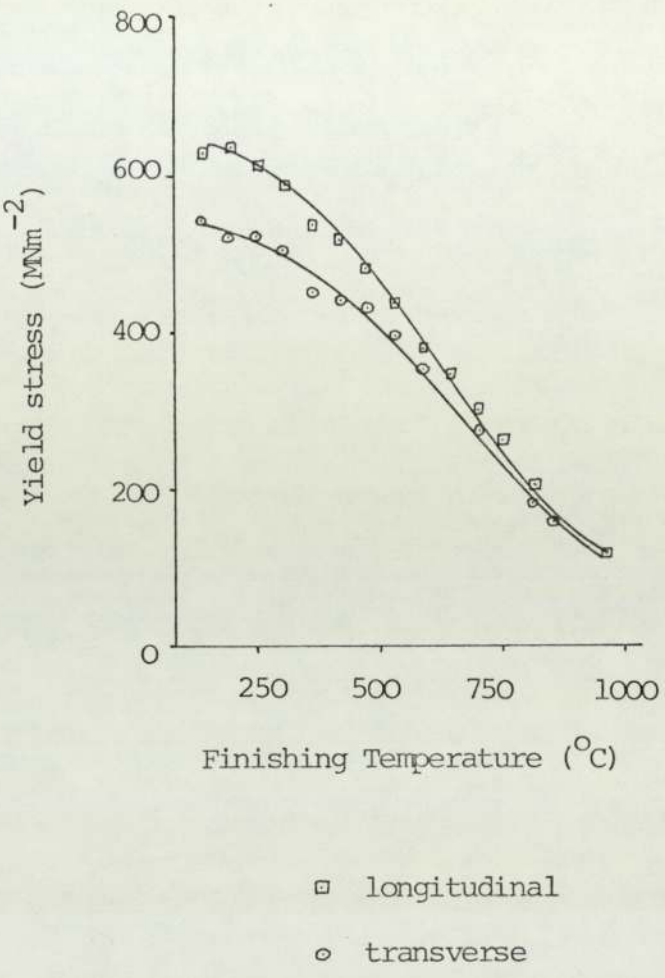

FIGURE 2.32 TENSILE PROPERTIES OF THE AS-ROLLED IRON-MANGANESE PLATES AS A FUNCTION OF FINISHING TEMPERATURE

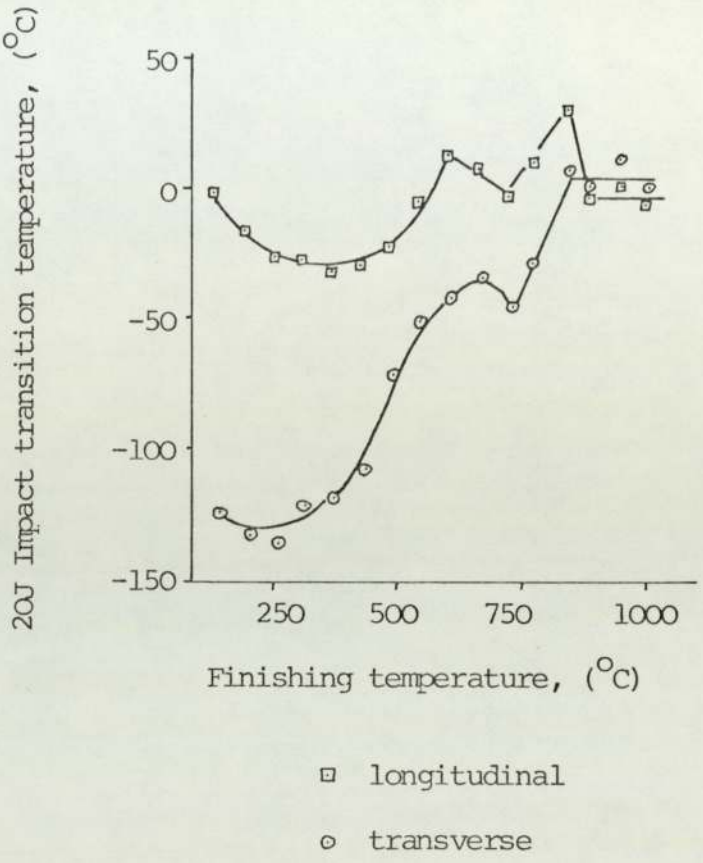

FIGURE 2.33 IMPACT PROPERTIES OF AS-ROLLED IRON-MANGANESE PLATES AS A FUNCTION OF FINISHING TEMPERATURE

3. EXPERIMENTAL PROGRAMME

3.1 INTRODUCTION

The development of high strength low alloy steels has taken place in conjunction with controlled rolling. The development has been aimed at obtaining a material with a high yield strength and good toughness properties.

These investigations have shown the importance of grain size as a means of both increasing the yield stress and reducing the impact transition temperature. It has also been shown that very fine precipitation of carbides and nitrides produces a significant increase in the yield strength, although at some detriment to the impact transition temperature.

Controlled rolling was developed as a thermo-mechanical treatment to optimise the refinement of the grain and sub-grain structure and produce a very fine dispersion of precipitates to gain maximum increase in strength with minimum loss of toughness.

The effect of reheating and deforming high strength low alloy steel, as opposed to deformation during cooling has received little attention. The work presented in this thesis is a study of the effect that re-heating and deformation of low alloy steels in the two phase ($\alpha + \gamma$) region, has on the structure and properties of the deformed material.

3.2 MATERIALS

Common micro-alloying additions used in high strength low alloy steels are niobium and vanadium. In this study, three steels were investigated, a plain carbon-manganese steel, one with vanadium addition, and one with a niobium addition. The composition of each steel is given in table 3.1.

The base composition chosen was typical of that used in many high strength low alloy steels (i.e 0.13%C, 1.57%Mn). Vanadium and niobium are commonly used micro-alloying addition. The vanadium forms precipitates with carbon and nitrogen (chiefly carbon), which are soluble in low temperature austenite. This opens the possibility for some secondary precipitation on cooling from the two phase region. The steel studied had a vanadium content of 0.091%. Niobium forms precipitates with carbon, which are stable at temperatures well into the austenitic region. Such precipitates have negligible hardening effect, but assist in grain refining by pining grain boundaries, and therefore preventing grain growth.

Using the following equations developed by Irvine et al[22] and Aaronson[39], the solution temperatures for V_4C_3 and Nb C were calculated.

For V_4C_3,

$$\log_{10}[V]^{\frac{4}{3}}[C] = \frac{-10,800}{T} + 7.05$$

Solution temperature = 817°C

For NbC,

$$\log_{10}[Nb][C] = \frac{-6,770}{T} + 2.26$$

Solution temperature = $1,354^{o}C$

In the above equations, T is the absolute temperature and the concentrations are given in atomic percent.

3.3 WARM DEFORMATION

Irrespective of the mode of deformation, problems are encountered when testing is carried out at elevated temperatures. This is due to the need to control and measure the temperature and extent of deformation.

There are four principal methods which can be used to study the effect of warm deformation, namely, scaled down practical working operations, tensile tests, compression tests (axisymmetric and plain strain), and torsion tests.

3.3.1 Scaled Down Practical Working Operations

The principal advantage of this form of deformation is that the test method and practical working operation for which the data is required, is the same. Such a test method is useful when studying a specific method of warm working rather than warm workability in general.

Extrusion experiments using scaled down equipment are an illustration of this form of testing, where important variables

which are specific to extrusion (e.g. die face angle and lubrication conditions) can be studied.

It is much more difficult to consider rolling in the same way. To reproduce the high deformation rates and intermittent deformation cycles currently used in modern continuous hot rolling mills, very expensive equipment would be required. In the case of cogging and slabbing mills, where lower rolling speeds and relatively long intervals between successive deformations are used, simulation using single stand mills can be used. In scaling up the measured rolling loads for production mills, care is necessary to account for differences in frictional conditions, temperature conditions and mill characteristics.

3.3.2 Tensile Tests

The strain rates obtainable with conventional tensile testing equipment are inadequate for warm working studies and therefore special equipment is required. At warm working temperatures, the flow stress is markedly dependent on the strain rate. A constant true strain rate can be obtained by driving the moving head of a tensile machine with a logarithmically shaped cam. In this way true stress - true strain curves at a constant true strain rate can be obtained for stress up to the point where necking begins to occur. Necking usually starts at a true strain of less than 0.7 (100% elongation). A study of the effect of hot deformation at strains greater than this involves the use of rather complex procedures.

3.3.3 Compression Tests

Two types of compression test have been used for metal working studies, namely, axisymmetric compression and plane strain compression, In the former, a cylindrical sample is compressed between flat platens whose cross-section is much larger than the initial cross-section of the samples. In the latter, a strip sample is compressed between two flat, narrow platens which overlap the edges of the samples.

Axisymmetric compression. - In common with the tensile tests, a constant true strain rate is achieved by driving the moving compression head with a cam of logarithmic shape. In this way, a true stress - true strain curve at a constant true strain rate can be obtained up to the strain at which 'barrelling' begins. This usually occurs at about 50% reduction in height (true strain 0.7), and arises due to friction between the platen and the end of the sample. Simulations involving true strains greater than 0.7 are not possible.

Plane strain compression. - In this form of compression testing, the area under compression remains constant, and true strains up to about 5 can be achieved at a constant true strain rate. This enables hot rolling to be studied since the true strain used in rolling is of the order of 5.

The problems associated with compression tests are due to:-

(i) surface friction between the platen and the sample;

(ii) platen breadth;

(iii) variation in sample geometry;

(iv) platen/sample temperature gradient.

3.3.4 Torsion Tests

In a torsion test the mode of deformation is shear, and deformation should occur without any change in dimensions of the sample. This means that by twisting the sample at a constant speed a constant true strain rate can be obtained up to the start of fracture. In certain cases this may correspond to strains of several hundred and is an important advantage over tensile and compression testing. Torsion testing has the additional advantage in that there are no frictional forces to be considered. Unfortunately, during twisting, samples tend to lengthen (aluminium) or shorten (most materials including steels), and to avoid this the specimen must be axially constrained. This imposes axial stresses on the specimen so that the stress state is not pure shear. In the case where the specimen is constrained, the constant geometry simplifies the conversion of torque (T) to surface shear stress (τ) as,

$$\tau = \frac{1}{2\pi r^3}\left[3T + \frac{\theta dT}{d\theta} + \frac{\dot{\theta} dT}{d\dot{\theta}}\right]$$

where r is the specimen radius and θ and $\dot{\theta}$ are the angle of twist per unit length and its time derivative respectively. The surface shear strain γ, and shear strain rate $\dot{\gamma}$ are related to θ and $\dot{\theta}$ as follows,

$$\gamma = r\theta$$

$$\dot{\gamma} = r\dot{\theta}$$

In practice, the number of tests required to calculate the variation of torque with angle of twist, means that calculation is time consuming. The test is useful for comparative purposes, and, because of its several advantages over other test methods, has become increasingly popular.

3.4 PROGRAMME

Warm deformation was carried out using torsion and rolling as the modes of deformation.

The torsion experiments enabled changes in the structure of the steel to be observed. The extent of deformation (shear strain) increases from zero at the centre to a maximum value at the surface. Some estimate of the effect on mechanical properties can be made from the hardness measurements.

The rolling experiments were used to assess the effect of warm deformation on the mechanical properties at room temperature.

3.4.1 Torsion Experiments

The torsion specimens used in this work are shown in figure 3.1. The machined specimens were initially heat treated in a vacuum furnace at 960^{o}C for 30 minutes and furnace cooled. This was done to anneal the steel and allow the vanadium carbide to be taken into solution and re-precipitate during the furnace cooling. A further stage in the initial work was to determine the extent of the two phase ($\alpha + \gamma$) region. This was done using dilatometry.

The specimens were tested at two temperatures within the two phase region, 740^{o} and 770^{o}C. Testing at these temperatures was done at a constant speed of rotation (angle of twist about the longitudinal axis of the specimen) of 30 rpm. This produces a strain and a strain rate gradient along the radius of the specimen. At the centre of the specimen the strain and strain rate is zero.

The values after twisting the specimen through 1 and 4 complete revolutions is tabulated below,

	1 Revolution	4 Revolutions
Surface strain	0.785	3.142
Surface strain rate (s^{-1})	0.393	0.393

At the end of deformation, the specimen was either allowed to cool in air, or sprayed with water. From these experiments, the effect of warm deformation on the structure, and particularly on the ferrite phase, could be assessed.

3.4.2 Rolling Experiments

The material used in rolling experiments was initially cold rolled to various thicknesses before heat treating in a vacuum furnace at 960^{o}C for 30 minutes. The material was then warm rolled in one pass to constant thickness. From the warm rolled materials specimens were prepared for tensile testing.

TABLE 3.1 COMPOSITION OF STEELS STUDIED

	Base Steel	Vanadium Steel	Niobium Steel
C	0.13	0.14	0.16
Mn	1.57	1.74	1.52
Si	0.03	0.03	0.06
S	0.010	0.009	0.010
P	<0.005	<0.005	<0.005
Al	<0.005	0.006	<0.005
V	0.023	0.091	0.016
Nb	<0.005	<0.005	0.029
Ti	<0.005	<0.005	<0.005
Ni	0.054	0.013	0.015
Cr	0.005	<0.005	0.007
Mo	0.010	0.008	0.008
Cu	0.013	<0.005	<0.005
Co	0.015	0.016	0.017
N	0.001	0.002	0.003

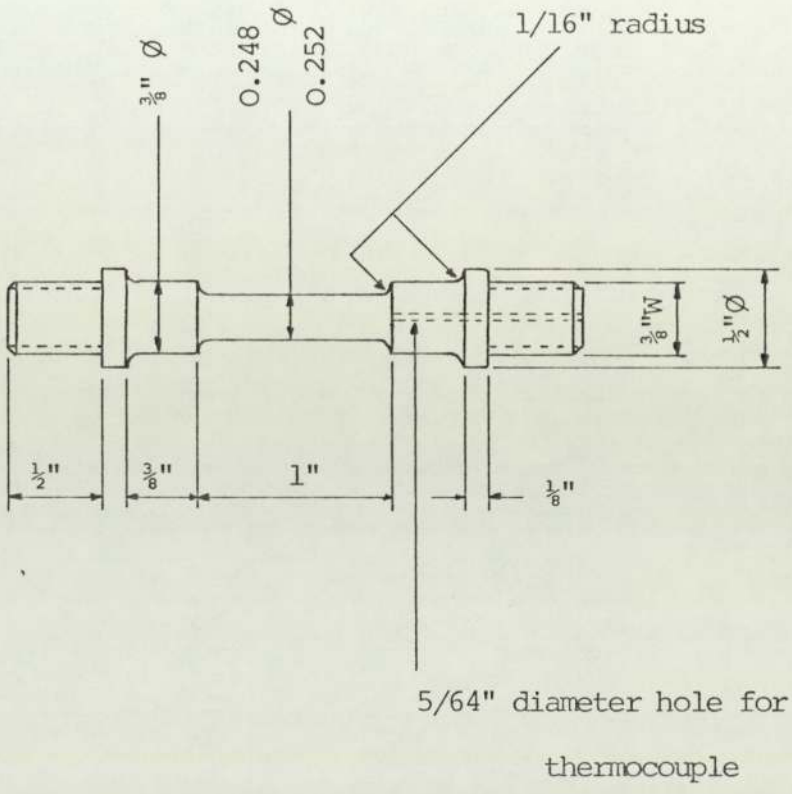

FIGURE 3.1 DIMENSIONS OF THE TORSION SPECIMENS

4. EXPERIMENTAL EQUIPMENT

4.1 TORSION EQUIPMENT

The torsion experiments were carried out using a lathe which had been suitably converted. On the lathe bed was fixed a carriage which enabled one end of the torsion specimen to be fixed while the other (screwed into the lathe chuck) was rotated. The general layout is shown schematically in figure 4.1.

The chuck was driven through a gearbox, giving spindle speeds in the range 21 - 480 rpm. In this study, all experiments were carried out using a spindle speed of 30 rpm. At this speed, dis-engaging the clutch simultaneously stopped the chuck without the need for an additional brake.

The specimen was heated using a high frequency induction coil operating at 5,000 Hz. The water cooled coil contained four turns, suitably spaced to ensure an even temperature along the gauge length of the specimen.

The carriage holding one end of the specimen fixed also contained a suitable arrangement for measuring the torque. A strain gauge was fixed to the arm which was constrained by a horizontal bar from rotating about the centre of the lathe. The output from the strain gauge was recorded on a UV recorder. Note: the response time for the standard pen recorders is not quick enough to give an accurate torque/strain plot).

The strain was measured accurately by producing a 'blip' on the UV recorder every quarter of a revolution. From these marks, and the timing marks automatically recorded on the chart every second, an accurate measurement of surface shear strain could be obtained. An illustration of the type of record produced by the UV recorder is shown in figure 4.2.

Water quenching of the specimen, when required, was arranged such that the specimen was immediately sprayed with water when the clutch was dis-engaged. Dis-engaging the clutch operated a micro-switch that switched off the power to the induction coil, and operated a water solenoid valve quenching the specimen.

The specimen temperature was controlled using a 'Pye Ether' electronic control unit. The temperature was measured by spot welding a sheathed chromel-alumel thermocouple(4) positioned as shown in figure 4.3(b).

4.1.1 Operational Problems

The main advantage of induction heating lies in the fact that the source of heating does not come into contact with the specimen to be heated. This is particularly useful since the specimens have to be tested by applying a torque at high temperature.

There are however, two major difficulties with high frequency induction heating. The eddie currents induced in the specimen being heated, interfere with the measurements of temperature and torque. In addition, accurate temperature measurement was difficult to achieve.

Interference with the output from the strain gauge occurs due to stray currents in the fixed side of the specimen. This interference on the torque curve was eliminated by earthing all parts of the equipment to a common earth point.

The problem of accurate temperature measurement was much more difficult to overcome. This difficulty was due not only to the use of high frequency induction heating of the specimen but also the fact that the temperature has to be controlled during the twisting of the specimen, and the usual problems that occur using a thermocouple to measure the temperature of relatively small specimens.

The temperature was measured, using chromel/alumel nimonic sheathed thermocouples, where the end had been broken off and a new bead formed. This allowed the hot juntion to be spot-welded directly to the specimen. The thermocouple was spot-welded at the end of a blind hole drilled in the fixed end of the specimen. The hole was drilled to the edge of the specimen gauge length. Fixing the thermocouple in this position enabled the temperature to be controlled during torsion since the thermocouple remained attached to the specimen during testing. The nimonic sheathing and ceramic insulation used in this type of thermocouple prevents the two wires from shorting-out on a cooler part of the specimen. Direct contact between the thermocouple's hot junction and the specimen was essential in order to obtain a good thermal contact during heating and testing of each specimen, since this thermocouple was used to control the temperature, and hence power in the induction coil.

4.1.2 Uniform Heating of Specimen

Uniform heating of the gauge length was achieved by altering the spacing between consecutive turns of the coil. The pitch of the coil was therefore smaller towards the end of the gauge length to compensate for the heat losses through the specimen grips.

Small thermocouples were spot-welded to the surface of the specimen at the middle and ends of the gauge length. The temperature was controlled using the thermocouple placed in the blind hole at the fixed end as already described.

Two problems were encountered with the surface thermocouples due to:

(i) variation in size of the 'hot junction' bead.
The thermocouple was formed by producing a bead on a junction of the two wires and spot-welding this to the surface of the specimen (figure 4.3(a)). The temperature at B will be lower than that at A, and it is the temperature at B that the thermocouple will record.

This problem, which it is thought can give a temperature difference between points A and B of up to 20^{o}C was avoided by spot-welding the wires separately on to the specimen.

(ii) pick up from eddy currents induced in the specimen.
Spot welding wires individually on to the specimen can cause a problem if the two wires are not close together. In particular, it is important that the two wires are on the same circumferential line in order to prevent the pick-up of eddy currents, induced in the specimen by the coil.

Thermocouples were fixed to the specimen as shown in figure 4.3(b), in order to obtain the correct coil pitch for uniform heating of the gauge length.

All thermocouples were chromel/alumel. Thermocouple 2 was used to control power supply. Thermocouples 1-3 were all individually spot-welded to the surface. Figure 4.4 shows the type of result obtained. The graph shows clearly the difference originally found between the temperature at the middle and ends of the gauge length. It also shows a curious effect with regard to thermocouple 4. It was thought that this might be due to a combination of eddy current pick-up and the fact that the temperature is approaching the curie temperature when iron changes from ferromagnetic to paramagnetic.

A similar experiment was carried out using a titanium sample where there is no curie temperature or phase change. The results presented in figure 4.5 show that all thermocouples have a constant relationship to one another.

The pitch of the coil was adjusted such that there was a uniform temperature along the gauge length of $\pm 10^{o}C$ over the range $720 - 860^{o}C$.

It was also recognised that the accurate measurement of temperature, using thermocouple 4, would depend on the size of bead produced when the two wires were joined, and the exact position in the blind hole where the spot weld was made. Clearly it is very difficult to determine the latter. These problems

could result in significant differences between the measured and actual temperature of the specimen. An alternative technique was therefore used to control the temperature of the specimen, using an optical pyrometer.

As a non-contact method of measuring the temperature, an optical pyrometer avoids the problems associated with the use of thermocouples. A pyrometer which could be focused on a spot 5mm in diameter at a distance of 125mm from the specimen was used. The positioning of the coil to obtain a uniform temperature enabled an appropriate area in the middle of the gauge length to be viewed by the pyrometer. The specimen was coated with 'aquadag', a suspension of graphite in water, to obtain black body radiation from the surface of the specimen. It also served to prevent oxidation and the formation of an oxide scale which would distort the results.

The calibration was achieved by plotting the specimen temperature as measured, using the optical pyrometer, against the power used by the induction coil. The calibration curve (figure 4.6) was obtained in the following manner:

- set the power level as required (arbitrary units);
- switch power on, the temperature of the specimen rises unhindered by the control thermocouple;
- after 5 minutes the temperature recorded by the optical pyrometer was stabilised by allowing the control thermocouple to operate;
- the temperature was then held constant for 10 minutes prior to testing of the specimen.

4.1.3 Uniformity of Strain along the Gauge Length

As a further check to ensure uniform heating of the specimen and constant surface shear strain, a specimen was marked with a straight line, using a metal scriber. The specimen was heated and twisted through four complete revolutions. The variation in twist with distance along the gauge length is shown in figure 4.7. This graph indicates that the surface shear strain is practically constant, along the gauge length.

4.2 ROLLING EQUIPMENT

The material to be warm rolled was initially cold rolled to various thicknesses, so that with one roll gap setting, a range of reductions could be achieved with a single pass. The length of each specimen was chosen so that a tensile specimen could be made from each warm rolled sample.

The specimens were heated in a muffle furnace under an argon atmosphere. The specimens were also coated with 'Burkatekt' to further reduce the oxidation of the surface. The furnace temperature was measured by a thermocouple placed directly on top of one of the samples. Once the specimens had reached the furnace temperature, they were soaked for 15 minutes.

The material was rolled using an experimental two high rolling mill. The furnace was placed adjacent to the rolling mill so that the specimens, attached to a length of nimonic wire, could be pulled from the furnace and through the rolling mill. This arrangement minimises the heat loss from the specimen prior to rolling. Before using the

rolling mill, a slab of copper approximately 10mm thick was heated to 800°C and rolled in order to raise the roll temperature. The rolled material was either immediately quenched in water, or allowed to cool in air.

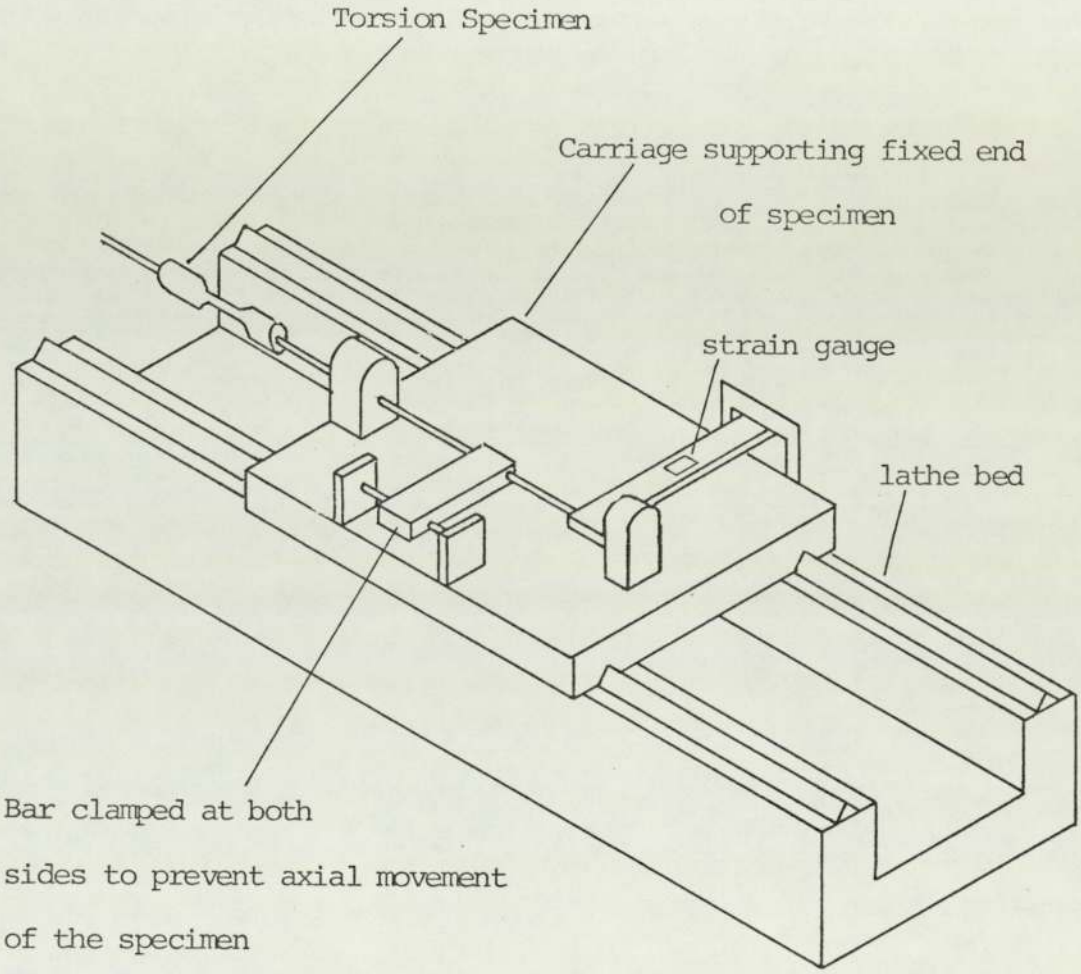

FIGURE 4.1 SCHEMATIC DIAGRAM OF TORSION APPARATUS

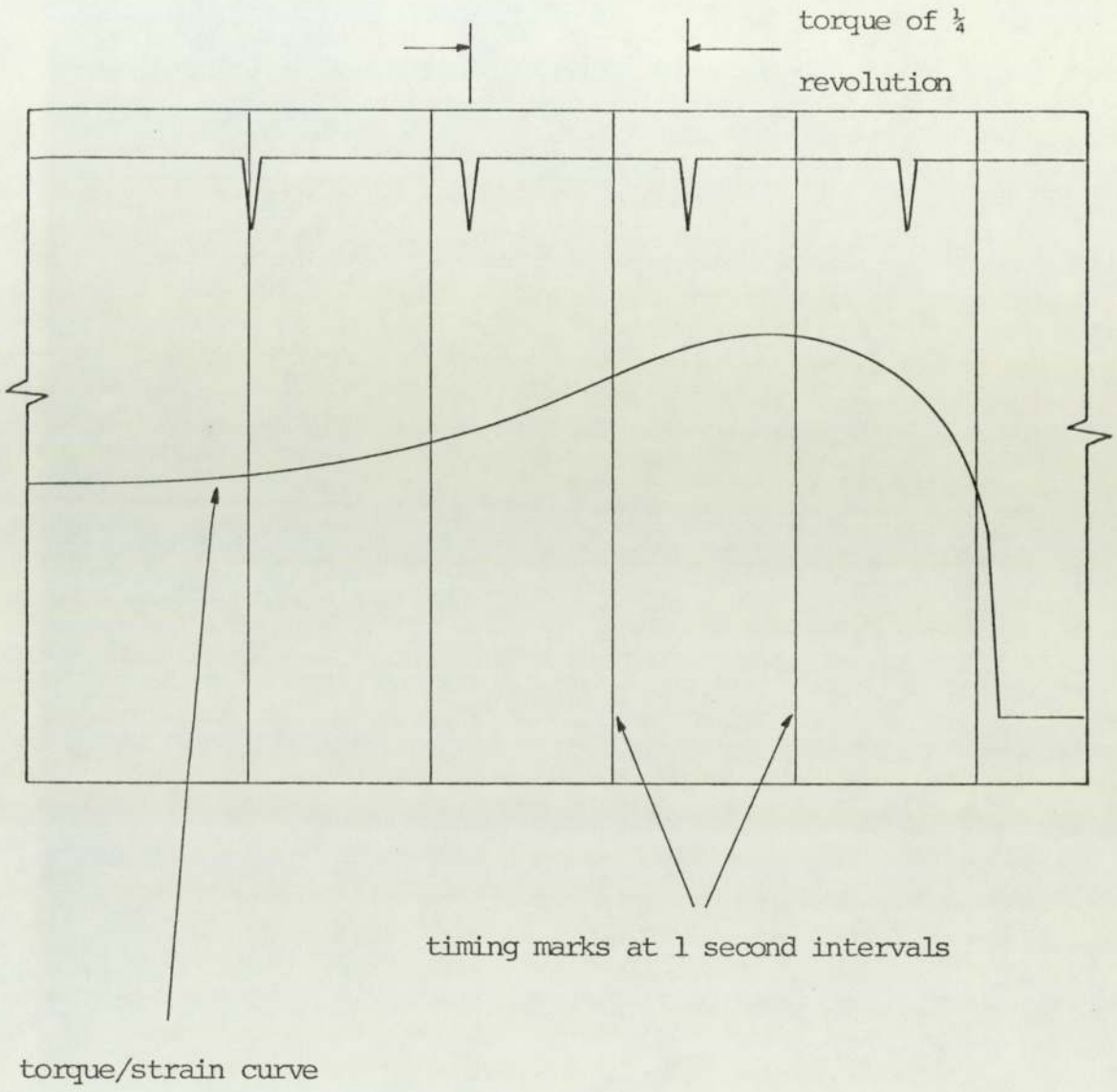

FIGURE 4.2 TYPICAL TRACE FROM THE UV CHART RECORDER

(a)

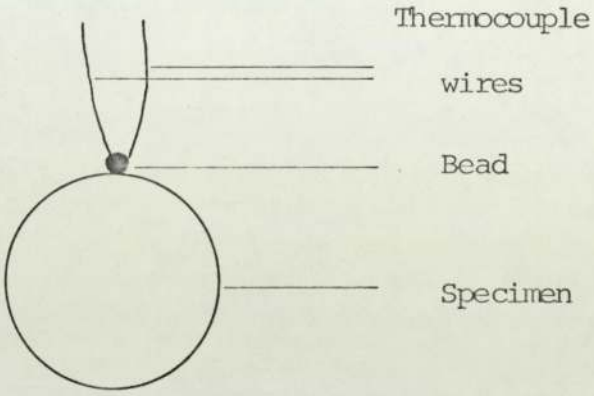

(b)

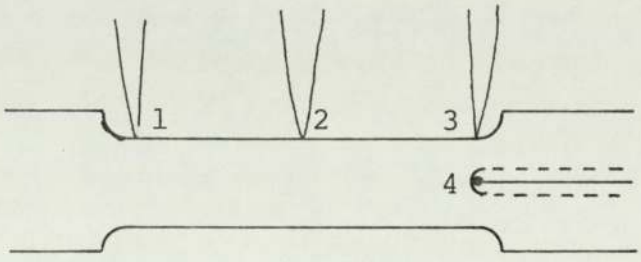

FIGURE 4.3 LOCATION OF THERMOCOUPLES

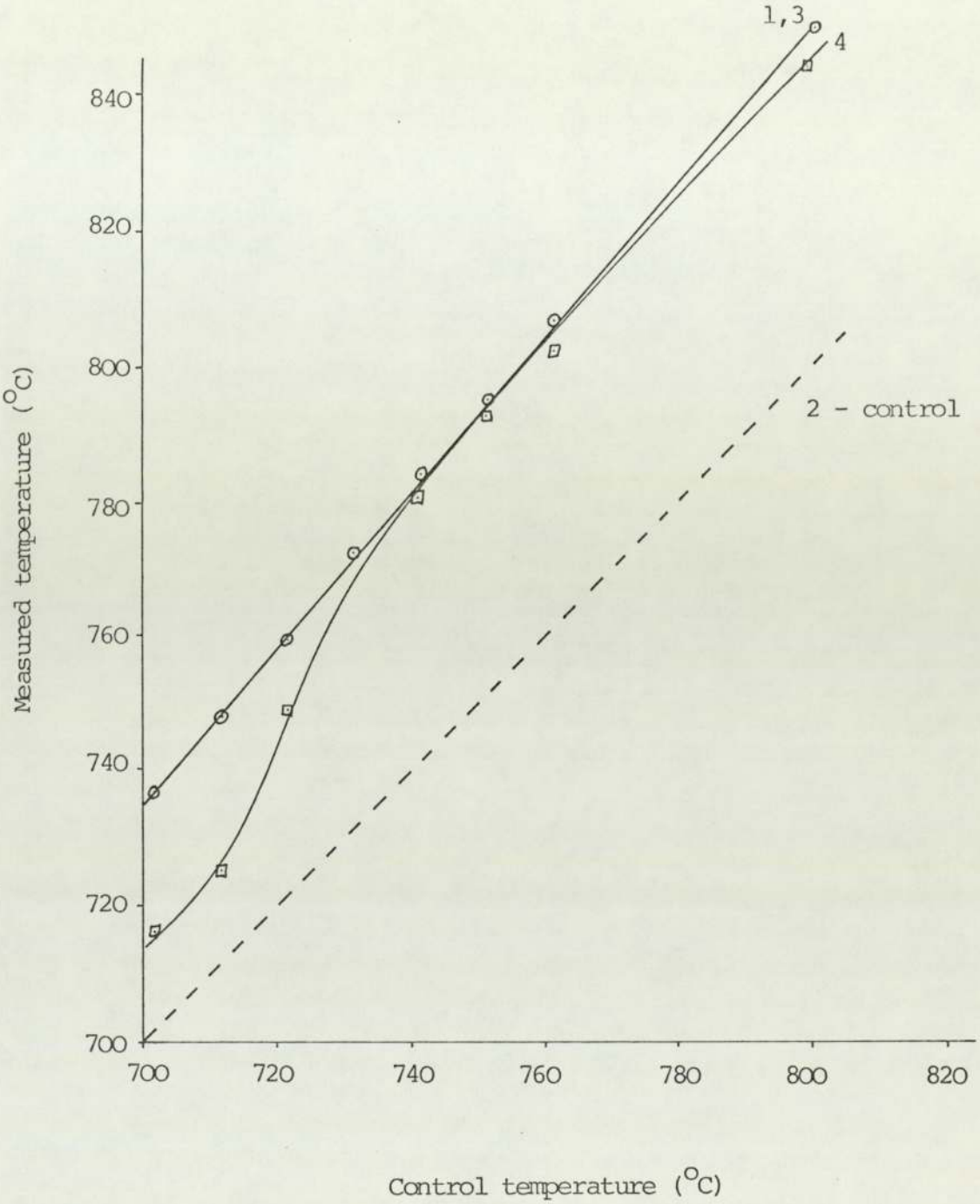

Data points

⊙ thermocouples 1 and 3

⊡ thermocouple 4

FIGURE 4.4 MEASURED TEMPERATURE PLOTTED AGAINST CONTROL TEMPERATURE (THERMOCOUPLE 2)

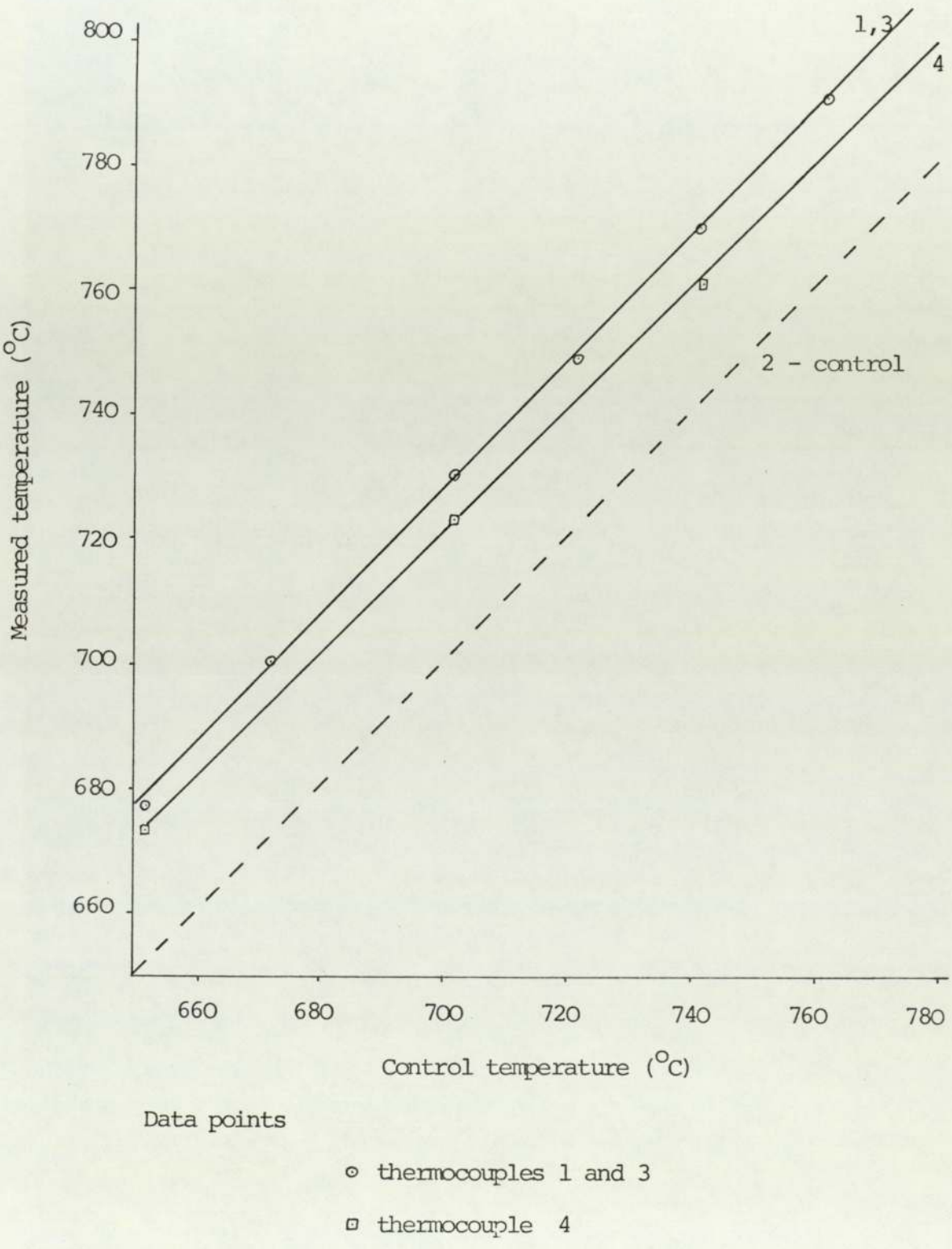

FIGURE 4.5 MEASURED TEMPERATURE PLOTTED AGAINST CONTROL TEMPERATURE (TITANIUM SPECIMEN)

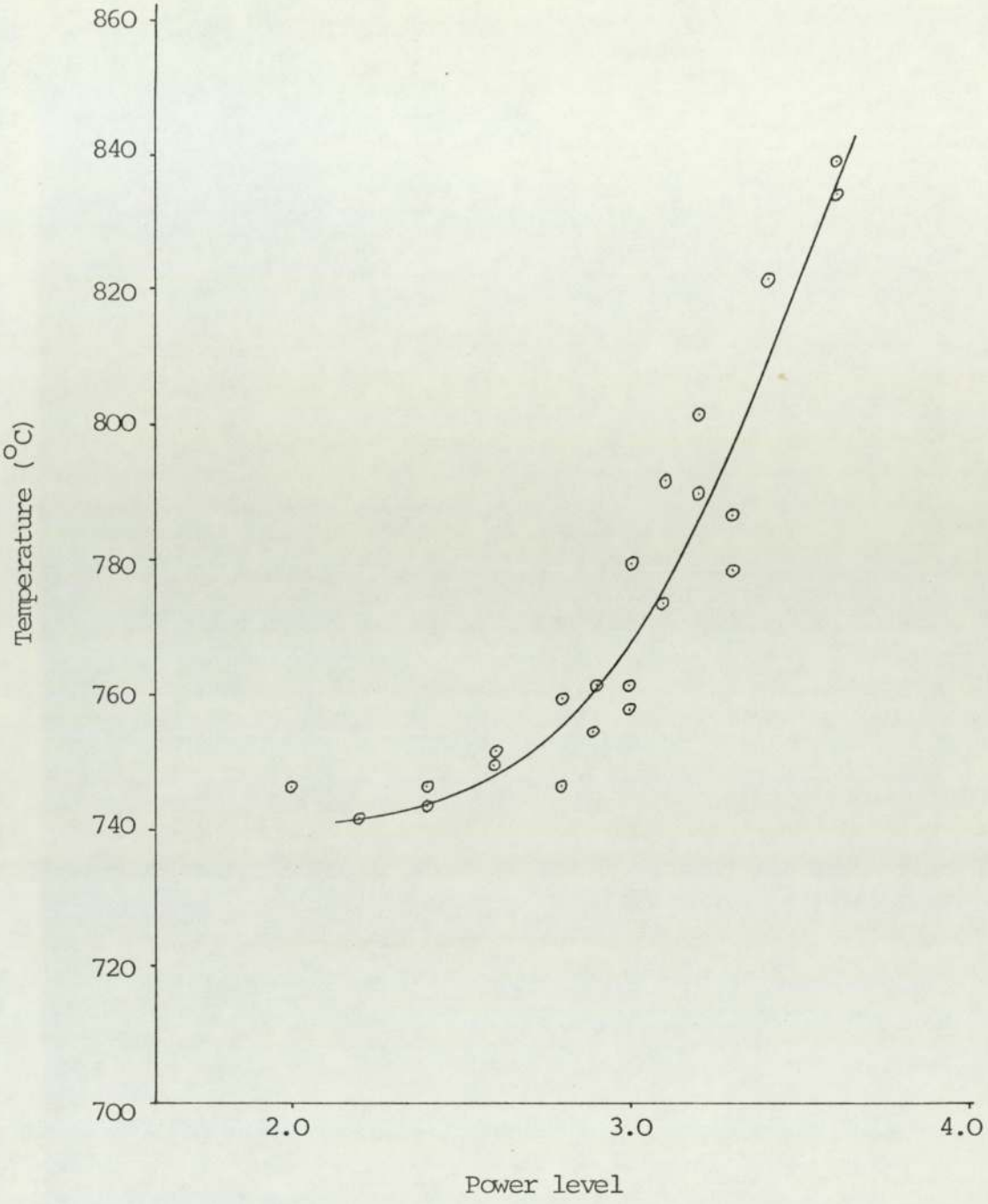

FIGURE 4.6 CALIBRATION CURVE SHOWING SPECIMEN TEMPERATURE AS A FUNCTION OF POWER

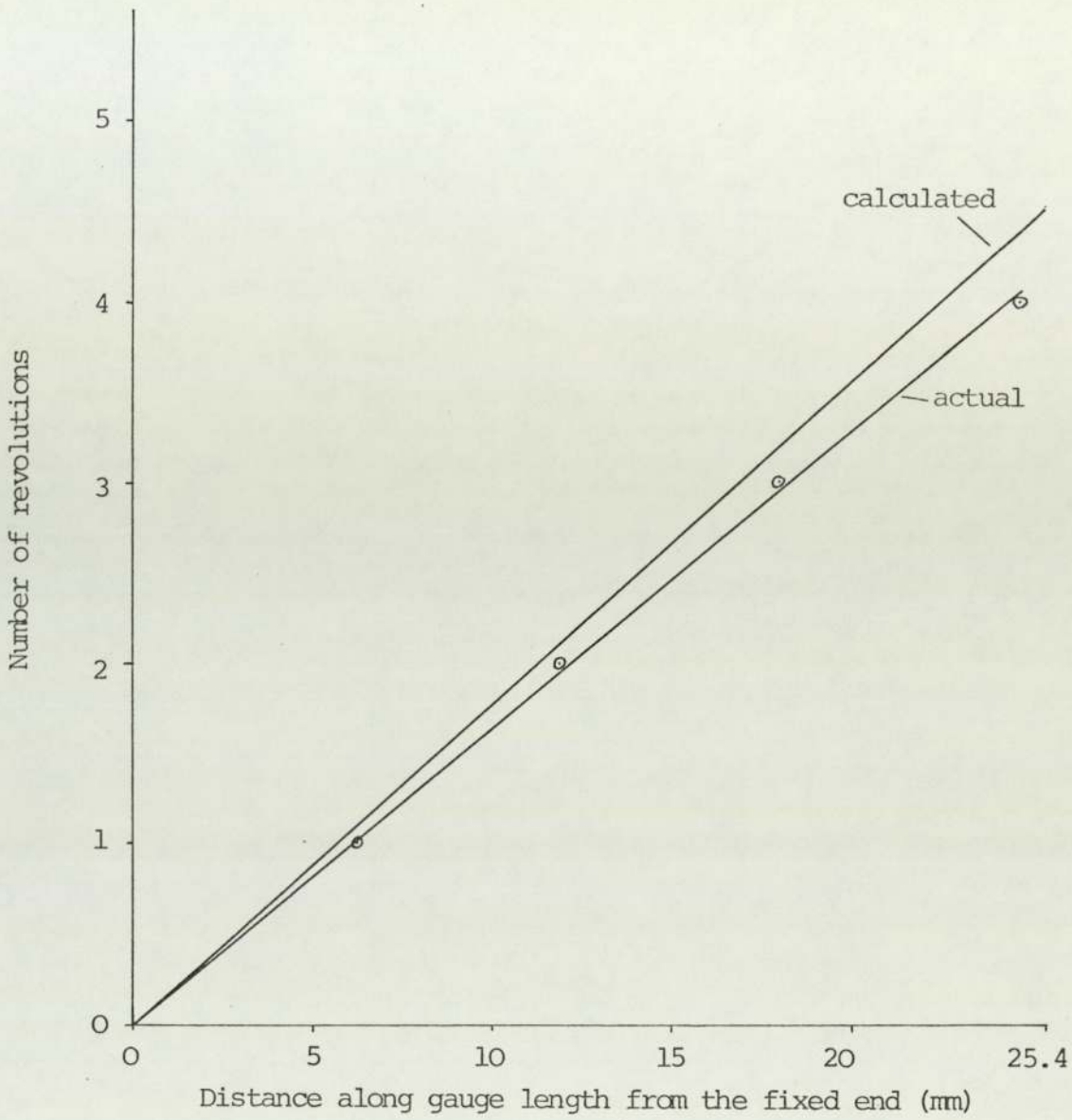

FIGURE 4.7 VARIATION IN SPECIMEN TWIST WITH DISTANCE MEASURED FROM THE FIXED END OF THE GAUGE LENGTH

5. METHODS OF ANALYSIS

5.1 TORQUE/STRAIN CURVES

The torque/strain curves were recorded on an ultra-violet light recorder as the specimens were twisted. This is only a macroscopic analysis, enabling the materials tested to be 'ranked' in order of yield stress, or categorised by the general shape of the plots obtained.

5.2 HARDNESS MEASUREMENTS

The torsion specimens were cut perpendicular to the longitudinal axis in the middle of the gauge length. The cut was made using a lubricated diamond impregnated slitting wheel. One half of the torsion specimen was screwed into a specially designed block (figure 5.1), and polished on emery paper to grade P1200. Hardness measurements were made on two orthogonal diameters using a Vickers hardness tester and a load of 2.5kg.

Care was taken to ensure that the minimum distance between the centres of adjacent indentations was greater than three times the width of the indentation measured across the diagonal. Vickers hardness tests were also carried out on a specimen that had been electro-polished to remove traces of mechanical damage, due to grinding, on the surface to be tested. Comparison with results from the same specimen without electro-polishing did not reveal any significant difference in the results.

The results were plotted against distance from the surface of the specimen. The best fit line was obtained using regression analysis.

5.3 SCANNING ELECTRON MICROSCOPY

5.3.1 Theory

The scanning electron microscope (SEM) was used to study the microstructure of the deformed torsion specimens. The microscope was used in the back scattered electron (BSE) mode rather than the normal secondary electron mode. This is a relatively new technique which significantly increases the capability of the scanning electron microscope[40].

In normal operation, the image is obtained using low energy secondary electrons. The image is enhanced by variations in surface topography that arise as a result of etching the sample.

Using back scattered electrons, there are two sources of image contrast in addition to surface topography, namely atomic number and crystal orientation. If the specimen is simply polished and not etched, then it is the variations in atomic number and crystal orientation that produce the contrast.

Regions of high atomic number back scatter electrons to a greater extent than those of low atomic number, and therefore appear brighter. In the case of solid solutions, the weighted mean atomic number of the phase will determine the level of contrast.

In the case of a pure metal or homogeneous alloy, the image contrast is only influenced by the orientation of the crystal with respect to the incident beam. In this way grains with a uniform orientation will have uniform contrast while distorted

grains will exhibit variations in contrast within the grain. This particular aspect of back scatter electron imaging was used to study the development of sub-grains and distortion resulting from warm working of the materials. Orientation of channelling contrast can also be used to determine the orientation of individual crystals. It is possible to operate the microscope in such a way that the beam remains fixed on one crystal in the specimen while using the scanning mechanism to vary the angle of incidence. The pattern of lines produced, known as a selected area channelling pattern, can be used to accurately determine the orientation of the crystal.

5.3.2 Specimen Preparation

It is essential to remove all traces of mechanical deformation due to mechanical polishing before the specimen can be examined using the BSE imaging technique. The specimen to be examined was therefore first electro polished in Morris's reagent. The composition of this reagent is given in table 5.2. A fresh solution is required, since the valency state of the chromium ions will change with time, rendering the solution ineffective. This is a slow polishing solution which was found to give a very highly polished surface. The specimens were polished for about 20 minutes using a voltage of 22V DC. On removing the specimen from the solution, it was immediately washed in water to prevent staining of the polished surface. The polishing solution was used at room temperature and was cooled using a water cooled coil.

Before inserting the specimen in the microscope, it was marked using a micro-hardness indentor, so that it could be aligned in the electron microscope to traverse across a known diameter.

5.4 TENSILE TESTING

The final thickness after warm rolling, of the rolled material was approximately 1mm. (The exact value for each specimen was measured with a micrometer). Simple parallel sided strips were machined from each sample with a gauge length of 100mm marked on each. The samples were tested on an Instron machine at a strain rate of 0.5mm/min.

TABLE 5.1 COMPOSITION AND USE OF MORRIS'S REAGENT

Composition

50g CrO_3

100ml glacial acetic acid

10ml distilled water

The solution requires stirring for 1-2 hours in order to dissolve the chromium trioxide.

The solution should be used fresh. The effectiveness of this solution deteriorates with time as the valence state of the chromium ions changes.

The solution should be used at room temperature with a potential of 22V DC between the anode (specimen) and the cathode (stainless steel container).

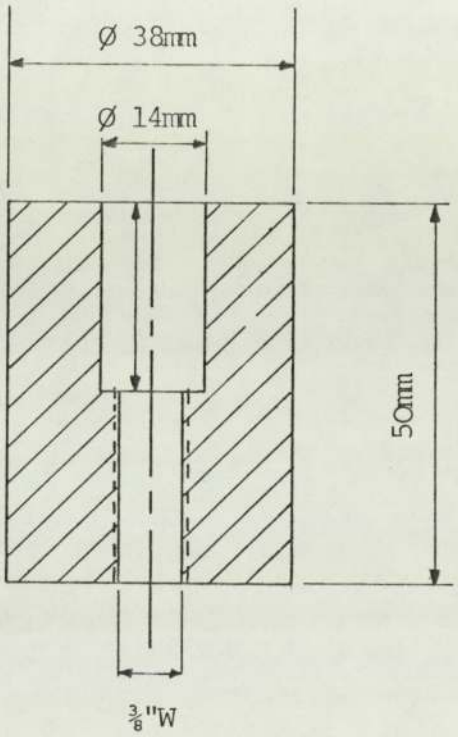

FIGURE 5.1 SECTION THROUGH HOLDER USED TO POLISH TORSION SPECIMEN

6. RESULTS

6.1 INITIAL CONDITION OF THE THREE STEELS

Before warm deformation, the steels were heat treated in a vacuum furnace for 30 minutes at 960°C, and furnace cooled to room temperature. The grain size for the three steels after this heat treatment were:

C-Mn	26μm
C-Mn-V	15μm
C-Mn-Nb	16μm

Some initial experiments were carried out to assess the hardenability of the steels used in later work. Using the torsion equipment, specimens were heated to 740°C or 780°C and after holding for 15 minutes were sprayed with water. The specimens were cut in the middle of the gauge length. A Vickers hardness traverse using a 2.5kg load was made on two orthogonal diameters.

The results for the C-Mn and C-Mn-V steels are shown in figures 6.1 and 6.2. They show little hardenability effect for the vanadium steel, but some hardenability effect for the plain carbon-manganese steel. The scatter in results is considerable, due to the fact that macro-hardness indentation will not distinguish between martensite and ferrite.

6.2 MEASUREMENT OF THE TRANSFORMATION TEMPERATURES

The A_1 and A_3 transformation temperatures were measured using a differential thermal expansion technique . The steel was heated

through the temperature range 650 - 850°C at a rate of 1°C/minute and cooled through the same range at the same rate. The results plotted as a change in length against temperature are shown in figure 6.3 for the vanadium steel. The results for this steel are typical of the three steels used. The A_1 and A_3 temperatures are tabulated below for heating and cooling:

$$\left.\begin{aligned} Ar_1 &= 725^{\circ}C \\ Ar_3 &= 771^{\circ}C \end{aligned}\right\} \text{cooling}$$

$$\left.\begin{aligned} Ac_1 &= 759^{\circ}C \\ Ac_3 &= 845^{\circ}C \end{aligned}\right\} \text{heating}$$

6.3 TORQUE CURVES

The torsion curves are shown in figure 6.4 for deformation at 740°C, and figure 6.5 for deformation at 770°C. Each curve represents an average of several tests using the steel and temperature as indicated.

From these curves the following general comments can be made:

(i) Flow stress

The torque (Nm) at the point of yield is shown for each steel in the following table:

	740°C	770°C
C-Mn	3.18	2.13
C-Mn-V	4.63	3.15
C-Mn-Nb	4.33	2.71

(ii) General shape of torque curves

The general shape of the torque curves is very similar for each steel.

At 740°C the curves for all three steels are approximately parallel. The curve for the plain C-Mn steel is significantly lower than that of the other two. The peak torque is reached after approximately the same surface shear strain for all specimens.

In the case of those materials tested at 770°C, the C-Mn and C-Mn-Nb steels exhibited a much greater reduction in torsional strength after the peak stress had been reached than was noted for the C-Mn-V steel. The maximum torsional stress occurred at greater strain for the C-Mn-V steel than the other two at 770°C.

6.4 HARDNESS MEASUREMENT OF TORSION SPECIMENS

The use of hardness testing is a convenient way in which it is possible to assess variations in mechanical properties across the radius of the torsion specimens. The hardness results do not correlate precisely with mechanical properties such as yield strength and tensile strength, but they do give some indication of the trend in mechanical property with increasing strain. The results contain considerable scatter, due to the fact that the structures contain more than one constituent phase typically martensite and ferrite, or ferrite and pearlite. The extent of the scatter is illustrated by the correlation coefficients obtained from the linear regression analysis. The

correlation coefficient r^2, is in the range 0.02 - 0.72 for water sprayed specimens and 0.02 - 0.93 for air-cooled specimens.

The results of the hardness testing are summarised in figures 6.6 - 6.8 for the air cooled specimens and figures 6.9 - 6.11 for the water quenched specimens.

6.4.1 Air cooled Material

The results obtained for the plain carbon-manganese steel show some increase in hardness with increase in strain for all conditions. After a surface shear strain of 0.785 (1 revolution) there is a significant increase in hardness from approximately 130HV2.5 to 150HV2.5. After a surface shear strain of 3.142 (4 revolutions), the surface hardness is comparable with that of 1 revolution, but the centre hardness is significantly higher. Clearly, the centre of the specimen has received some strain, since the centre hardness should be independent of surface strain (at constant temperature). At 770°C, the surface hardness after 1 revolution of deformation is about 10 points higher than after 4 revolutions. The centre hardness values are approximately the same. It is also interesting to note that the strain at a depth of 2.38mm (strain rate $0.098s^{-1}$), in the specimen deformed through 4 revolutions, is equal to the surface strain in the specimens deformed 1 revolution (strain rate $0.393s^{-1}$). The data presented below shows that the strain rate in this range has little effect on hardness.

	1 revolution surface hardness (HV2.5)	4 revolutions hardness at depth of 2.38mm (HV2.5)
740°C	151	148
770°C	146	138

Data from air-cooled C-Mn-V steel specimens shows that the hardness is significantly greater than that for the plain C-Mn steel. The centre hardness in the vanadium steel is about 175HV2.5 compared with an average of 137 for the centre hardness of the plain carbon steel. The results show a significant variation in hardness with strain in the specimens deformed 4 revolutions at 740°C, but little variation at 770°C. This would suggest that a degree of recrystallisation has occurred at 770°C which was not present at 740°C.

Data for the niobium-containing steel shows hardness values again higher than those for the plain carbon manganese steel and comparable with those of the vanadium steel. The difference in hardness at the centre of the specimens deformed at 780°C indicates that the central region is strained to some extent after 4 revolutions deformation.

In the table below, hardness values at the surface of the specimen deformed by 1 revolution are compared with values for the same strain obtained from the 4 revolution specimen.

	1 revolution surface hardness (HV2.5)	4 revolutions hardness at depth of 2.38mm (HV2.5)
740°C	184	170
780°C	160	166

6.4.2 Water Sprayed Material

The hardness of the water sprayed material is significantly influenced by the martensite content. Since the micro-structure is a mixture of ferrite and martensite, there is a substantial scatter in the results as the macro-hardness measurements do not distinguish between these two phases. In all cases, the martensite content did not vary between the centre and the surface of the specimen.

Carbon-manganese Steels

There is a significant variation in the hardness between the centre and surface of most of the carbon-manganese specimens. The data presented in figure 6.9 shows a much smaller variation in hardness across the radius of the specimen for higher deformation (4 revolutions) and higher temperatures. This may be due to either recrystallisation of the ferrite phase under these conditions, or strain in the centre of the specimen raising the hardness in the centre.

Vanadium Steel

The results for the vanadium steel (figure 6.10) indicate a higher hardness for a given temperature and deformation than the carbon-manganese steel.

Niobium Steel

The hardness results plotted in figure 6.11 show that for a given temperature, the hardness of the steel is greater than that found in the vanadium steel. There is only a very small variation in hardness with increasing deformation at a given temperature.

6.5 SCANNING ELECTRON MICROSCOPE

6.5.1 General Observations

The structure of the warm worked steels were examined using the Scanning Electron Microscope in the Back Scattered Electron mode (BSE). The contrast in this case is 'channelling contrast' due to crystal orientation. Before describing in detail the microstructures observed, it is useful to make some general comments on the structures that can be seen using channelling contrast.

In the microstructures observed, martensite and ferrite or pearlite and ferrite can be seen depending on whether the steel was water sprayed or air-cooled to room temperature.

Martensite

Using the BSE mode, martensitic structures are often difficult to distinguish. This is likely to be due to the variation in orientation of the martensitic needles to the surface being observed. In some cases however, the needle structure of martensite has been observed and is shown in photomicrograph 6.1. A prior austenite grain growing into the ferrite can also be seen in the bottom left hand corner of photomicrograph 6.1a. Some prior austenite grain boundaries are also visible, although they are difficult to distinguish (photomicrograph 6.1b).

Pearlite

The detailed microstructure in the pearlitic regions of the structure cannot be readily distinguished using the Scanning Electron Microscope in the BSE mode. Some examples of the lamellar carbide structure typical of pearlite can be seen occasionally, and examples are shown in photomicrograph 6.2.

Ferrite

Ferrite is the phase about which most information can be observed using the BSE mode. Using channelling contrast, variations in crystal orientation within individual grains can be clearly seen, as can the development of a sub-grain structure as the shear strain is increased.

In the centre of the torsion specimens, the structure is only slightly deformed. Large grains of ferrite can be seen with uniform or almost uniform contrast (Photomicrograph 6.3). The photomicrographs also show a Widmanstatten ferrite in the ferrite structure of the carbon-manganese steel heated to 740^{o}C. This was not apparent in the other steels tested, or in the carbon-manganese steel heated to 755^{o}C.

The effect of deformation on the structure of the ferrite will be considered in the following section, when the effect of warm deformation is considered in detail.

Precipitation

The only evidence for precipitation that could be seen using the SEM was found in the niobium steel at the ferrite grain boundaries (Photomicrograph 6.4). The precipitates are typically 0.1 - 0.2μm in size.

6.5.2 Ferrite Grain Size and Structure

The principal use of the SEM in the back-scattered electron mode was to investigate the development of subgrain structures in the ferrite phase. From the photomicrographs, estimates of the sub-grain size were obtained.

Carbon-manganese Steel

Results for the carbon-manganese steel were obtained for the following three combinations of temperature and deformation:-

740°C, 1 revolution deformation - air-cooled and water sprayed
740°C, 4 revolutions deformation - air-cooled and water sprayed
755°C, 1 revolution deformation - water sprayed

The variation in ferrite grain size with distance from the surface of the specimen is plotted in figures 6.12 - 6.14. In the case for the specimen deformed at 740°C, both air-cooled and water sprayed results were available, and are plotted on the same graph. In general, it is clear that the grain size is independent of the cooling rate, although the results for the water sprayed material after 1 revolution of deformation are a little lower than the air-cooled results. After only 1 revolution of deformation the grain size at any one position varies considerably, giving a large scatter in the results. After 4 revolutions of deformation at 740°C, the limiting sub-grain size has been achieved and there is little scatter in the results.

The measured grain sizes are summarised in the table below:

	Surface Grain Size (μm)	Centre Grain Size (μm)
740°C, 1 revolution	5.5	22
740°C, 4 revolutions	4.7	25
755°C, 1 revolution	3.3	24

In addition to the above figures, it is also of interest to note that the sub-grain size measured at a depth of 2.38mm from the surface on the specimen deformed through 4 revolutions is 7.5μm. This position has the same strain as the surface of the specimen deformed by 1 revolution where the sub-grain size is 5.5μm.

At 755°C, the result shows that the sub-grain size at the surface is significantly lower than the comparable value obtained at 740°C, indicating that the limiting grain size decreases as the temperature increases.

The microstructures obtained are shown in photomicrographs 6.5 - 6.9.

Carbon-Manganese-Vanadium Steel

Results for this steel were obtained from the following three combinations of temperature and deformation:

740°C, 1 revolution deformation - water sprayed
740°C, 4 revolutions deformation - air-cooled and water sprayed
755°C, 4 revolutions deformation - water sprayed

The variation in ferrite grain size with distance from the surface of the specimen is plotted in figures 6.15 - 6.17. Where data from the two cooling rates is available, these are plotted on the same graph. The results are summarised in the following table:

	Surface Grain Size (μm)	Centre Grain Size (μm)
740°C, 1 revolution	3.5	24
740°C, 4 revolutions	4.2	9.5
755°C, 4 revolutions	2.6	11

The results show a similar trend to those for the base steel except that the grain size in the centre of the specimens deformed by 4 revolutions is significantly lower than that found in the comparable plain carbon-manganese steels. It is quite likely that the centre of these specimens is subject to a small strain after 4 revolutions, and this must be sufficient to cause some sub-grains to develop in the structure. Comparing the specimens deformed at 740°C, it was noted that the grain size at the surface of the specimen is lower in the case of the vanadium containing steel. It was noted that the grain size after deformation at 755°C was smaller than that found after deformation at 740°C (compare figure 6.17 with figure 6.16). The effect of strain rate on grain size can again be compared by comparing the following points of equal strain:

(i) the grain size at the surface of the specimen deformed by 1 revolution (3.5μm)

(ii) the grain size at a depth of 2.38mm in the specimen deformed by 4 revolutions (7μm)

As with the plain carbon-manganese steel, the results show that the grain size is strain rate dependent. The strain rates in the two cases considered are respectively $0.393s^{-1}$ and $0.098s^{-1}$.

The structure as seen in the SEM is shown in photomicrographs 6.10 - 6.12.

Carbon-manganese-Niobium

Results for the niobium steel were obtained for deformations of 1 and 4 revolutions at 740°C, and two cooling rates (air-cooled and water sprayed.) The variation in ferrite grain size with distance along the specimen radius is shown in figures 6.18 and 6.19.

For each deformation, the data from the air-cooled and water sprayed specimens are plotted in the same graph. The grain sizes observed are briefly summarised in the following table:

	Surface Grain Size (μm)	Centre Grain Size (μm)
740°C, 1 revolution	6.3	23
740°C, 4 revolutions	3.2	8.5

After deformation of 1 revolution, the graph (figure 6.18) shows a very similar trend to that seen in the base and vanadium steels i.e. a significant decrease in grain size is observed between the centre and the surface of the specimen. The results obtained after 4 revolutions of deformation (figure 6.19) are very similar

to those for the vanadium steel, with some sub-grains formed near the centre of the specimen. The results also show that for a constant strain rate, the grain size decreases as the strain increases (compare surface grain size after 1 and 4 revolutions).

The effect of strain rate can be seen by comparing the following data points, for a strain of 0.785:

(i) the sub-grain size at the surface of the specimen deformed by 1 revolution (6.3μm)

(ii) the sub-grain size at a dpeth of 2.38mm in the specimen deformed by 4 revolutions (6.2μm)

Clearly a strain rate in the range 0.098 to 0.393s^{-1} has no effect on the sub-grain size after a strain of 0.785.

The structure of the niobium steel is shown in photomicrographs 6.13 - 6.16.

6.6 TENSILE TESTING

The 0.5% proof stress for each steel is plotted in figures 6.20 - 6.22 for the warm rolled and air-cooled materials and figures 6.23 - 6.25 for the warm rolled and water quenched materials.

The results for the air-cooled specimens show that the rolling temperature has little effect on the strength. As the percentage reduction by warm rolling increases, the proof stress increases. This is particularly noticeable in the case of the niobium steel.

The results for the water quenched specimens are heavily dependent on the martensite content, and hence the significant variation in proof stress with rolling temperature.

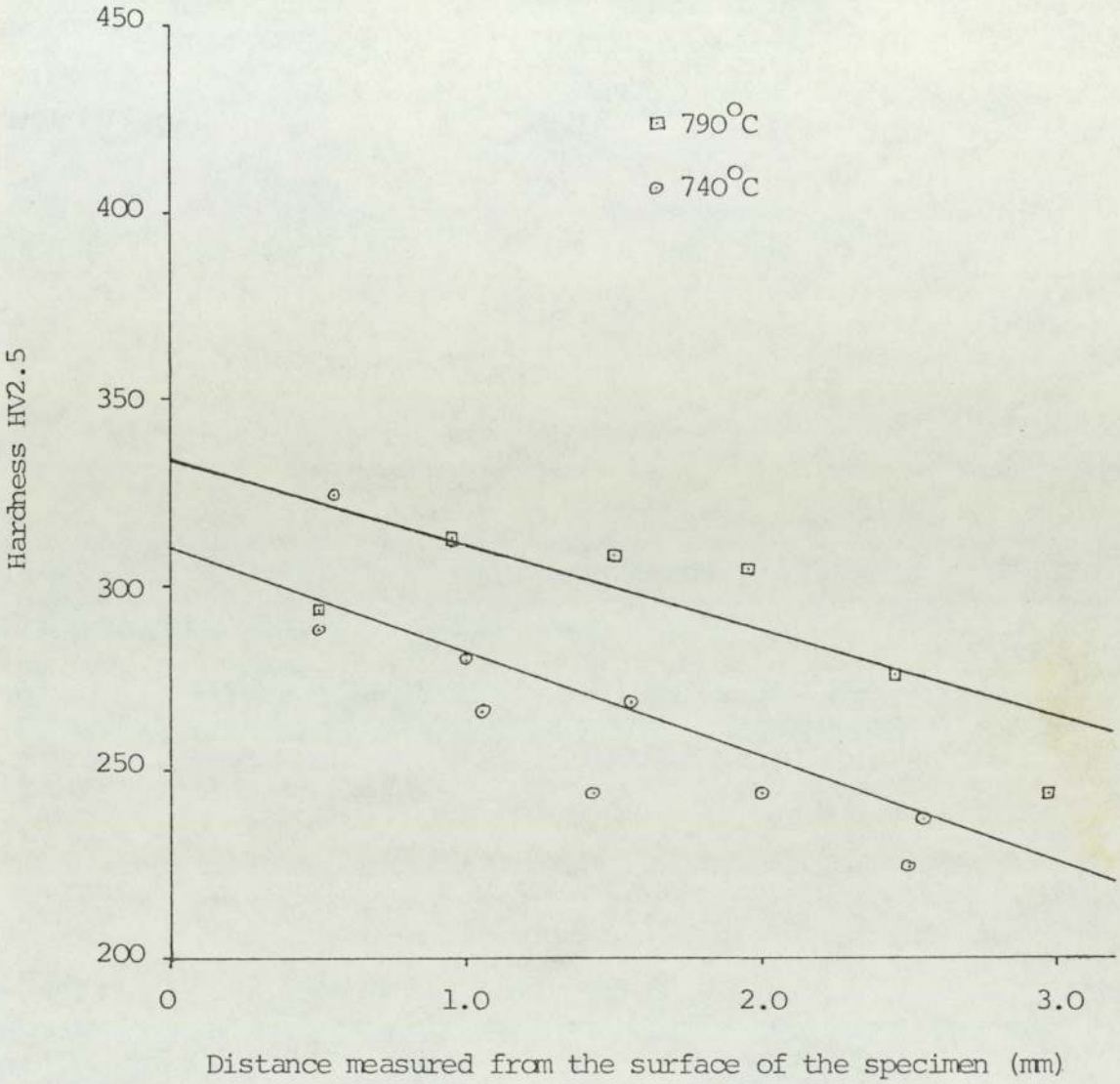

FIGURE 6.1 HARDNESS MEASUREMENTS ON TORSION SPECIMENS HEATED TO THE TEMPERATURE INDICATED WITHOUT DEFORMATION AND WATER SPRAYED. C-Mn STEEL

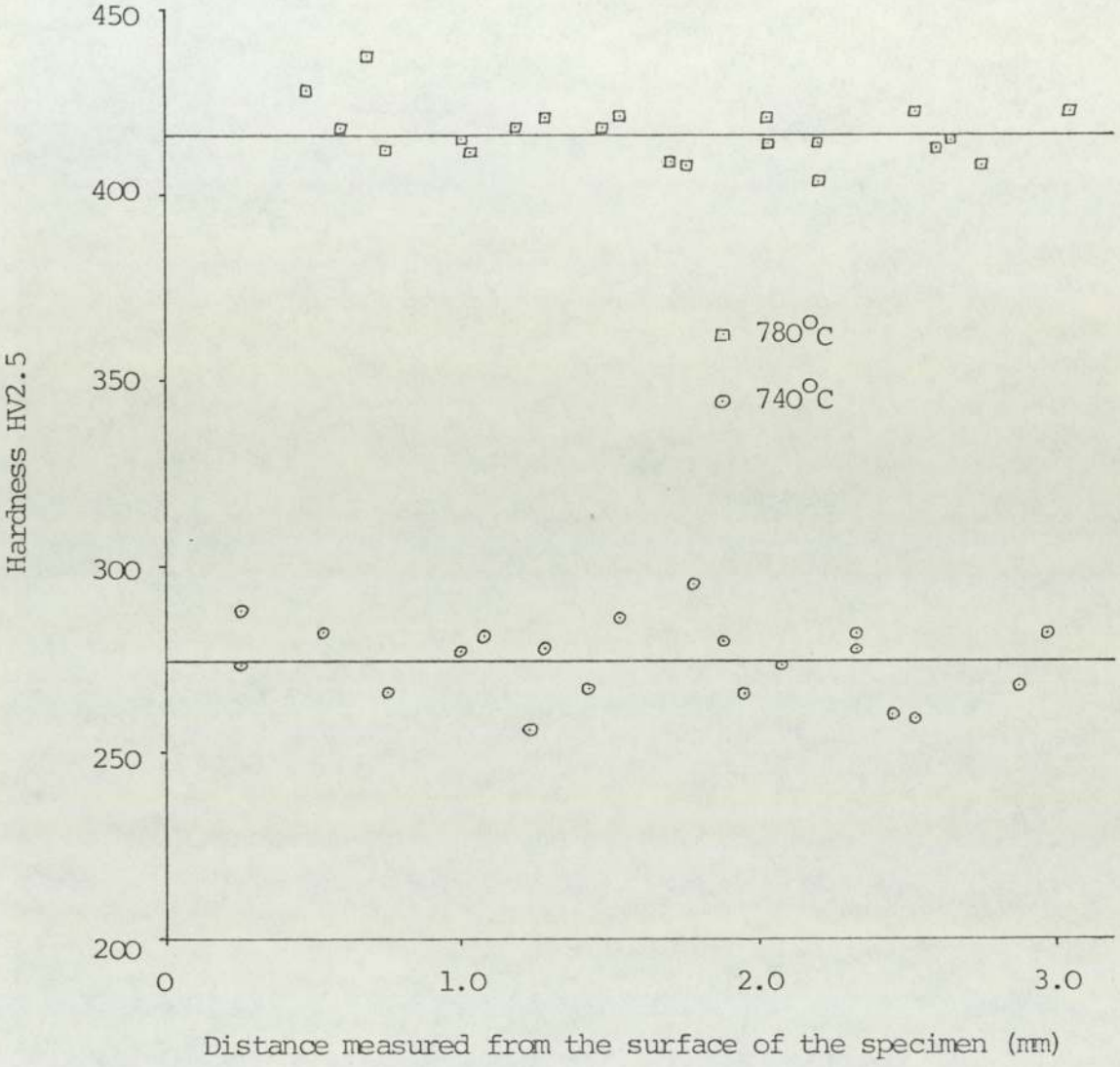

FIGURE 6.2 HARDNESS MEASUREMENT ON TORSION SPECIMEN HEATED TO THE TEMPERATURE INDICATED, WITHOUT DEFORMATION AND WATER SPRAYED. C-Mn-V STEEL

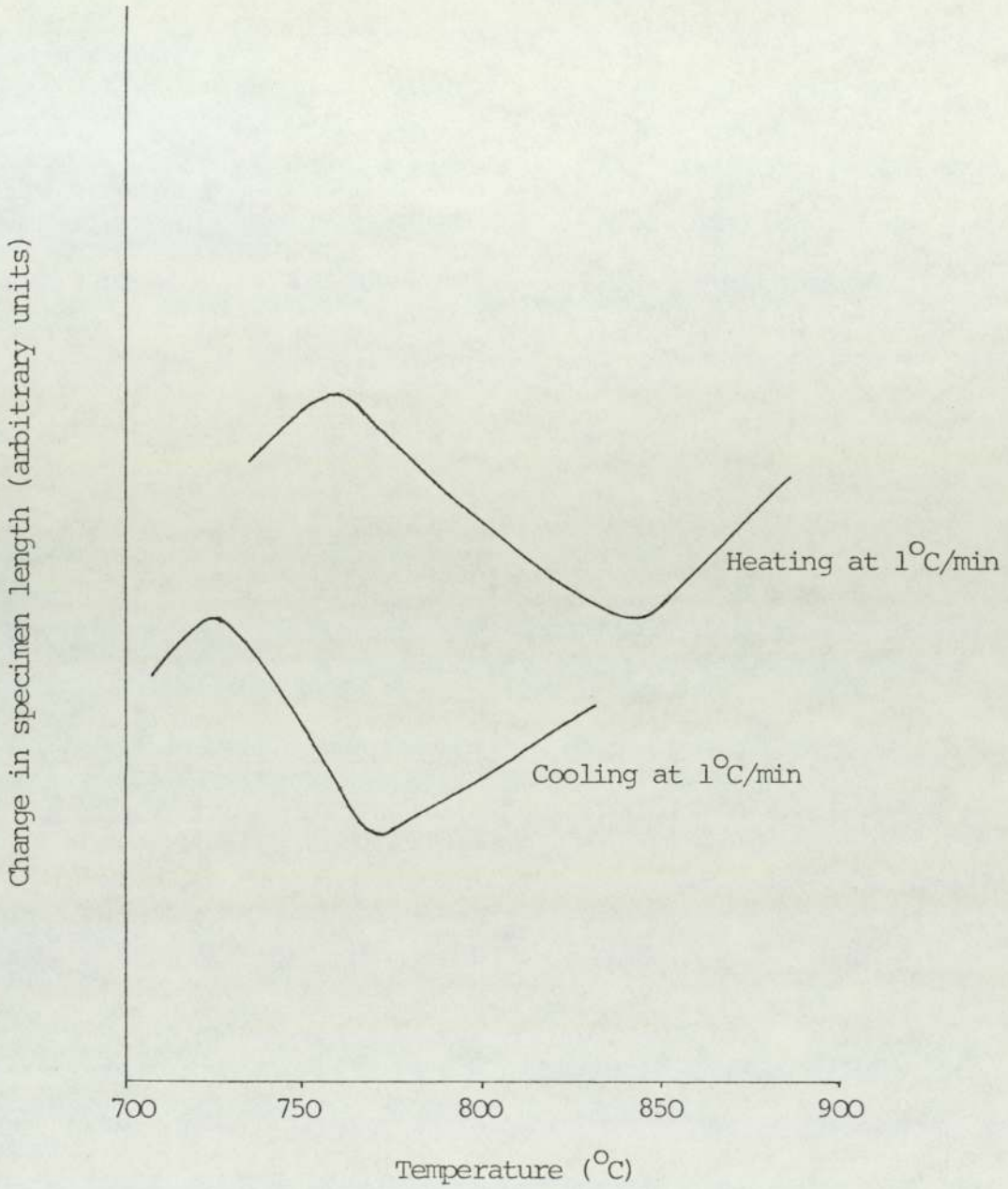

FIGURE 6.3 THE CHANGE IN SPECIMEN LENGTH AS A FUNCTION OF TEMPERATURE

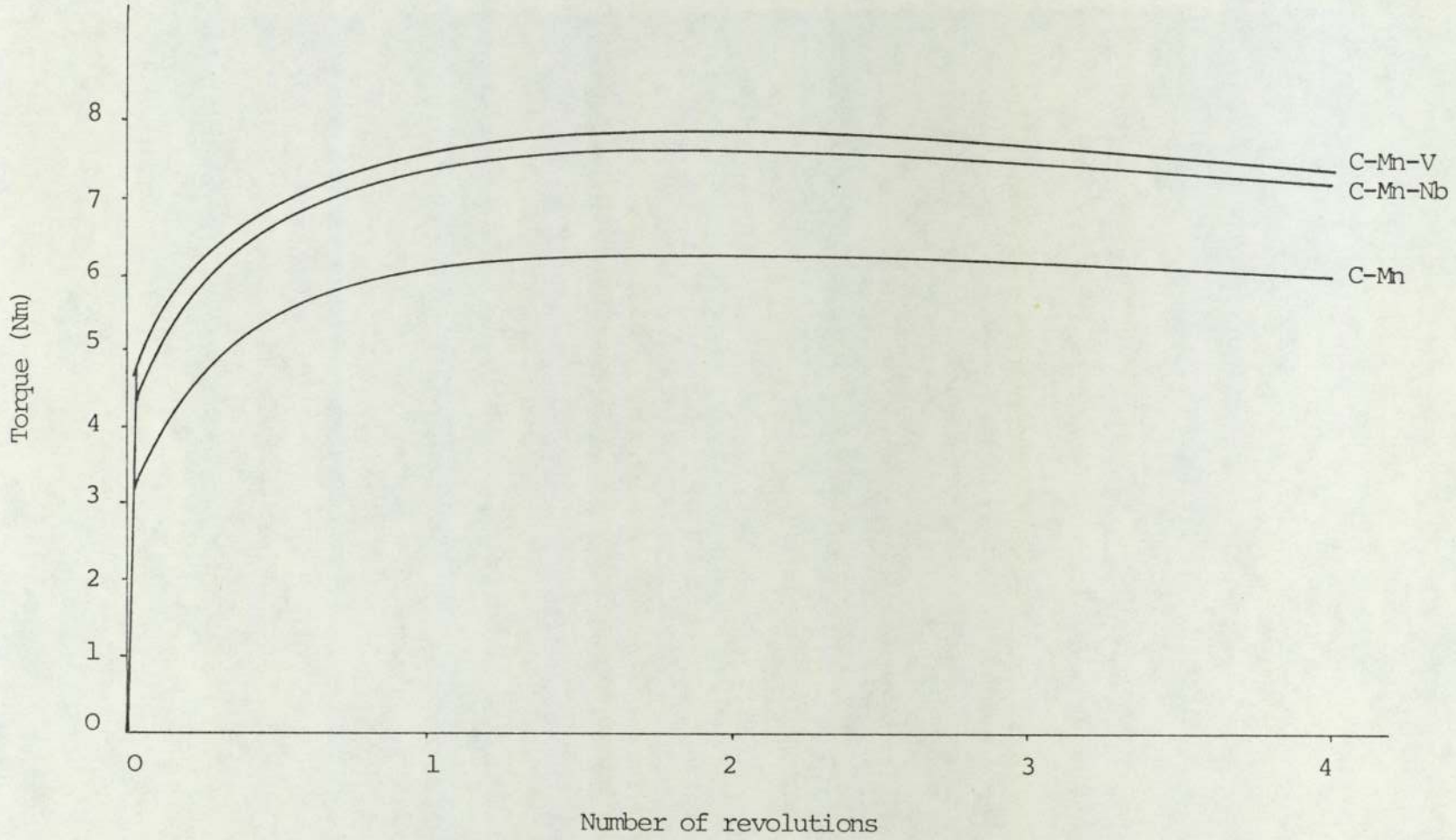

FIGURE 6.4 TORSIONAL DEFORMATION AT 740°C

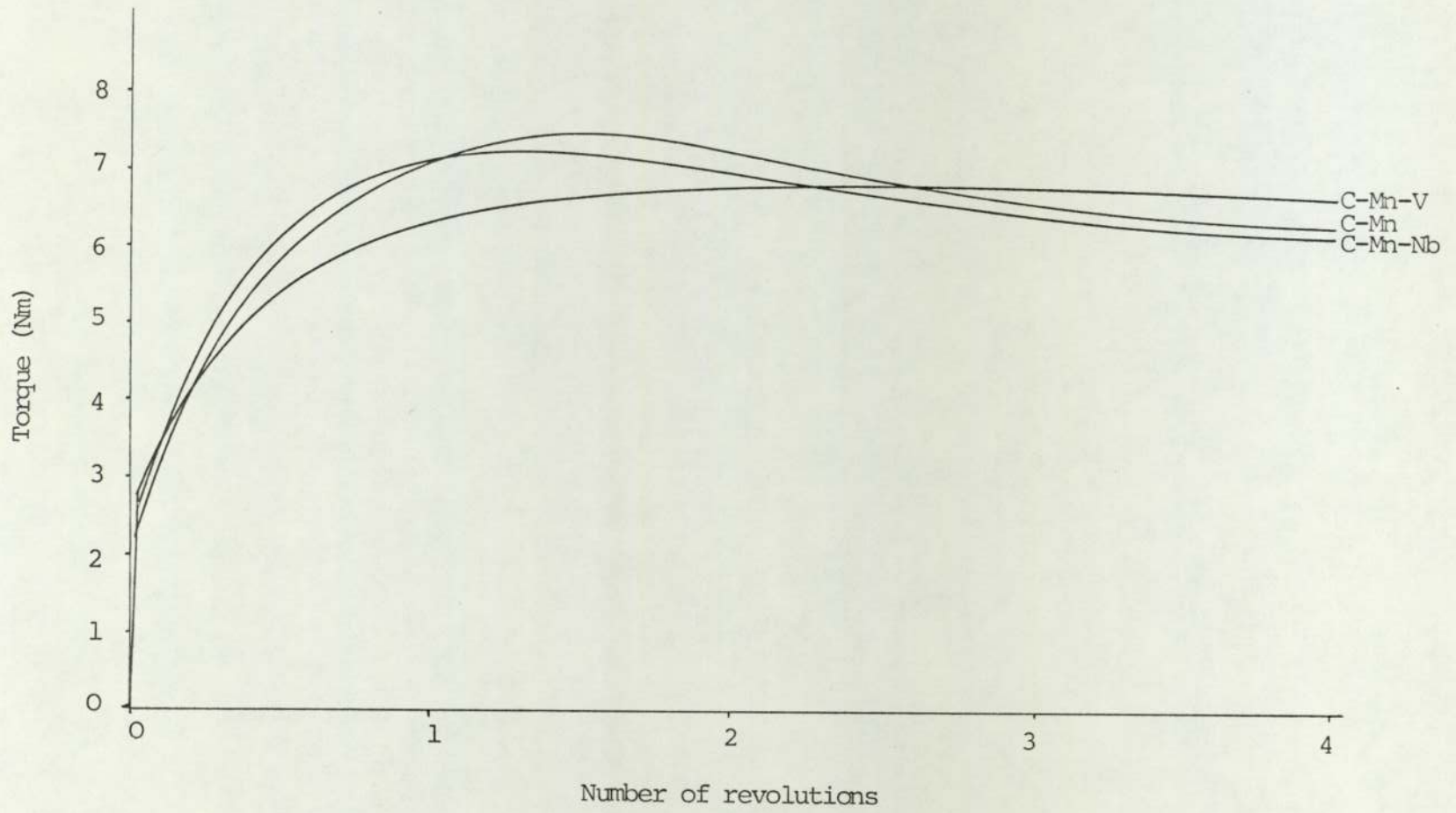

FIGURE 6.5 TORSIONAL DEFORMATION AT 770°C

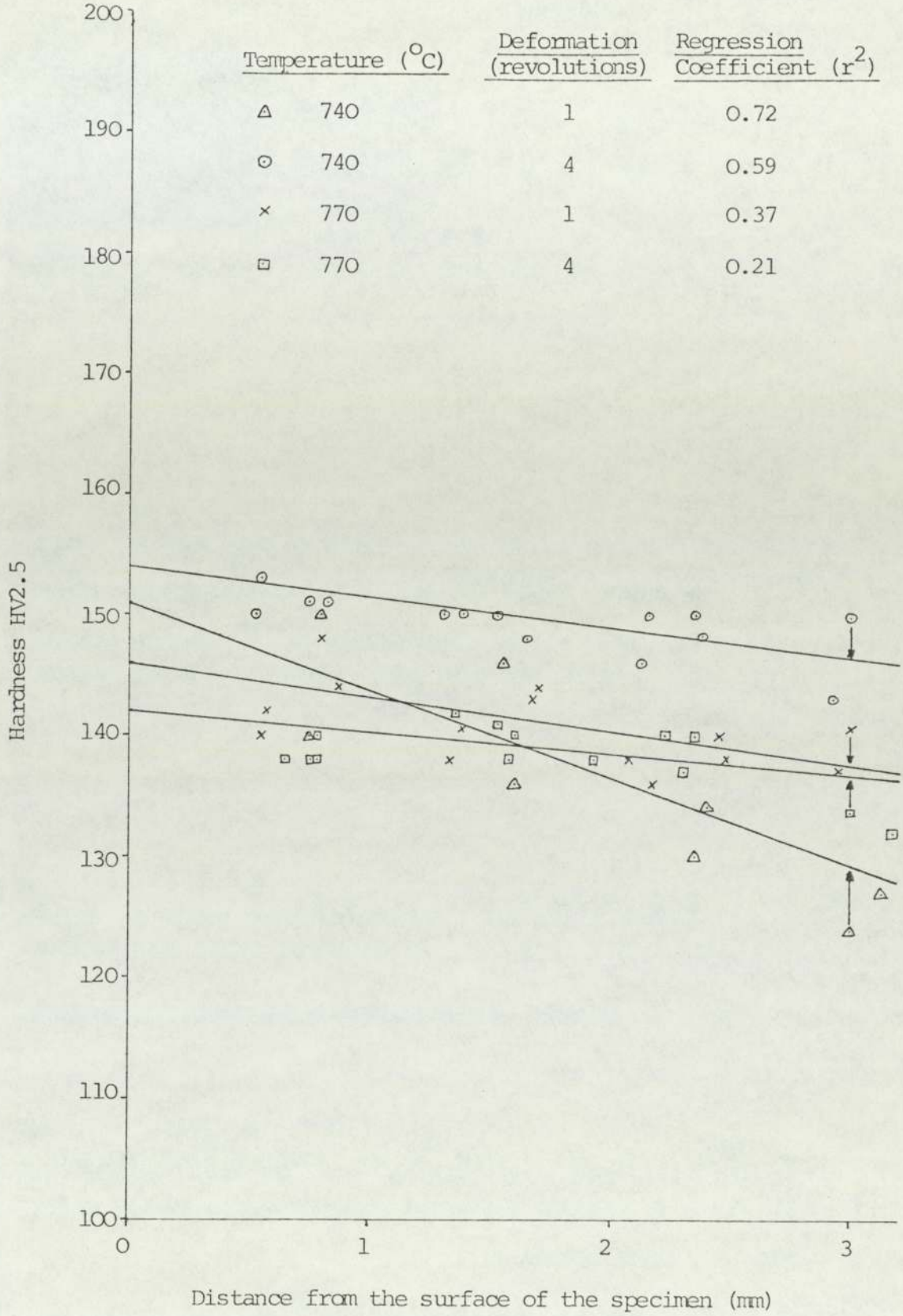

FIGURE 6.6 HARDNESS DATA FOR THE C-Mn STEEL - AIR-COOLED

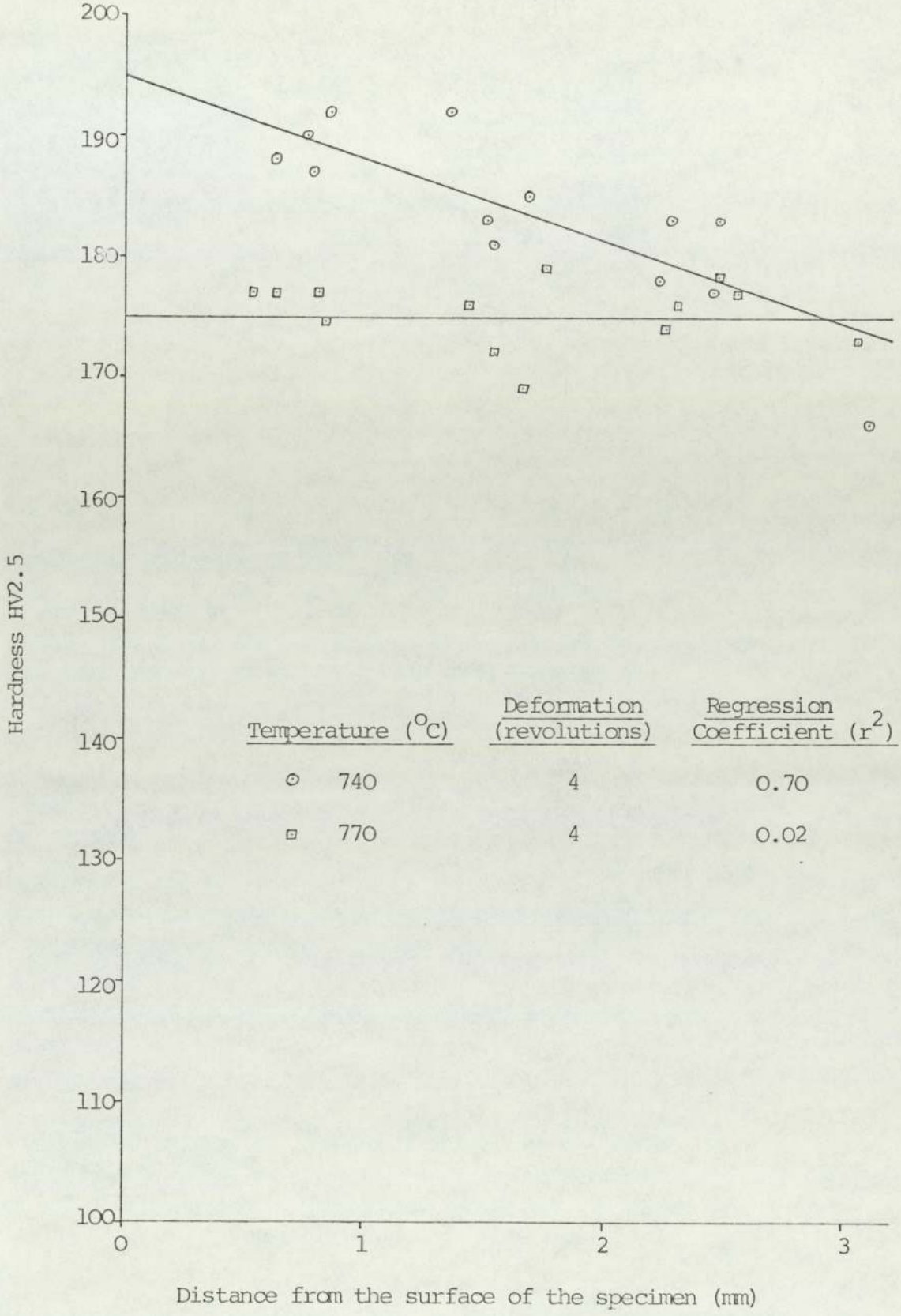

FIGURE 6.7 HARDNESS DATA FOR THE C-Mn-V STEEL - AIR-COOLED

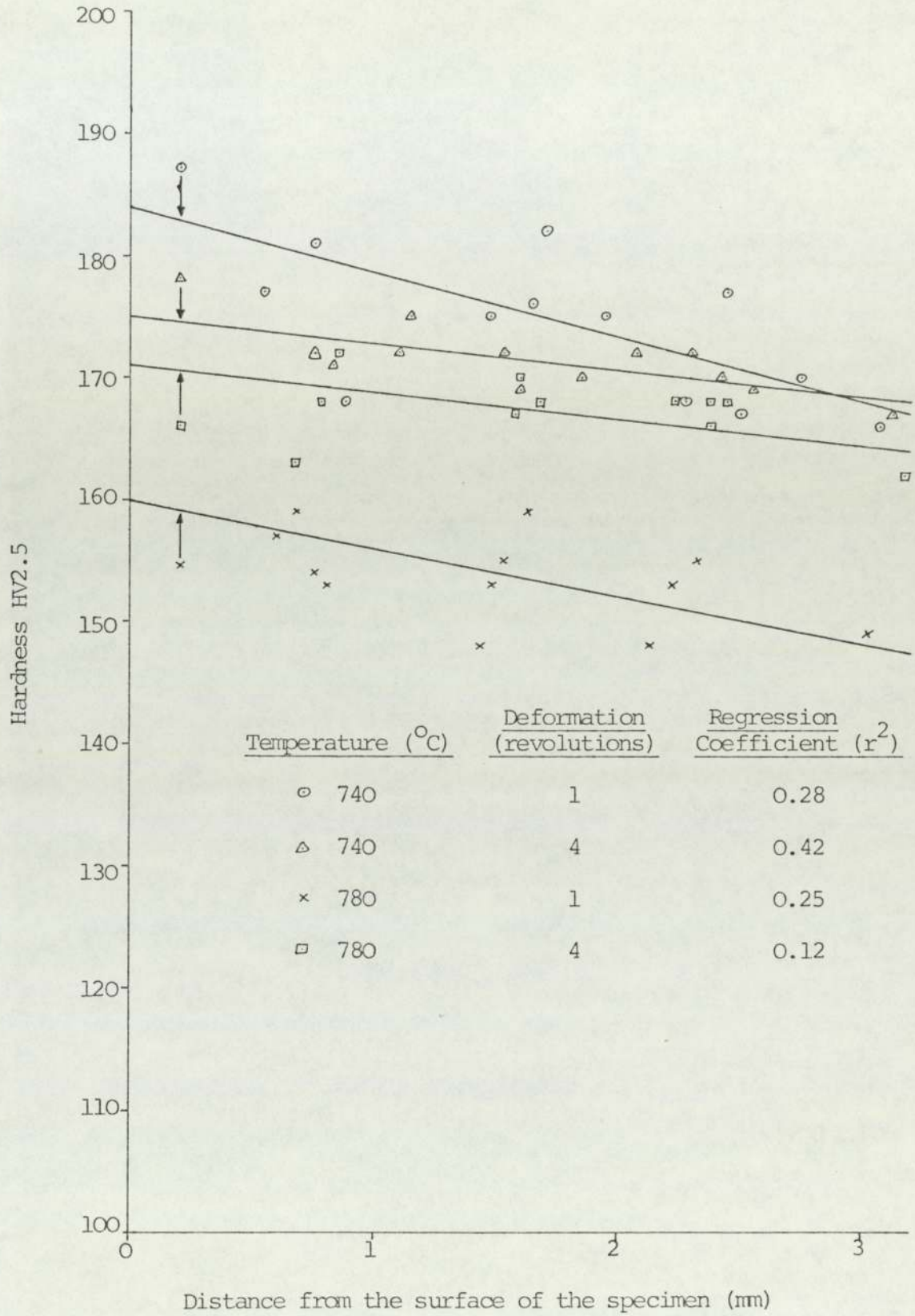

FIGURE 6.8 HARDNESS DATA FOR THE C-Mn-Nb STEEL - AIR-COOLED

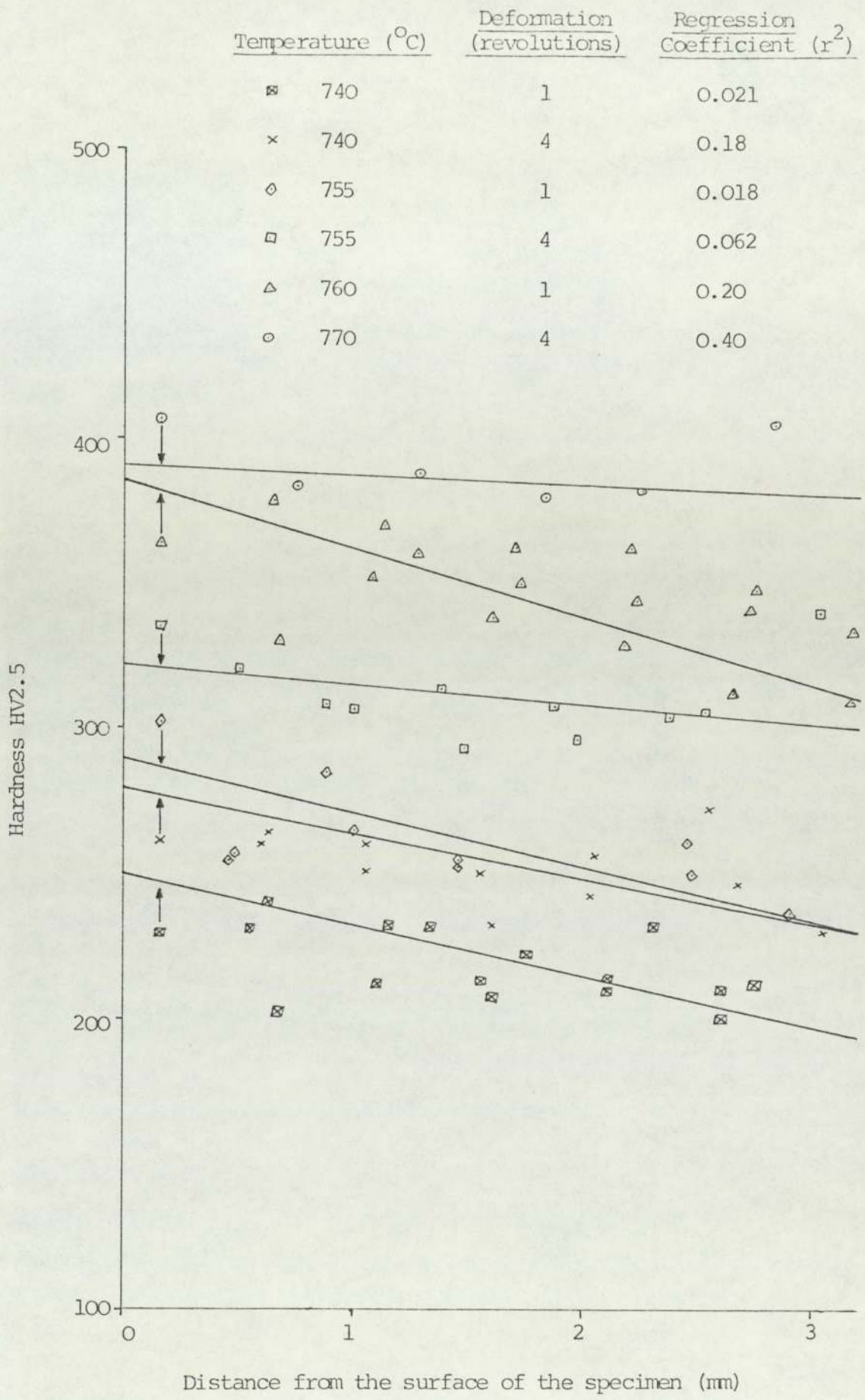

FIGURE 6.9 HARDNESS DATA FOR THE C-Mn STEEL - WATER SPRAYED

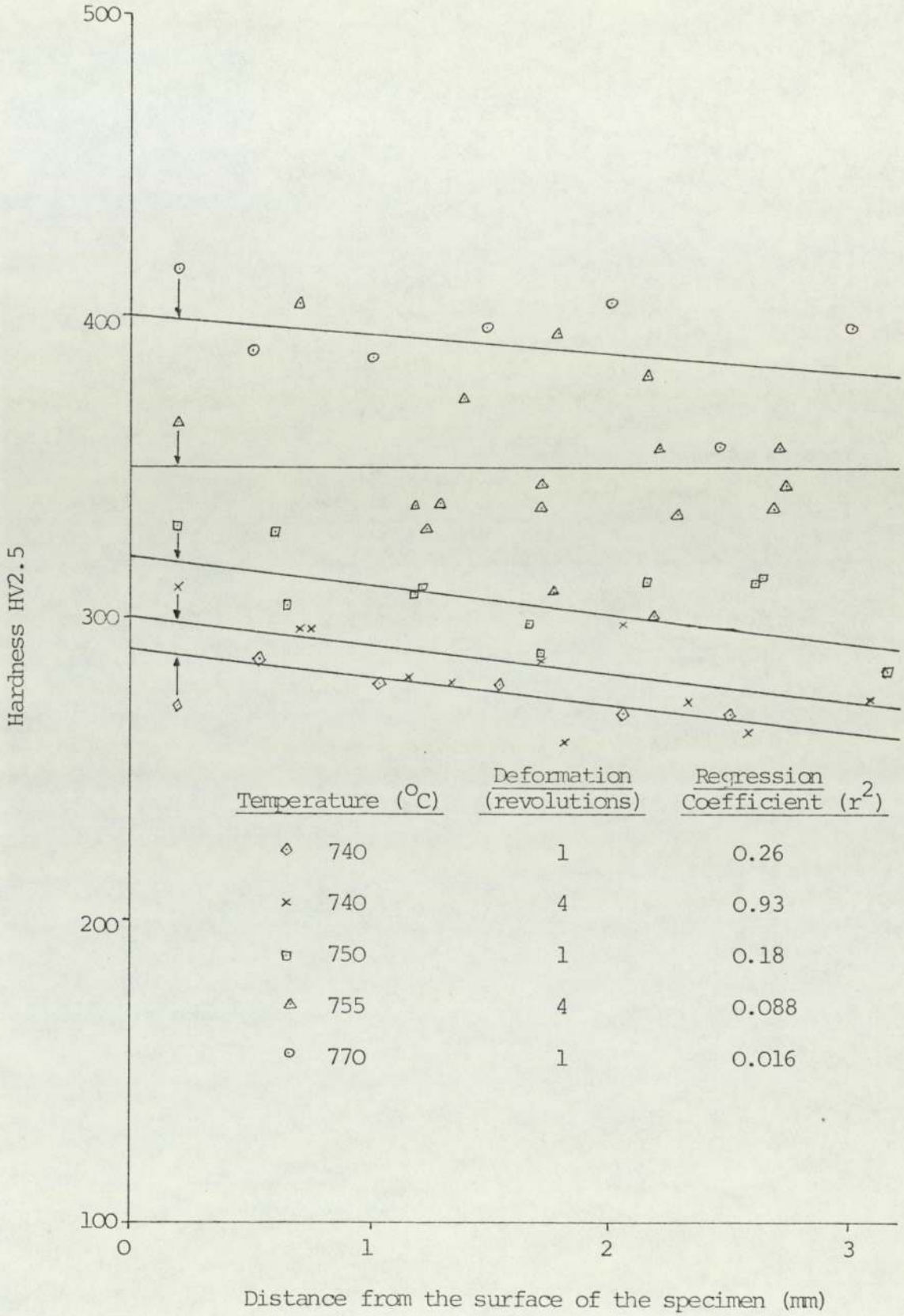

FIGURE 6.10 HARDNESS DATA FOR THE C-Mn-V STEEL - WATER SPRAYED

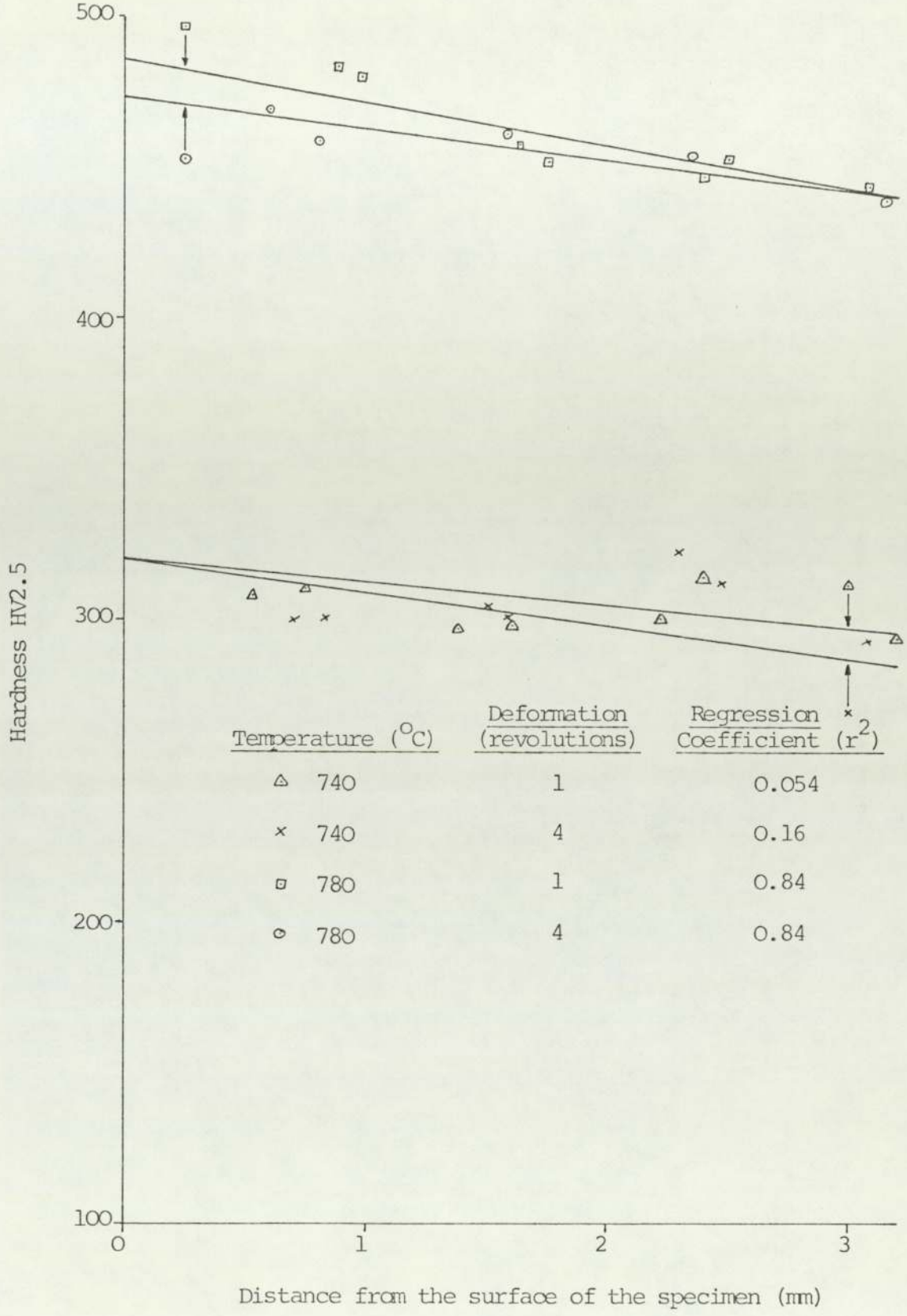

FIGURE 6.11 HARDNESS DATA FOR THE C-Mn-Nb STEEL - WATER SPRAYED

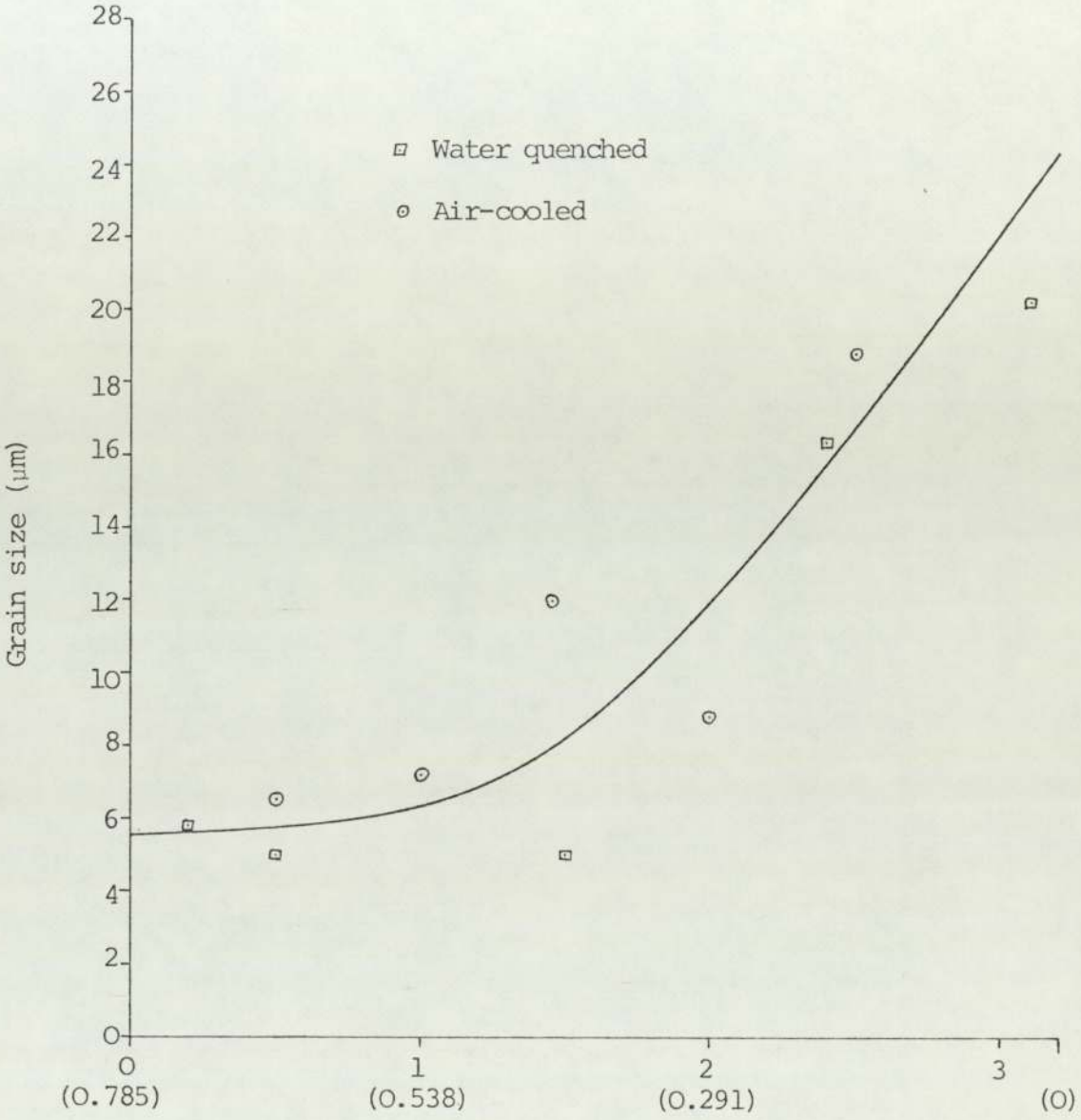

FIGURE 6.12 VARIATION OF GRAIN SIZE WITH STRAIN

C-Mn STEEL DEFORMED 1 REVOLUTION AT 740°C

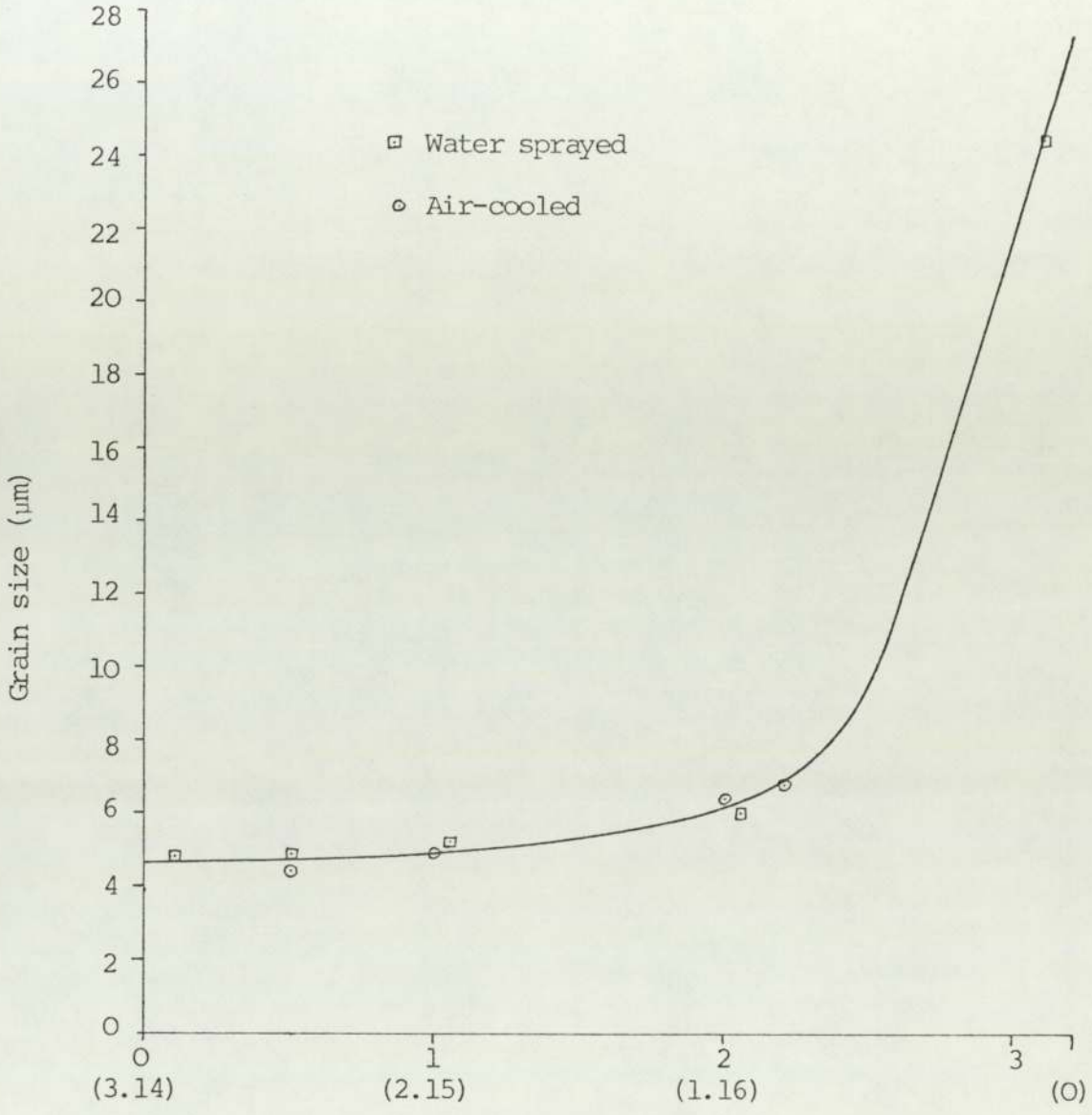

FIGURE 6.13 VARIATION OF GRAIN SIZE WITH STRAIN

C-Mn STEEL DEFORMED 4 REVOLUTIONS AT 740°C

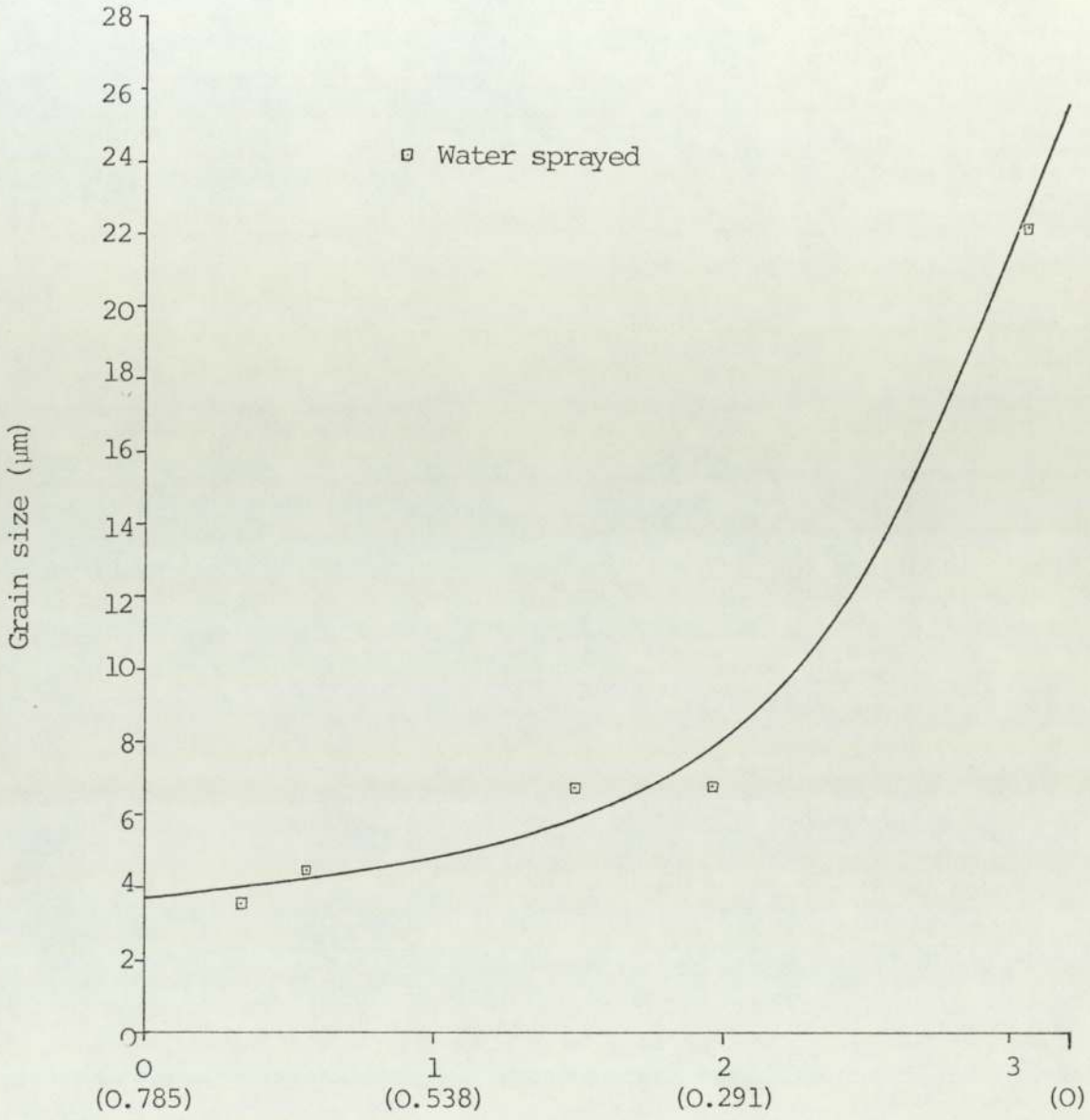

FIGURE 6.14 VARIATION OF GRAIN SIZE WITH STRAIN

C-Mn STEEL DEFORMED 1 REVOLUTION AT 755°C

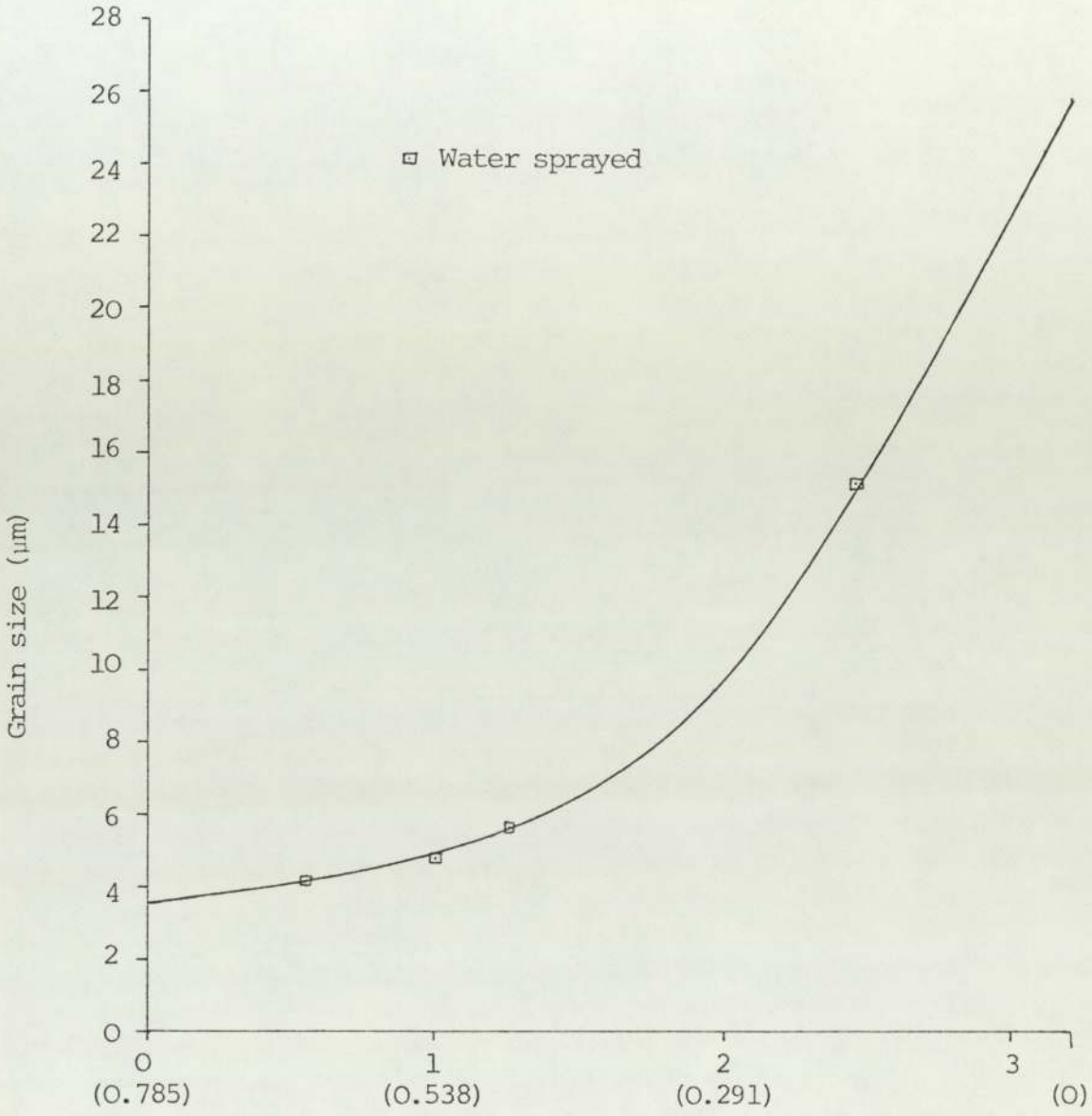

FIGURE 6.15 VARIATION IN GRAIN SIZE WITH STRAIN

C-Mn-V STEEL DEFORMED BY 1 REVOLUTION AT 740°C

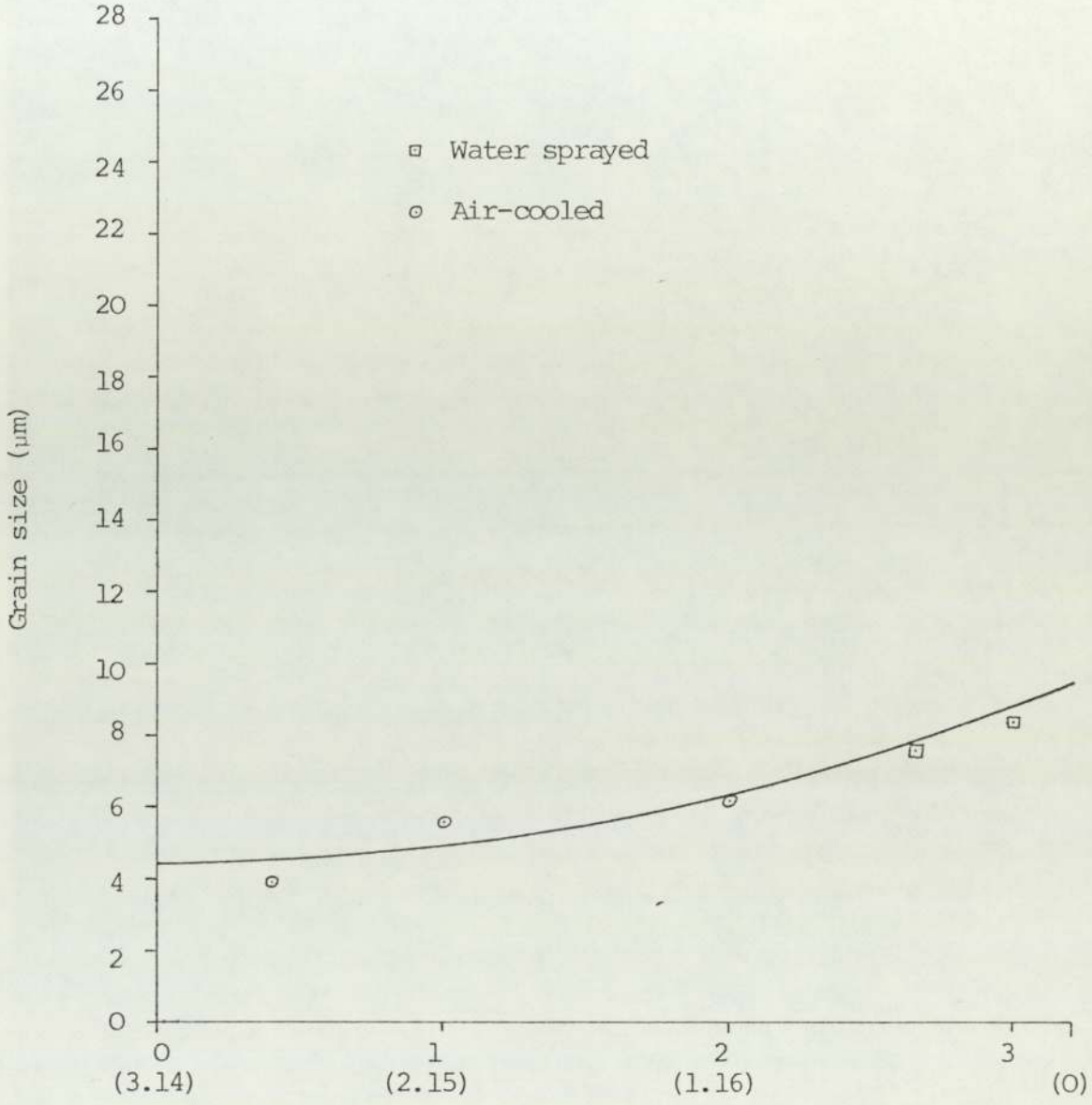

FIGURE 6.16 VARIATION IN GRAIN SIZE WITH STRAIN

C-Mn-V STEEL DEFORMED BY 4 REVOLUTIONS AT 740°C

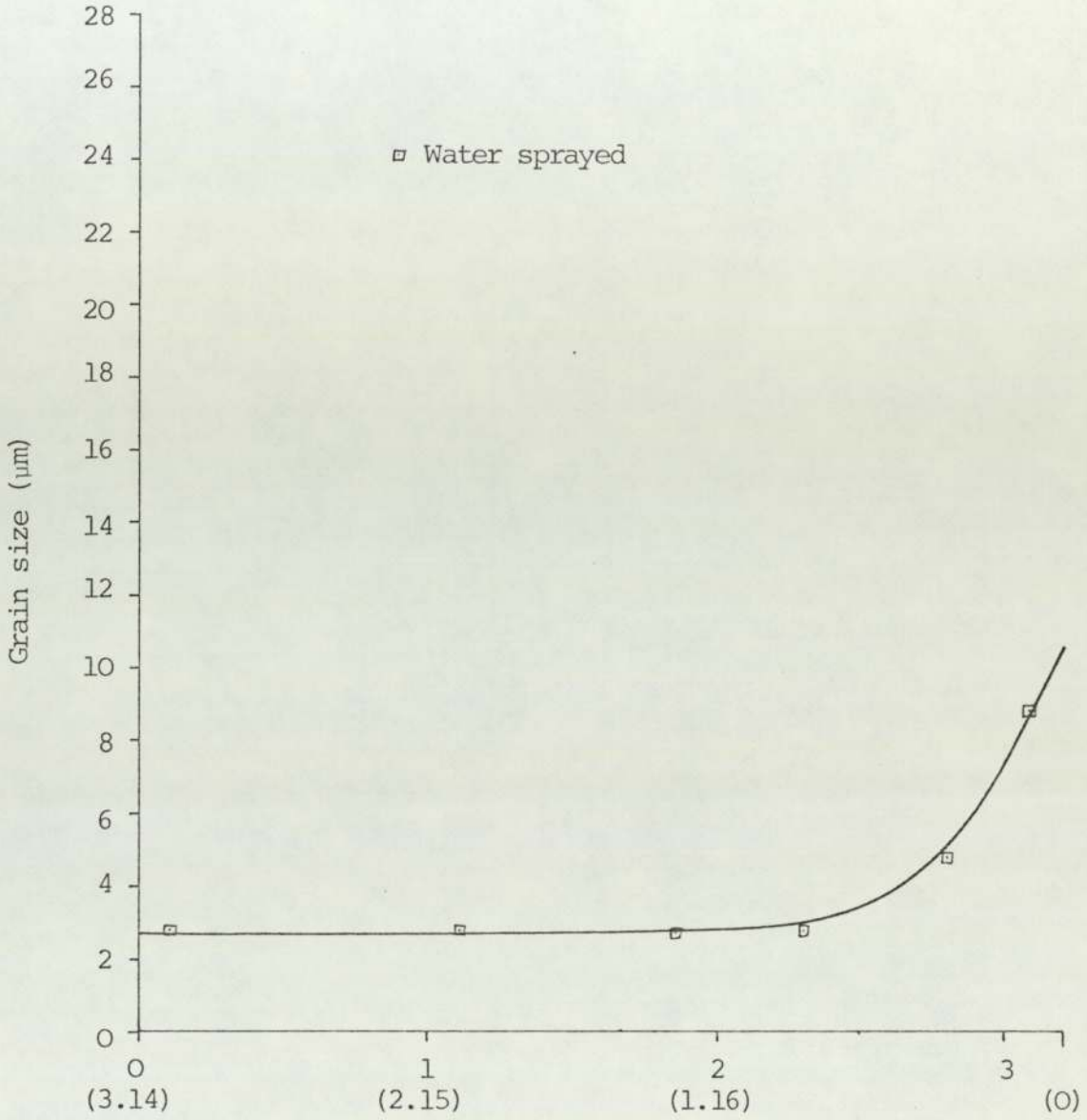

FIGURE 6.17 VARIATION IN GRAIN SIZE WITH STRAIN

C-Mn-V STEEL DEFORMED BY 4 REVOLUTIONS AT 755^{o}C

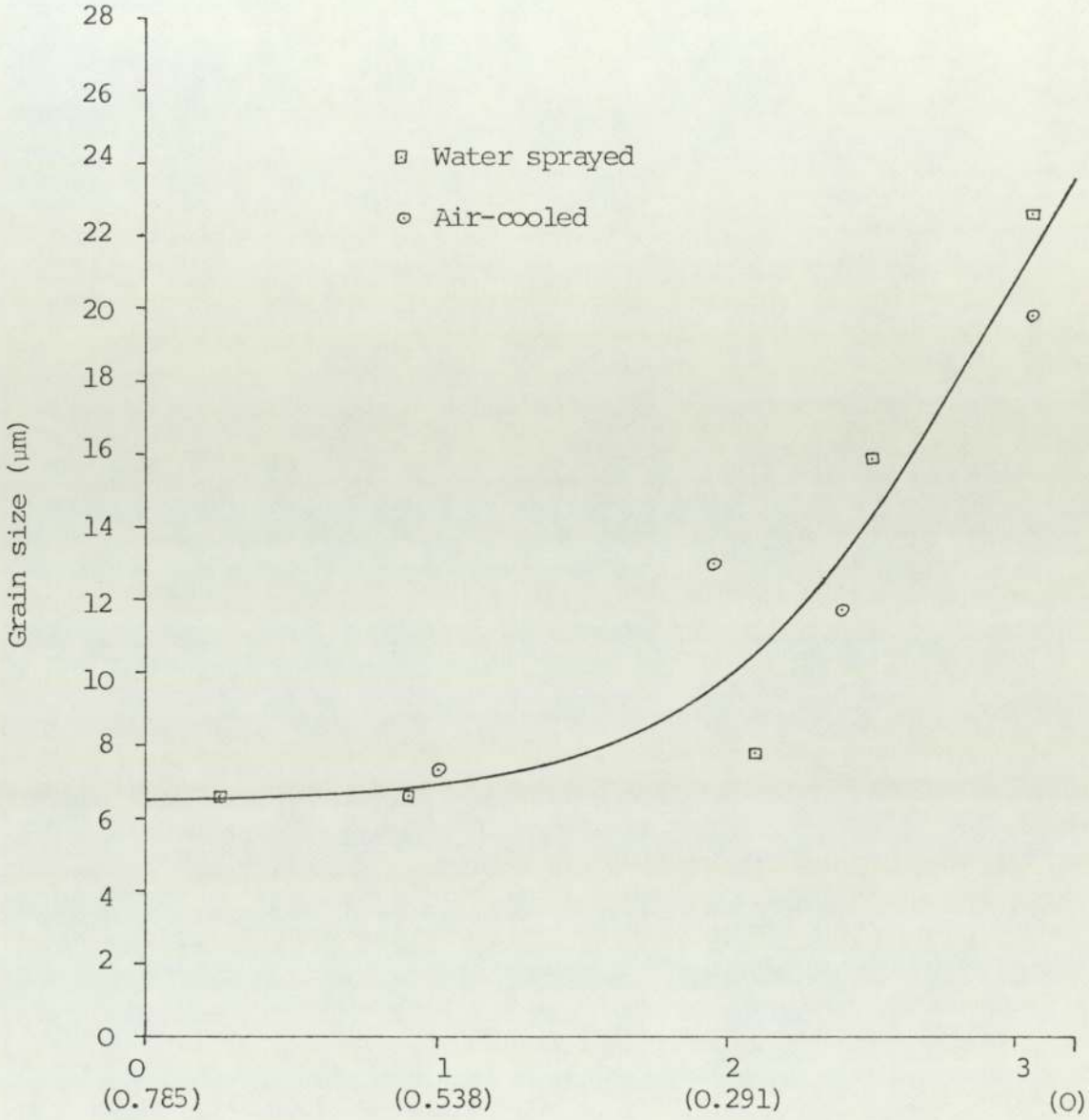

FIGURE 6.18 VARIATION IN GRAIN SIZE WITH STRAIN

C-Mn-Nb STEEL DEFORMED 1 REVOLUTION AT 740°C

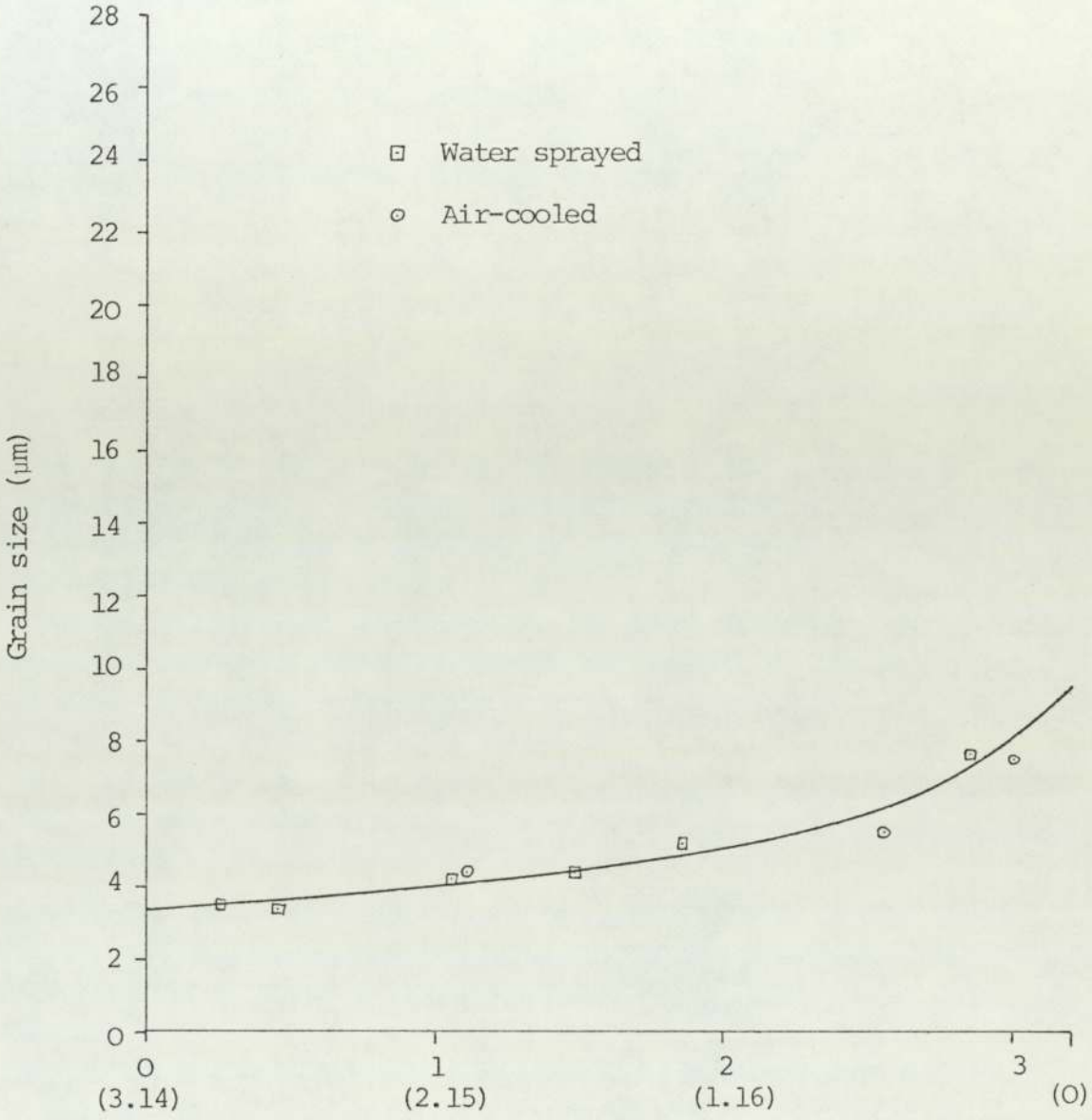

FIGURE 6.19 VARIATION OF GRAIN SIZE WITH STRAIN

C-Mn-Nb STEEL DEFORMED 4 REVOLUTIONS AT 740^{o}C

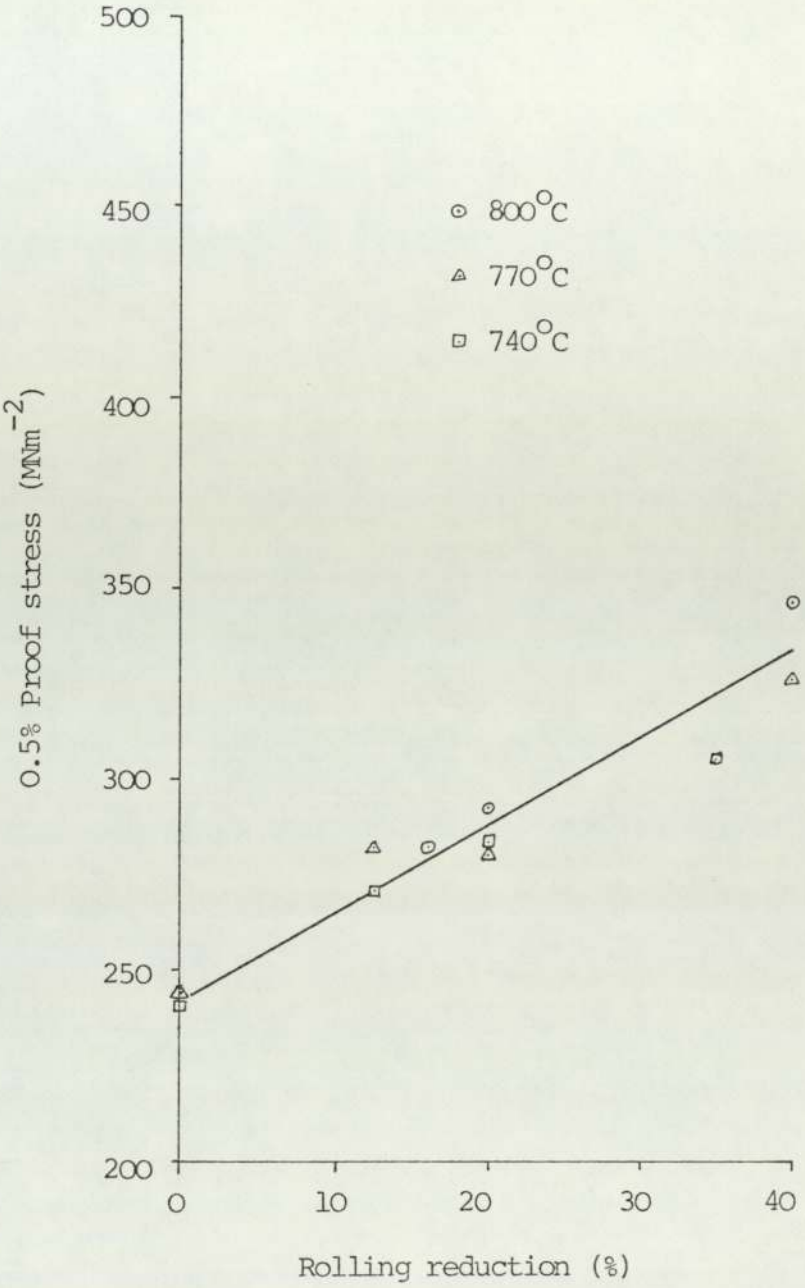

FIGURE 6.20 VARIATION IN PROOF STRESS WITH ROLLING REDUCTION

C-Mn STEEL AIR-COOLED AFTER ROLLING

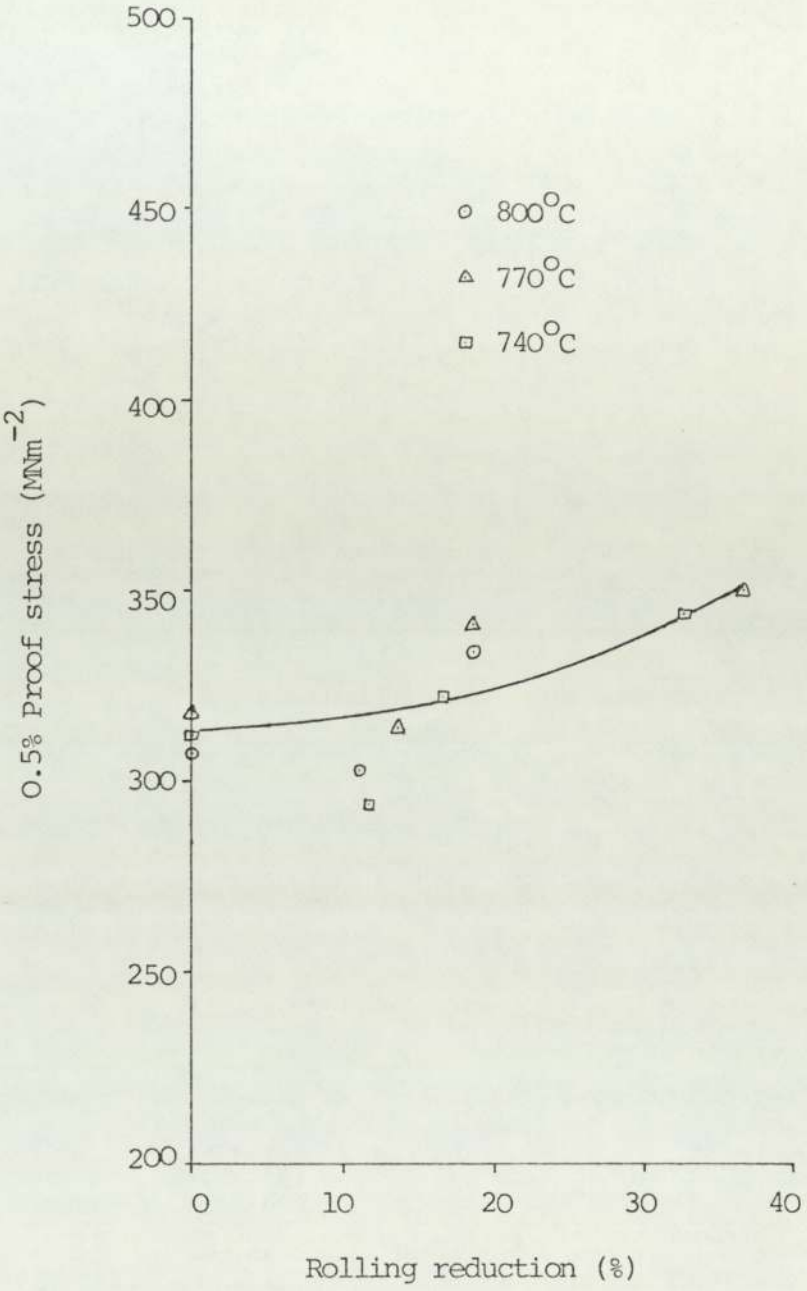

FIGURE 6.21 VARIATION IN PROOF STRESS WITH ROLLING REDUCTION

C-Mn-V STEEL AIR-COOLED AFTER ROLLING

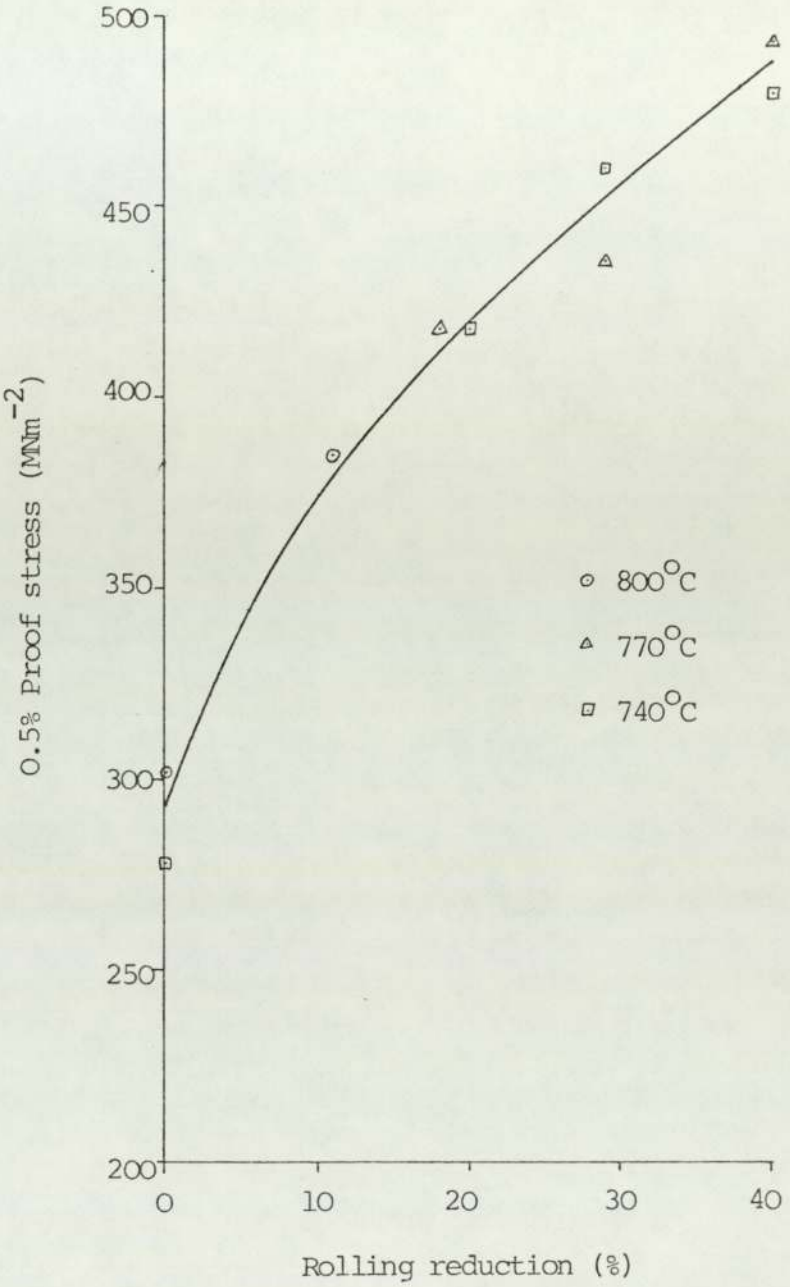

FIGURE 6.22 VARIATION IN PROOF STRESS WITH ROLLING REDUCTION

C-Mn-Nb STEEL AIR-COOLED AFTER ROLLING

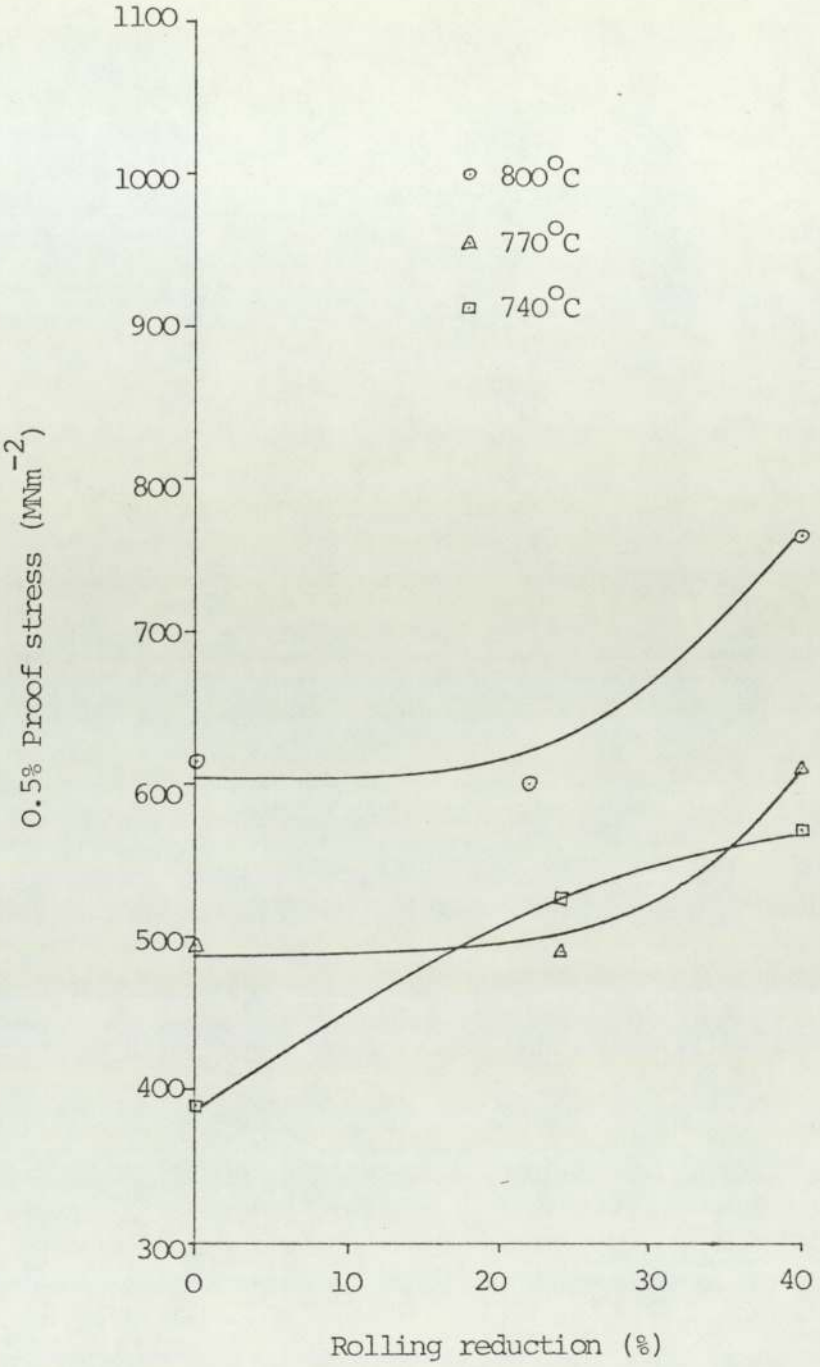

FIGURE 6.23 VARIATION IN PROOF STRESS WITH ROLLING REDUCTION

C-Mn STEEL WATER QUENCHED AFTER ROLLING

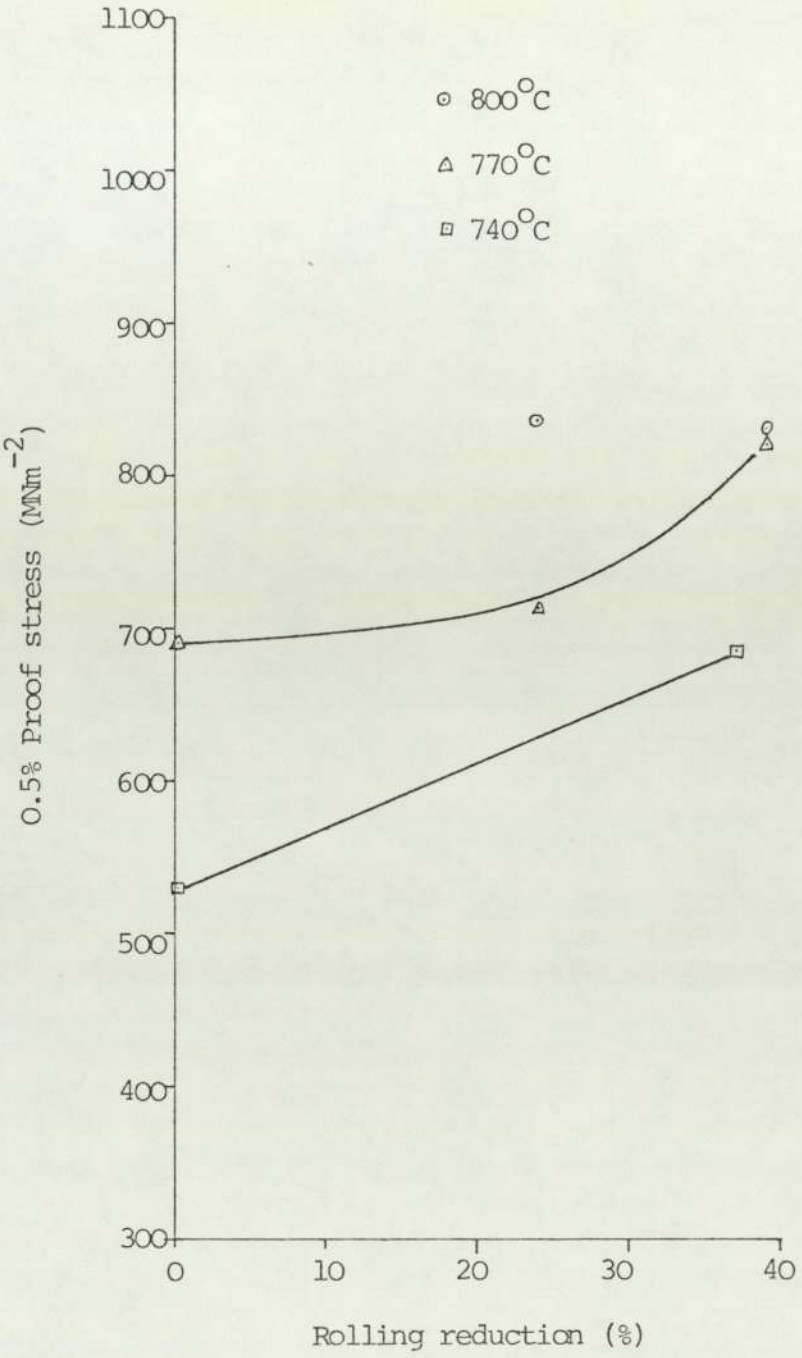

FIGURE 6.24 VARIATION IN PROOF STRESS WITH ROLLING REDUCTION

C-Mn-V STEEL WATER QUENCHED AFTER ROLLING

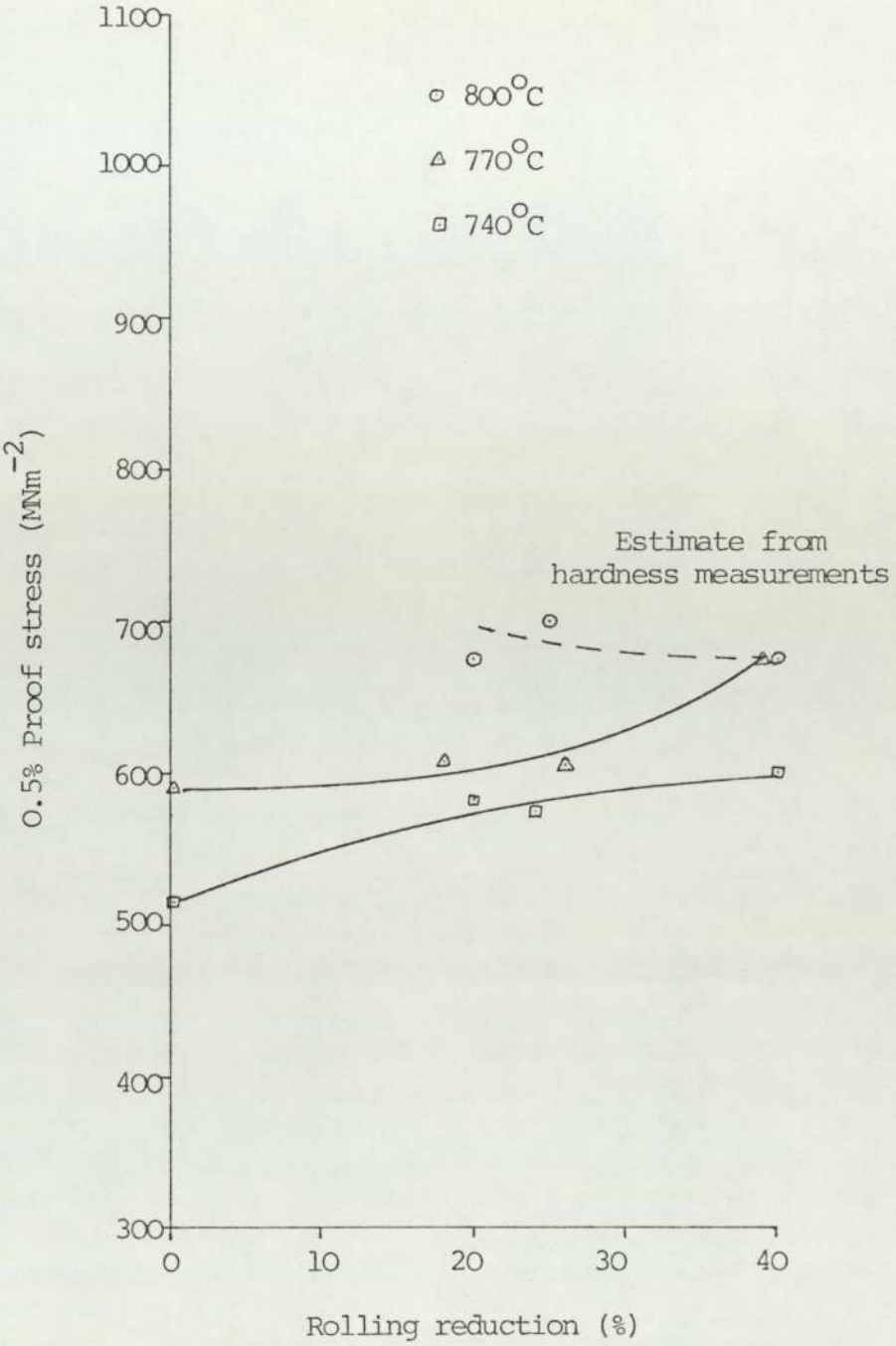

FIGURE 6.25 VARIATION IN PROOF STRESS WITH ROLLING REDUCTION

C-Mn-Nb STEEL WATER QUENCHED AFTER ROLLING

(a) Vanadium steel magnification x 1500

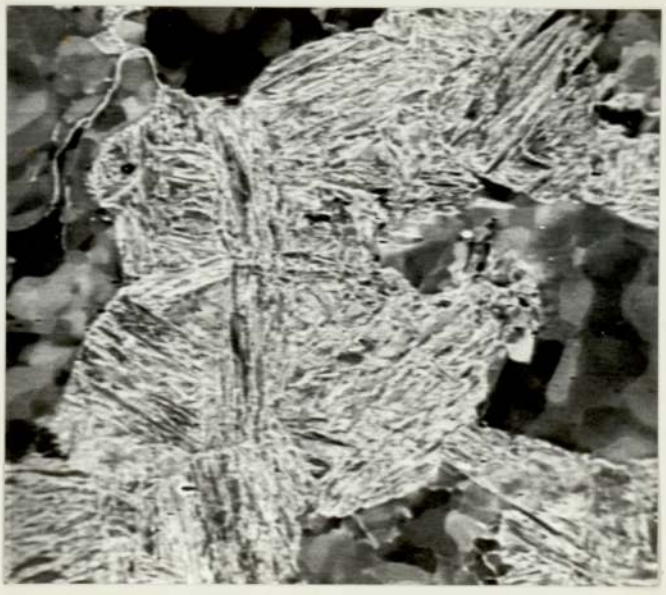

(b) Carbon-manganese steel magnification x 1000

PHOTO. 6.1 STRUCTURE OF MARTENSITE SEEN IN THE SEM USING BSE MODE

(a) Niobium steel - magnification x 1000

(b) Carbon-manganese steel - magnification x 1000

PHOTO. 6.2 SEM (BSE MODE) PHOTOMICROGRAPHS WHICH SHOW SMALL AREAS OF PEARLITE

(a) Carbon-manganese steel - magnification x 500

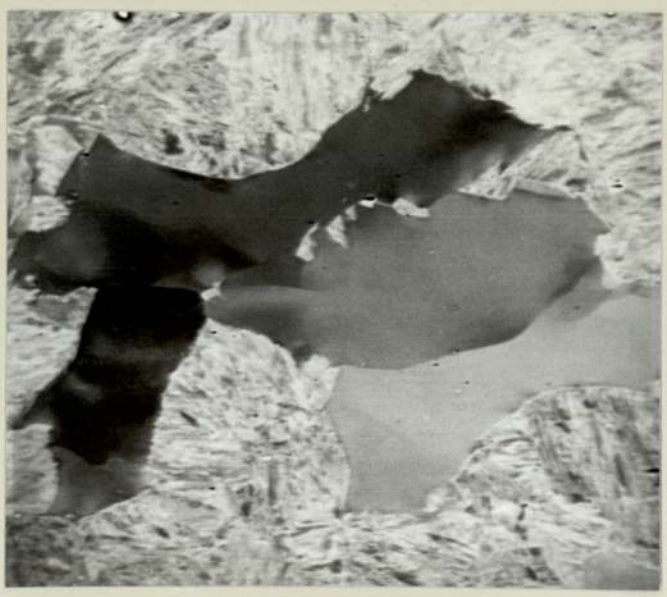

(b) Carbon-manganese steel - magnification x 1000

PHOTO. 6.3 UNDEFORMED FERRITE CLOSE TO THE CENTRE OF TORSION SPECIMENS

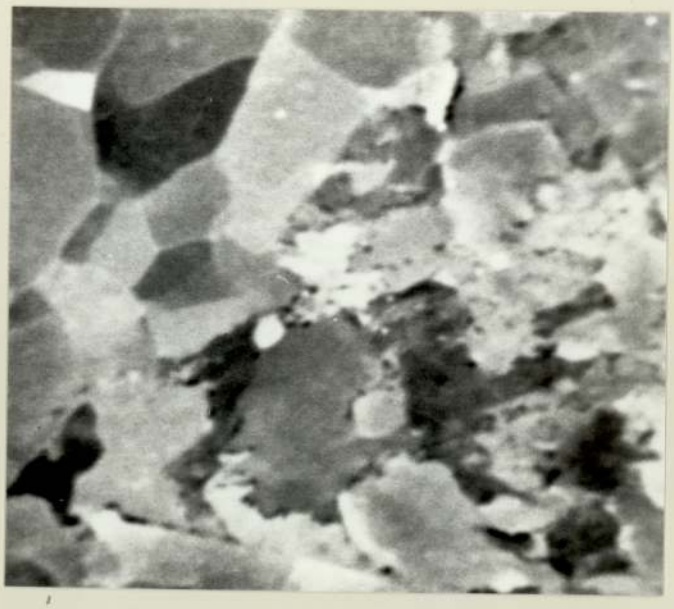

Magnification x 5000

PHOTO. 6.4 PRECIPITATION IN THE NIOBIUM STEEL

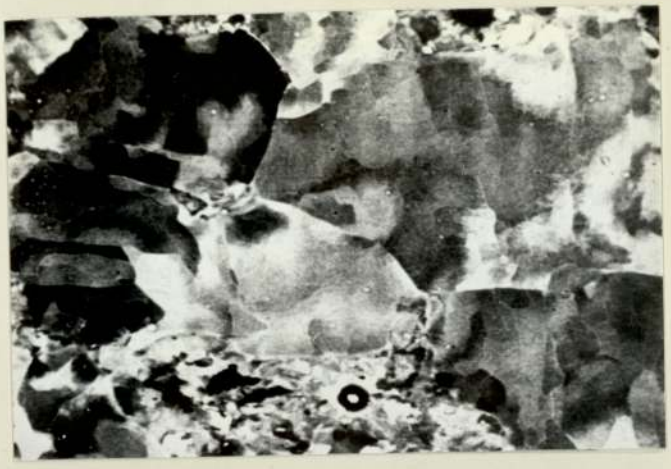

Shear strain = 0.165

2.5mm*

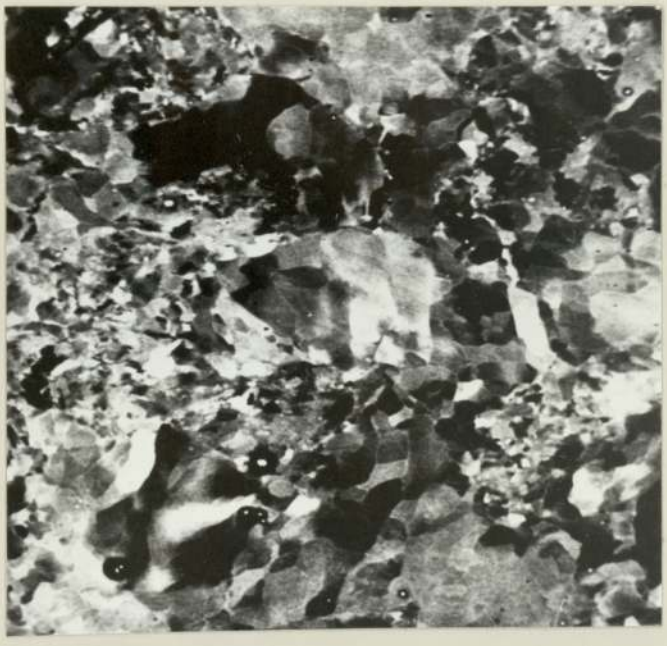

Shear strain = 0.535

1.00mm*

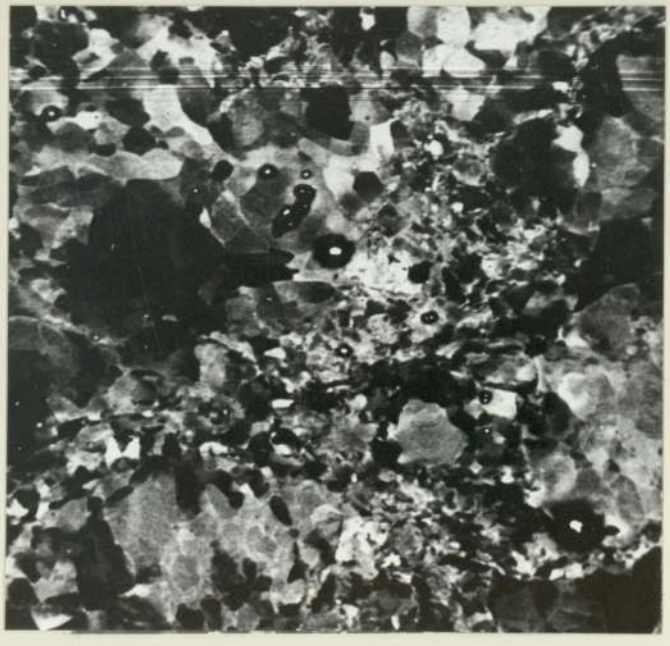

Shear strain = 0.66

0.50mm*

*distance measured from the surface

PHOTO. 6.5 C-Mn STEEL DEFORMED 1 REVOLUTION AT 740°C AND AIR-COOLED (MAGNIFICATION x 1000)

Shear strain = 0.19

2.39mm*

Shear strain = 0.66

0.5mm*

Shear strain = 0.735

0.2mm*

*distance measured from the surface

PHOTO. 6.6 C-Mn STEEL DEFORMED 1 REVOLUTION AT 740°C AND WATER SPRAYED (MAGNIFICATION x 1000)

Shear strain = 0.72

2.44mm*

Shear strain = 2.14

1.00mm*

Shear strain = 2.6

0.5mm*

*distance measured from the surface

PHOTO 6.7 C-Mn STEEL DEFORMED BY 4 REVOLUTIONS AT 740°C AND AIR-COOLED (MAGNIFICATION x 1000)

Shear strain = 1.12

2.04mm*

Shear strain = 2.10

1.04mm*

Shear strain = 2.94

0.19mm*

*distance measured from the surface

PHOTO. 6.8 C-Mn STEEL DEFORMED BY 4 REVOLUTIONS AT 740^{o}C AND WATER SPRAYED (MAGNIFICATION x 1000)

Shear strain = 0.30

1.94mm*

Shear strain = 0.48

1.47mm*

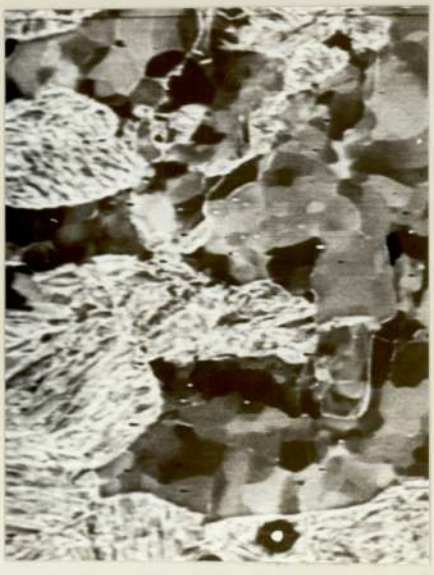

Shear strain = 0.645

0.55mm*

*distance measured

from the surface

PHOTO. 6.9 C-Mn STEEL DEFORMED BY 1 REVOLUTION AT 755^{o}C AND WATER SPRAYED (MAGNIFICATION x 1000)

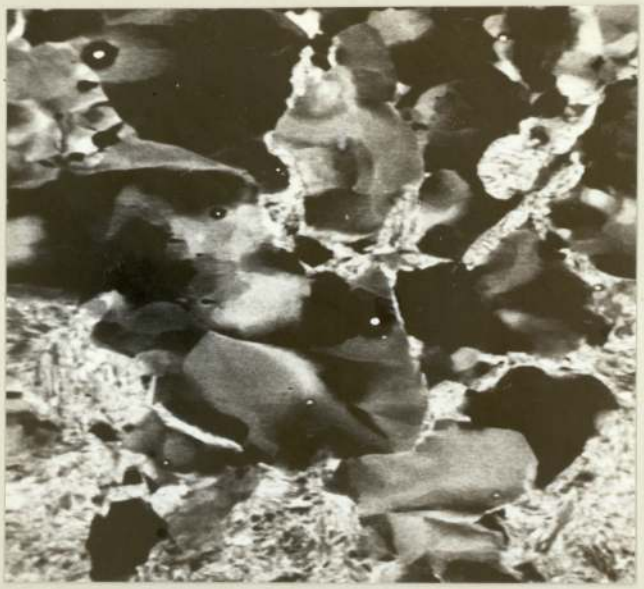

Shear strain = 0.18

2.45mm*

Shear strain = 0.425

1.45mm*

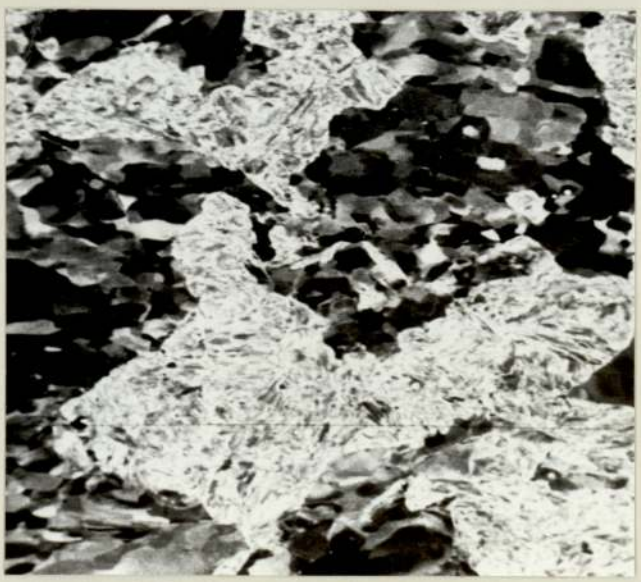

Shear strain = 0.645

0.55mm*

*distance measured from the surface

PHOTO. 6.10 C-Mn-V STEEL DEFORMED BY 1 REVOLUTION AT 740°C AND WATER SPRAYED (MAGNIFICATION x 1000)

Shear strain = 0.12

3.04mm*

Shear strain = 1.16

2.0mm*

Shear strain = 2.12

1.02mm*

Shear strain = 2.72

0.40mm*

*distance measured from the surface

PHOTO. 6.11 C-Mn-V STEEL DEFORMED BY 4 REVOLUTIONS AT 740°C AND AIR-COOLED (MAGNIFICATION x 1000)

Shear strain 0.10

3.08mm*

Shear strain = 0.36

2.8mm*

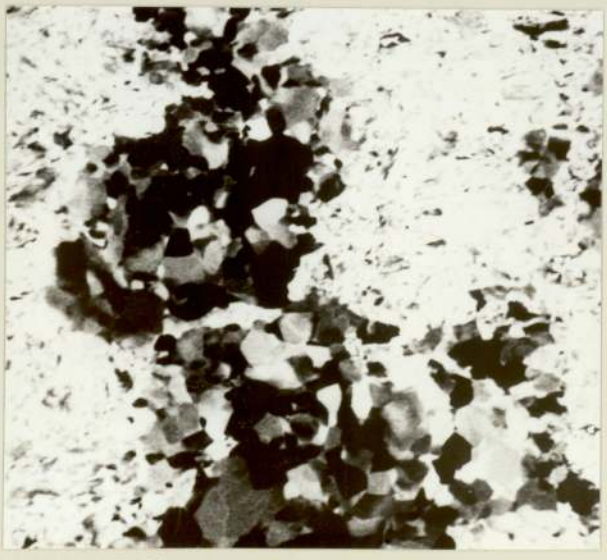

Shear strain = 2.04

1.1mm*

*distance measured from the surface

PHOTO. 6.12 C-Mn-V STEEL DEFORMED BY 4 REVOLUTIONS AT 755^{o}C AND WATER SPRAYED (MAGNIFICATION x 1000)

Shear strain = 0.30

1.96mm*

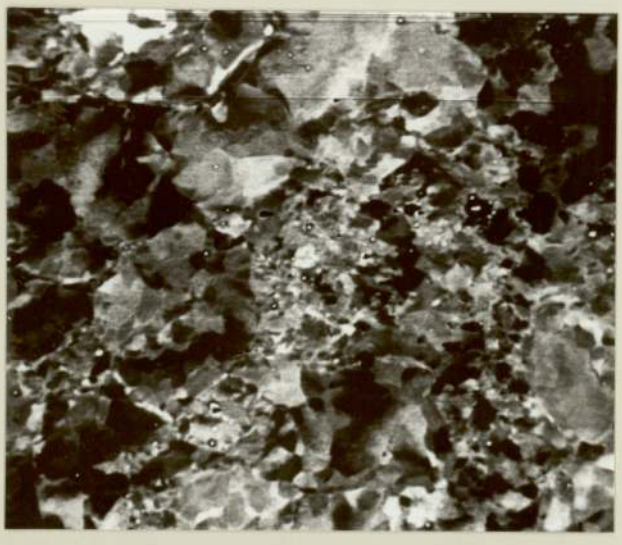

Shear strain = 0.525

1.000mm*

Shear strain = 0.66

0.48mm*

*distance measured from the surface

PHOTO. 6.13 C-Mn-Nb STEEL DEFORMED BY 1 REVOLUTION AT 740°C AND AIR-COOLED (MAGNIFICATION x 1000)

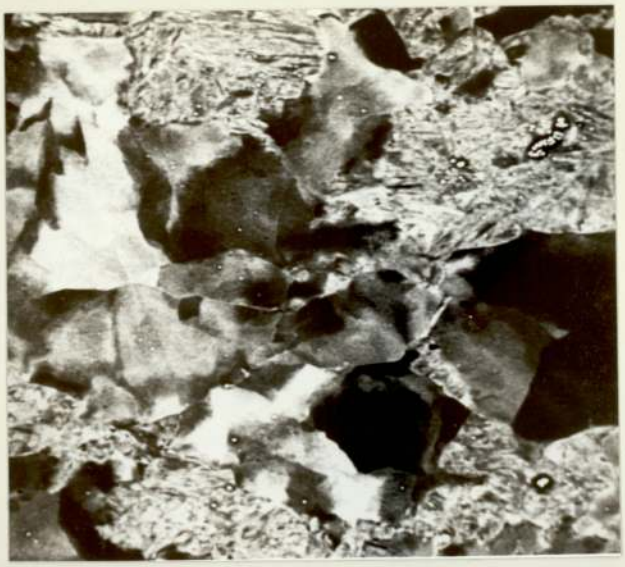

Shear strain = 0.165

2.51mm*

Shear strain = 0.55

0.92mm*

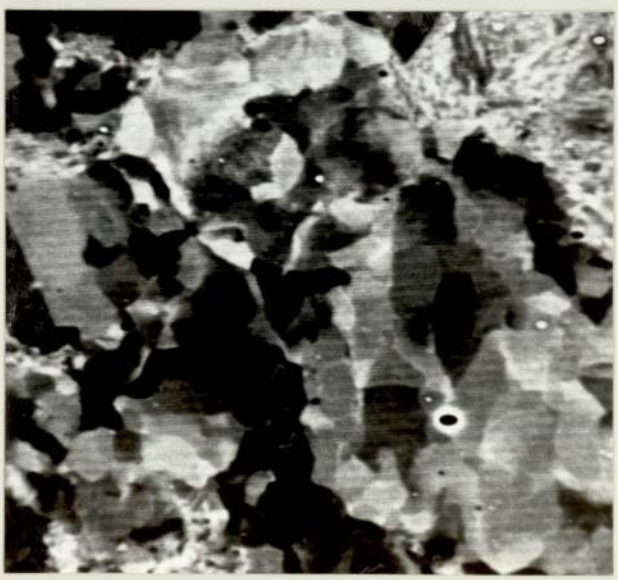

Shear strain = 0.72

0.25mm*

*distance measured from the surface

PHOTO. 6.14 C-Mn-Nb STEEL DEFORMED BY 1 REVOLUTION AT 740°C AND WATER SPRAYED (MAGNIFICATION x 1000)

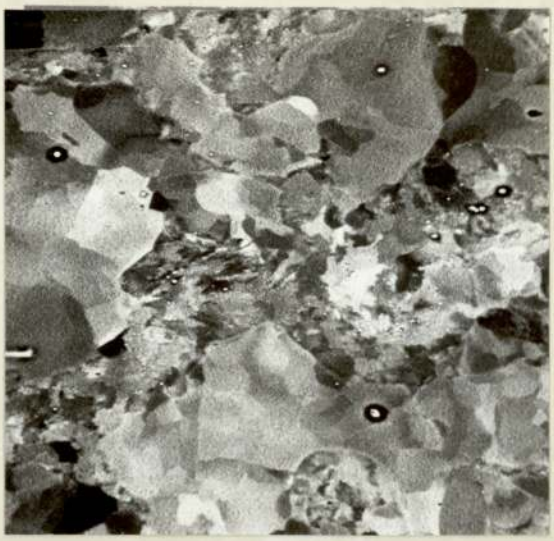

Shear strain = 0.14

3.02mm*

Shear strain = 0.60

2.55mm*

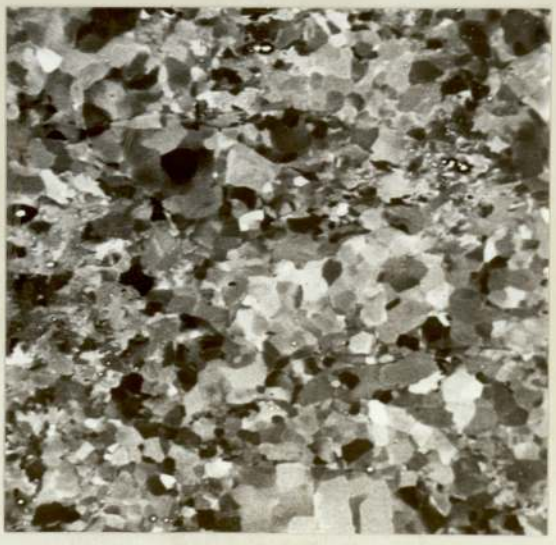

Shear strain = 2.06

1.11mm*

*distance measured

from the surface

PHOTO. 6.15 C-Mn-Nb STEEL DEFORMED BY 4 REVOLUTIONS AT 740°C AND AIR-COOLED (MAGNIFICATION x 1000)

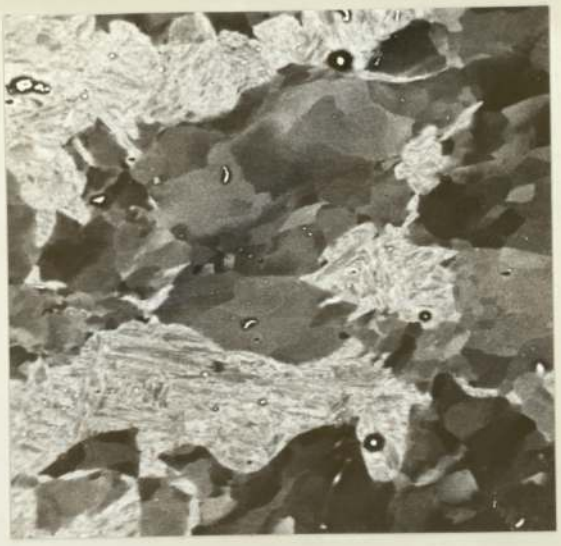

Shear strain = 0.30

2.86mm*

Shear strain = 1.28

1.86mm*

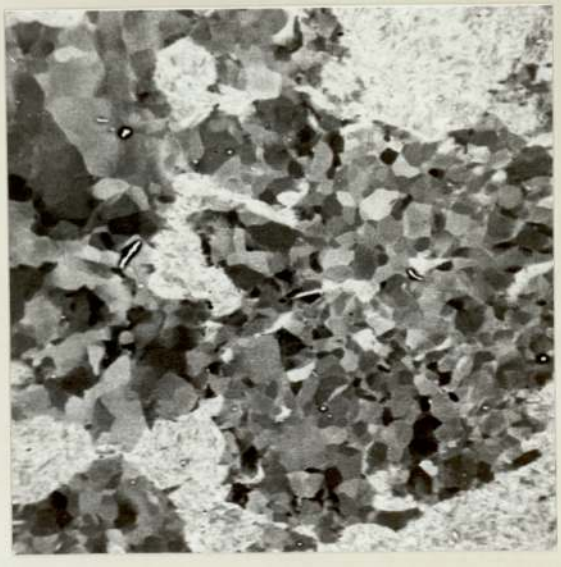

Shear strain = 1.66

1.48mm*

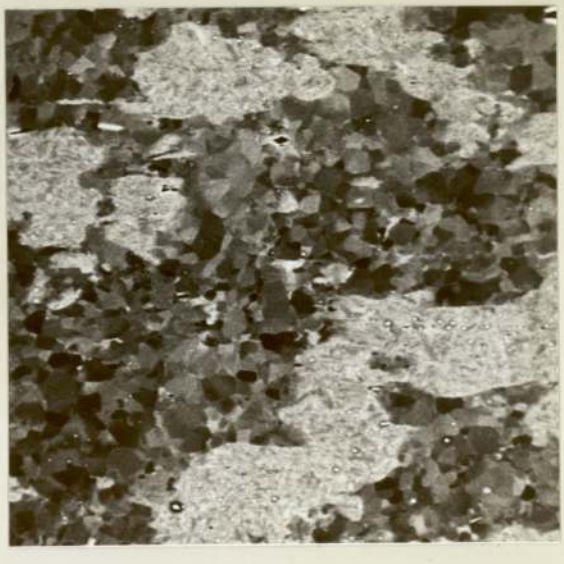

Shear strain = 2.68

0.46mm*

*distance measured

from the surface

PHOTO. 6.16 C-Mn-Nb STEEL DEFORMED BY 4 REVOLUTIONS AT 740°C AND WATER SPRAYED (MAGNIFICATION x 1000)

7. DISCUSSION

7.1 TORQUE - STRAIN CURVES

The torque - strain curves presented in figures 6.4 and 6.5 enable the three materials studied to be ranked in order of their strength.

The results show the expected decrease in the torque at the point of yield with increase in temperature. It is also clear that small additions of vanadium and niobium significantly increase the yield point with respect to that of the carbon manganese steel. This is due to the grain boundary pinning effect of niobium and vanadium carbide precipitates, with possibly some precipitation hardening from the vanadium carbide present.

These torque curves indicate that the vanadium steel has the greatest flow stress, followed by the niobium steel and finally the plain carbon manganese steel. This order is also apparent from the hardness measurements of the three steels. The surface hardness of the three steels deformed by 4 revolutions at 740^{o}C and air cooled were:

C-Mn	154 HV2.5
C-Mn-Nb	175 HV2.5
C-Mn-V	196 HV2.5

At 740^{o}C, the curves for the three steels are very similar in shape. This is not the case at 770^{o}C. At this higher temperature, the curves for the C-Mn and C-Mn-Nb steels show a much greater decrease in torque after the maximum has been reached than the vanadium steel. The torque - strain curves for the plain carbon and niobium steels at 770^{o}C are

typical of a steel under-going a process of dynamic recrystallisation[41] rather than dynamic recovery.

7.2 CORRELATION OF TORSION AND ROLLING EXPERIMENTS

7.2.1 Hardness Measurement and Mechanical Properties

The only form of mechanical property data available from the torsion specimens was Vickers hardness measurement using a 2.5kg load. Sandin[42] made hardness tests on metals cold-drawn up to 60% reduction and also determined the 0.2% proof stress σ_p, of the material. He found the following linear relation at each stage for copper, aluminium, carbon steel and stainless steel:-

$$HV = K_1\sigma_p + K_2 \qquad (7.1)$$

where,

HV = Vickers hardness number

σ_p = 0.2% proof stress

K_1, K_2 = constants

As part of this study, specimens of the three steels were deformed by rolling after soaking at a temperature in the range of 740 - 800°C. From these rolled materials, tensile properties were measured together with the Vickers hardness number. Data for the 0.5% proof stress and the Vickers hardness (HV10) were obtained for material after the following thermo-mechanical heat treatments:

(i) C-Mn, C-Mn-V, C-Mn-Nb — Heated to 740, 770 or 800°C and air cooled to room temperature without any rolling deformation.

(ii) C-Mn, C-Mn-V, C-Mn-Nb — Heated to 740, 770 or 800°C and water quenched to room temperature without any rolling deformation.

(iii) C-Mn-Nb — Heated to 740°C and deformed 20, 24 or 40% by rolling before quenching in water to room temperature.

(iv) As (iii) above but heated to 770°C before rolling.

(v) As (iii) above but heated to 800°C before rolling.

(vi) C-Mn-Nb — Heated to 740°C and deformed 20, 24 or 40% by rolling followed by air cooling to room temperature.

(vii) As (vi) above but heated to 770°C before rolling.

(viii) As (vi) above but heated to 800°C before rolling.

In figure 7.1 the Vickers hardness number is plotted against the 0.5% proof stress for all of the above thermo-mechanical treatments. The line was fitted using a linear regression analysis giving a regression coefficient (r^2) of 0.94 and can be represented by the following equation:

$$\sigma_p = 2.24HV - 21.22 \qquad (7.2)$$

where, σ_p is the 0.5% proof stress (N/mm^2).

This analysis of the rolling result was then used to determine the 0.5% proof stress for the steels deformed by torsion. The results are plotted in figures 7.2 and 7.3 for the air cooled material and figures 7.4 - 7.6 for the water quenched material.

The results are plotted to show the variation in 0.5% proof stress with temperature for the following conditions:

(i) the centre of the torsion specimen (nominally zero shear strain);

(ii) the surface of the torsion specimen deformed by 1 revolution (surface shear strain of 0.785);

(iii) the surface of the torsion specimen deformed by 4 revolutions (surface shear strain of 3.142)

(iv) undeformed material heated in a muffle furnace (results shown dotted in each case)

7.2.2 Deformation by Rolling and Torsion

In order to correlate the results of the torsion experiments with those obtained by rolling it is necessary to equate deformation produced by the two modes.

Rolling

The true strain ε, for a tensile test specimen is defined by,

$$\varepsilon = \ln\left[\frac{L}{L_o}\right] \qquad (7.3)$$

where, L_o = initial length of specimen

L = final length of specimen

Since the specimen has constant volume,

$$t_o.W_o.L_o = t.W.L \qquad (7.4)$$

where, t_o = initial thickness

W_o = initial width

t = final thickness

W = final width

Assuming that the width remains constant,

$$\frac{L}{L_o} = \frac{t_o}{t} \qquad (7.5)$$

The true strain in the warm rolled material is therefore given by,

$$\varepsilon = \ln\left[\frac{t_o}{t}\right] \qquad (7.6)$$

Torsion

The true strain at the periphery of the torsion specimens is given by the following equation[43],

$$\varepsilon = \frac{2\pi NR}{L\sqrt{3}} \qquad (7.7)$$

where,

N = number of revolutions

R = radius of specimen (3.175mm)

L = length of specimen (25.4mm)

The true strain of the periphery of the torsion specimens after 1 and 4 revolutions is respectively 0.453 and 1.814.

7.2.3 General Observations

Figures 7.7 - 7.12 show the relationship between true strain at temperatures in the range 740 - 800°C, and the proof stress of that material at room temperature. Figures 7.7 - 7.9 show the results obtained when the steel concerned is air-cooled to room temperature, and figures 7.10 - 7.12, for steels water quenched after deformation. For comparison, the rolling and torsion results for the same steel and thermo-mechanical treatment are plotted on the same graph. In the case of the torsion experiments, data is only presented for the periphery of the specimen. At the centre of these specimens, the strain is nominally zero, however, this is unlikely in practice, particularly after 4 revolutions deformation.

Generally, there is reasonable agreement between the results obtained from the rolling and torsion data. The exception is the niobium steel (figures 7.9 and 7.12) where significant discrepancies are apparent.

7.3 WARM DEFORMATION AND STRENGTH

7.3.1 Air-cooled Steels

The results for the steels deformed at temperatures in the range 740 - 800°C and air-cooled are shown in figures 7.9 - 7.11. The results for the carbon-manganese steel and the vanadium steel are very similar in form. In both cases the proof stress is increased by warm deformation. From the rolling results particularly, it is clear that the proof stress is independent of the temperature in the range 740 - 800°C, and strains up to 1.0 (C-Mn steel) and 0.5 (C-Mn-V steel). For larger strains, the temperature has an effect on the proof stress. As the temperature of deformation increases the room temperature proof stress decreases. In the case of the carbon-manganese steel, the difference in proof stress is 28 MNm^{-2} at a true strain of 1.8. For the vanadium steel, the difference is 47 MNm^{-2} after a true strain of 1.8.

7.3.2 Water Quenched Steels

The results for the steels deformed at temperatures in the range 740 - 800°C and water quenched are shown in figures 7.10 - 7.12. As expected, the proof stress varies significantly with the temperature of deformation since the volume fraction of

martensite in the microstructure is temperature dependent. In all cases, the proof stress increases with strain at constant deformation temperature.

7.4 STRUCTURE/PROPERTY RELATIONSHIPS

7.4.1 Introduction

The mechanical properties of materials vary significantly with changes in composition and microstructure.

In the case of the three steels studied, the compositional effects on mechanical properties will be due to small variations in the manganese content, and the effect of vanadium carbide and niobium carbide precipitates.

The microstructural features found in these steels, which will influence the mechanical properties are:-

(i) ferrite grain size and sub-grain size, together with the effect of dislocation density which will vary between cold worked and recrystallised grains. The contribution to strength will also vary with the volume fraction of ferrite present in the microstructure.

(ii) the carbon content of martensite will affect the properties of the water quenched materials. The extent of deformation in the prior austenite grains may also have an effect on hardenability.

(iii) the volume fraction of pearlite in the air-cooled materials.

7.4.2 Predicted Strength

Many studies have been carried out to establish empirical relationships relating compositional and micro-structural features to yield strength.

Air-cooled Steels

For air-cooled steels containing less than 30% pearlite, the following relationship[4] relates yield stress to grain and some compositional factors,

$$\underset{(MNm^{-2})}{\sigma_y} = K + 37(\%Mn) + 83(\%Si) + 2918(N_f) + 15.1(d^{-\frac{1}{2}}) \qquad (7.8)$$

where K = 88 MNm^{-2} for an air-cooled material and
62 MNm^{-2} for a furnace cooled material

d = grain size defined as the mean linear intercept of the polygonal ferrite grains expressed in mm

N_f = weight percent of free nitrogen.

The above equation applied to plain carbon-manganese steels which have been cooled from the austenite range without deformation.

For the manganese, silicon and nitrogen contents given in table 3.1, the yield stress predicted can be calculated. Equation 7.1 then becomes:-

for the C-Mn and C-Mn-Nb steels,

$$\sigma_y = 155 + 15.1(d^{-\frac{1}{2}}) \text{ N/mm}^2 \qquad (7.9)$$

for the C-Mn-V steel,

$$\sigma_y = 164 + 15.1(d^{-\frac{1}{2}}) \text{ N/mm}^2 \qquad (7.10)$$

The difference between these two equations is due to the slightly higher manganese content in the vanadium steel.

In figure 7.13, equation 7.9 is plotted together with the 0.5% proof stress for the base and niobium steel. Data is included for the material deformed at 740^{o}C, since the pearlite content is less than 30%. A similar graph for the vanadium steel is plotted in figure 7.14.

The results presented in figure 7.13 do not very readily fit the line that represents equation 7.9. This is due to the fact that the steels have been deformed in the austenite - ferrite temperature range. The much finer grain structure that develops during deformation is due to the formation of a sub-grain structure. From the work of Manganon[28], the effect of sub-grains on the strength can be assessed. The following relationship can be used to determine the increase in yield stress with sub-grain size.

$$\Delta\sigma_{SG} = -125 + 13.6d^{-\frac{1}{2}} \qquad (7.11)$$

where, d = sub-grain size

$\Delta\sigma_{SG}$ = change in yield stress

Consider the results for the carbon-manganese steel deformed at 740°C:

Deformation		Grain Size	
		surface(μm)	centre(μm)
740°C	1 revolution	5.5	22
740°C	4 revolutions	4.7	25

From this data, the initial grain size of the carbon-manganese steel is taken as 25μm. Using the equation 7.9, the predicted yield stress is 251 MNm^{-2}. The ferrite structure at the surface of the specimens is assumed to be composed completely of sub-grains, the values given therefore representing the sub-grain size. Using equation 7.11 developed by Manganon, the increase in yield stress due to sub-grain strengthening can be calculated. The sub-grain strengthening calculated for a ferrite content of 75% is given below.

	740°C - 1 revolution	740°C - 4 revolutions
Predicted yield stress from grain size	251	251
Sub-grain strengthening	44	55
Predicted yield stress	295	306
0.5% proof stress calculated from hardness measurement	317	324

These results show a close agreement between the 0.5% proof stress calculated from hardness measurement and that predicted from the grain and sub-grain size.

In order to consider further the results from the vanadium and niobium steels, account must also be taken of the effect of precipitation. The following data was obtained from the material heated to 740°C in a muffle furnace without deformation by warm rolling.

	0.5% Proof stress (MNm^{-2})	$\Delta\sigma$
C-Mn	243	-
C-Mn-V	307	64
C-Mn-Nb	278	35

The difference betweent the vanadium and niobium steels and the base steel is due to the precipitation of vanadium and niobium carbides.

For the vanadium steel, the grain size is 15μm (see section 6.1). Using the same equations as before, the predicted yield stress can be calculated from the following components.

	740°C - 4 revolutions
Predicted yield stress from grain size	287
Sub-grain strengthening (sub-grain size 4.2μm)	64
Precipitation effect	84
Predicted yield stress	415 MNm^{-2}

	740°C - 4 revolutions
0.5% proof stress calculated from hardness measurement	418 MNm^{-2}

For the niobium steel, the grain size is 16μm (see section 6.1), and the sub-grain sizes are 6.3μm and 3.2μm after 1 and 4 revolutions deformation respectively at 740°C. The predicted yield strength can be calculated from the following components.

	740°C - 1 revolution	740°C - 4 revolutions
Predicted yield stress from grain size	274	274
Sub-grain strengthening	35	86
Precipitation effect	35	35
Predicted yield stress	344	395
0.5% Proof stress calculated from hardness measurement	390	371

There is fairly close agreement between the predicted yield stress and the 0.5% proof stress calculated from the hardness measurement after 4 revolutions of deformation. This is not however the case after 1 revolution. From an examination of the photo-micrographs 6.13 and 6.15, it is clear that after 4 revolutions of deformation a uniform sub-structure has developed at the periphery of the specimen. This is not the case after only 1 revolution.

Water Quenched Steels

In the case of the water quenched steels, the yield strength depends on the percentage and carbon content of the martensite phase. In the steels studied, the mean carbon content was 0.14% by weight. As the quantity of martensite in the micro-structure decreases, its carbon content will increase. The martensite hardness as a function of the martensite content is shown in figure 7.15[4].

Using figure 7.15, the martensite hardness in each water quenched specimen was calculated. From the measured hardness of each torsion specimen, and using a simple law of mixtures, the hardness of the ferrite phase at both the centre and the surface was calculated. These values are summarised in table 7.1[44].

From these results in table 7.1, it is clear that this analysis of the hardness contributions from the ferrite and martensite phases is inaccurate. An alternative approach is used below to assess the hardness of the ferrite and martensite phases.

From a knowledge of the grain size, and the sub-grain size of the ferrite phase, it is possible to predict the yield stress of the ferrite phase. Using the equation derived earlier to relate the 0.5% proof stress to the hardness, the approximate hardness of the ferrite phase can be calculated. From the measured hardness of the material and the proportion of ferrite and martensite in the structure, the hardness of the martensite phase can then be calculated using a simple law of mixtures. The results of this

analysis are presented in tables 7.2 - 7.4 for the three steels investigated.

These results show that, after deformation at 740°C, the martensite hardness is significantly lower than that predicted by figure 7.15. The only exception to this is the C-Mn-Nb steel deformed by 1 revolution at 740°C when the predicted and calculated values are in fairly close agreement (table 7.4). In the case of the base and the vanadium steels, the calculated and predicted martensite hardness values are in close agreement for deformation at 755°C (tables 7.2 and 7.3). The C-Mn-Nb steel deformed at 780°C and water quenched, produced a fully martensite structure. From figure 7.15, the predicted martensite hardness is 320, compared with a measured value at the surface of 475 (1 revolution) and 485 (4 revolutions).

At low temperatures in the two phase $\alpha + \gamma$ region, the hardenability of the austenite phase is reduced by deformation. In figure 7.1, the hardness of torsion specimens quenched without deformation is shown. At 740°C the surface hardness achieved at the periphery of base steel specimens deformed at 740°C.

Results from figure 6.2 for undeformed vanadium steel specimen shows that the surface hardness of a steel quenched from 740°C is 274HV2.5, lower than values obtained from the surface of deformed specimens. Deformation would not therefore appear to reduce the hardenability of the vanadium steel as predicted in the above analysis.

TABLE 7.1 HARDNESS OF MARTENSITE AND FERRITE PHASES IN THE WATER SPRAYED MATERIAL

C-Mn steel

Deformation	% Martensite	Martensite Hardness	Ferrite Hardness Centre	Hardness Surface
740°C 1 revolution	28	725	-11	46
750°C 1 "	58	440	-60	83
760°C 1 "	73	375	1.3	416
740°C 4 revolutions	30	700	29	100
755°C 4 "	53	465	114	167
770°C 4 "	95	330	1330	1550

C-Mn-V steel

740°C 1 revolution	38	585	61	109
750°C 1 "	50	480	100	160
770°C 1 "	85	350	550	683
740°C 4 revolutions	34	640	79	125
755°C 4 "	67	395	259	259

C-Mn-Nb steel

740°C 1 revolution	30	700	121	157
780°C "	100	320	-	-
740°C 4 revolutions	30	700	107	157
780°C 4 "	100	320	-	-

TABLE 7.2 HARDNESS AND YIELD STRENGTH OF THE WATER SPRAYED C-Mn TORSION SPECIMENS

Specimen Designation	740/1	740/4	755/4
Contribution to yield stress of ferrite			
- grain size	251	251	251
- sub-grain size	58	73	112
Predicted yield stress of ferrite (MNm^{-2})	309	324	363
Equivalent hardness of ferrite	147	154	172
Material hardness (HV2.5)	250	280	325
Martensite hardness (from figure 7.15)	725	700	465
Martensite hardness (calculated)	515	574	461

Notes:

(i) all measurements relate to the surface of each specimen

(ii) the specimen designation gives the temperature first followed by the number of revolutions of deformation.

TABLE 7.3 HARDNESS AND YIELD STRENGTH OF THE WATER SPRAYED C-Mn-V TORSION SPECIMENS

Specimen Designation	740/1	740/4	755/4
Contribution to yield stress			
- grain size	287	287	287
- sub-grain size	105	85	142
- precipitation	64	64	64
Predicted yield stress of ferrite (MNm^{-2})	456	436	493
Equivalent hardness of ferrite	213	204	230
Material hardness (HV2.5)	290	300	350
Martensite hardness (from figure 7.15)	585	640	395
Martensite hardness (calculated)	415	486	409

Notes:

(i) all measurements relate to the surface of each specimen

(ii) the specimen designation gives the temperature first, followed by the number of revolutions of deformation.

TABLE 7.4 HARDNESS AND YIELD STRENGTH OF THE WATER SPRAYED C-Mn-Nb TORSION SPECIMENS

Specimen Designation	740/1	740/4
Contributions to yield stress of ferrite		
- grain size	274	274
- sub-grain size	46	115
- precipitation	35	35
Predicted yield stress of ferrite (MNm^{-2})	355	424
Equivalent hardness of ferrite	168HV	199HV
Material hardness (HV2.5)	320	320
Martensite hardness (from figure 7.15)	700	700
Martensite hardness (calculated)	675	602

Notes:

(i) all measurements relate to the surface of each specimen

(ii) the specimen designation gives the temperature of deformation in degrees Centigrade first, and then the number of revolutions of deformation.

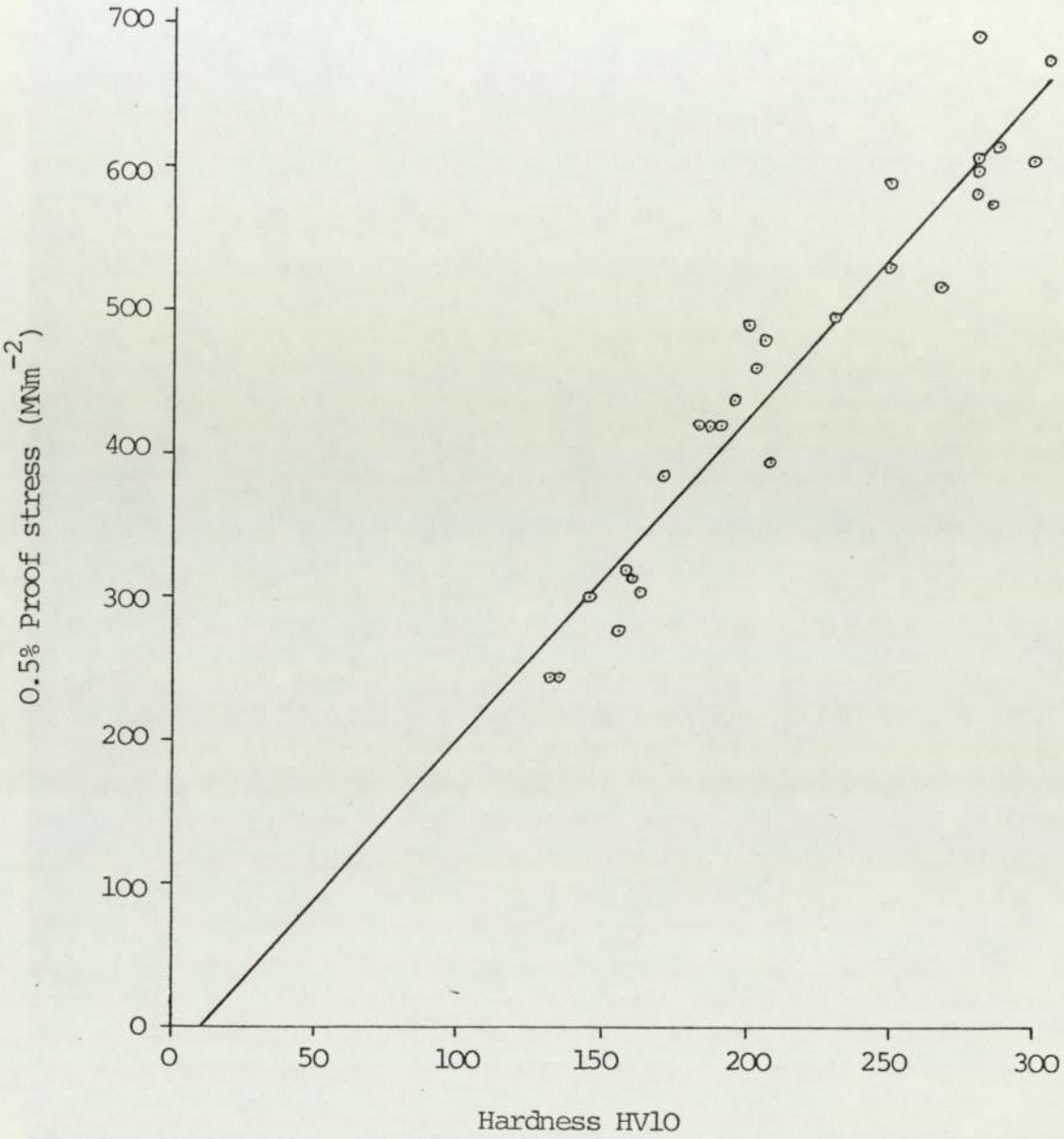

FIGURE 7.1 CORRELATION BETWEEN PROOF STRESS AND VICKERS HARDNESS MEASUREMENT

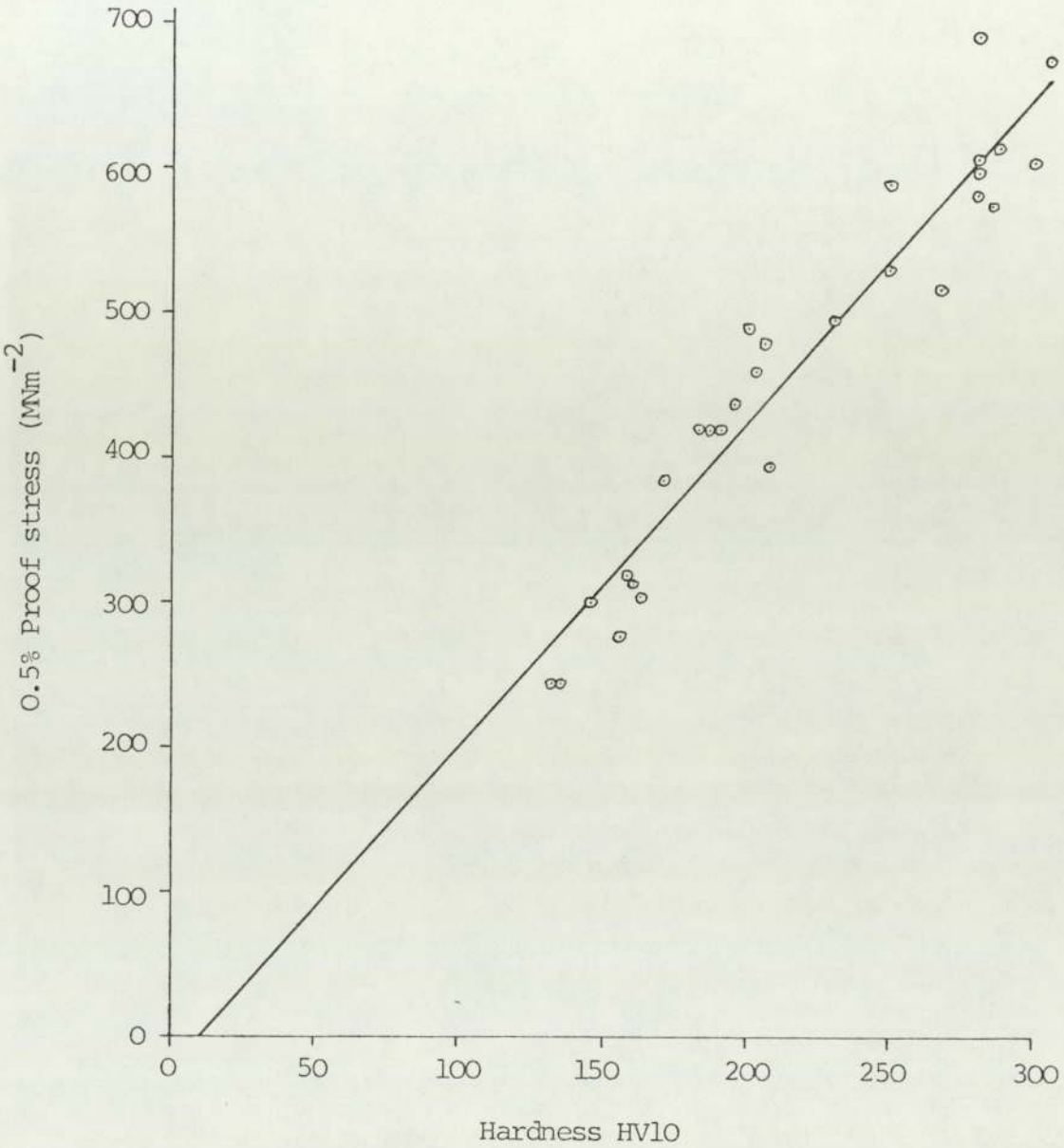

FIGURE 7.1 CORRELATION BETWEEN PROOF STRESS AND VICKERS HARDNESS MEASUREMENT

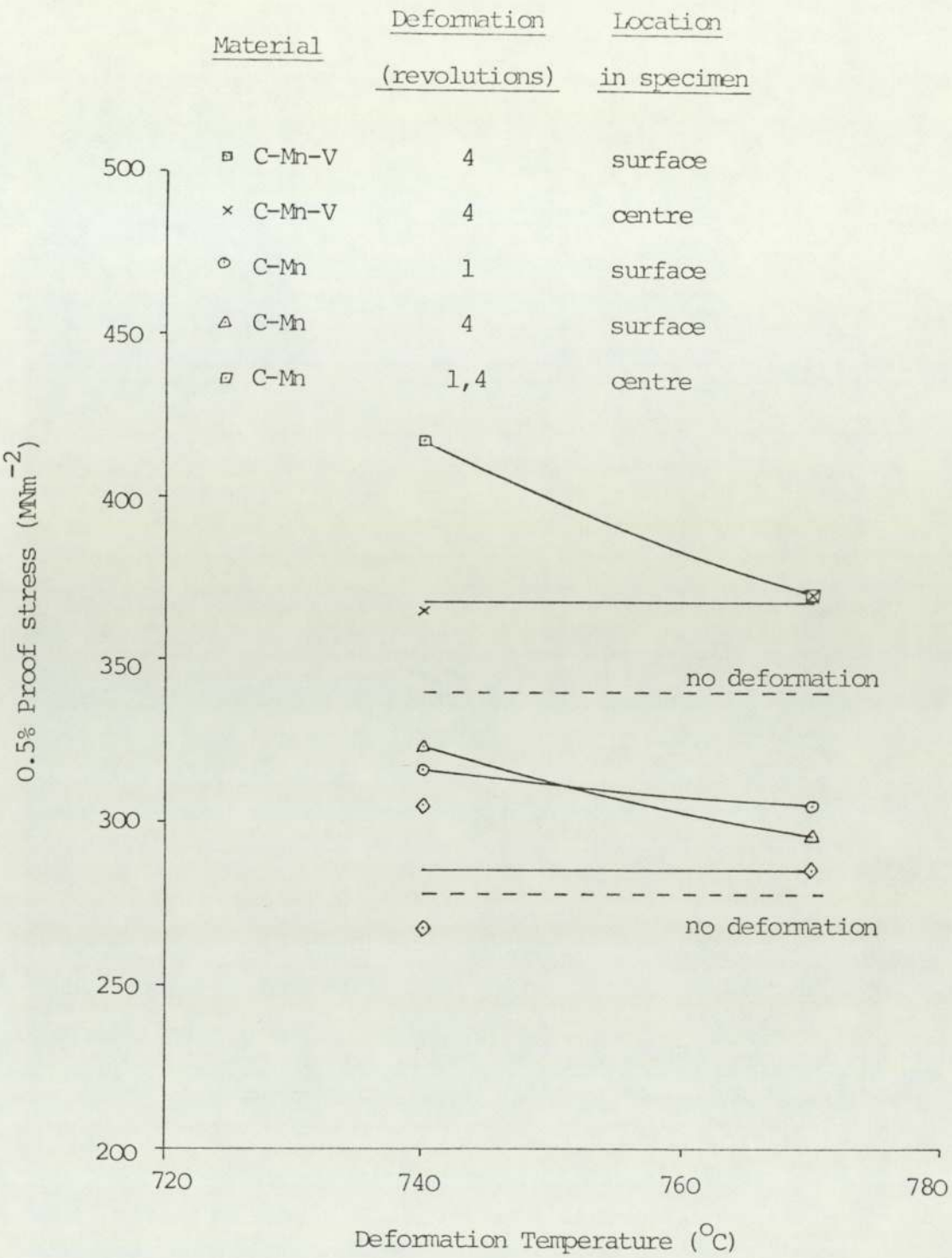

FIGURE 7.2 VARIATION IN PROOF STRESS WITH TEMPERATURE AND DEFORMATION FOR THE C-Mn AND C-Mn-V STEEL TORSION SPECIMENS (AIR-COOLED AFTER DEFORMATION)

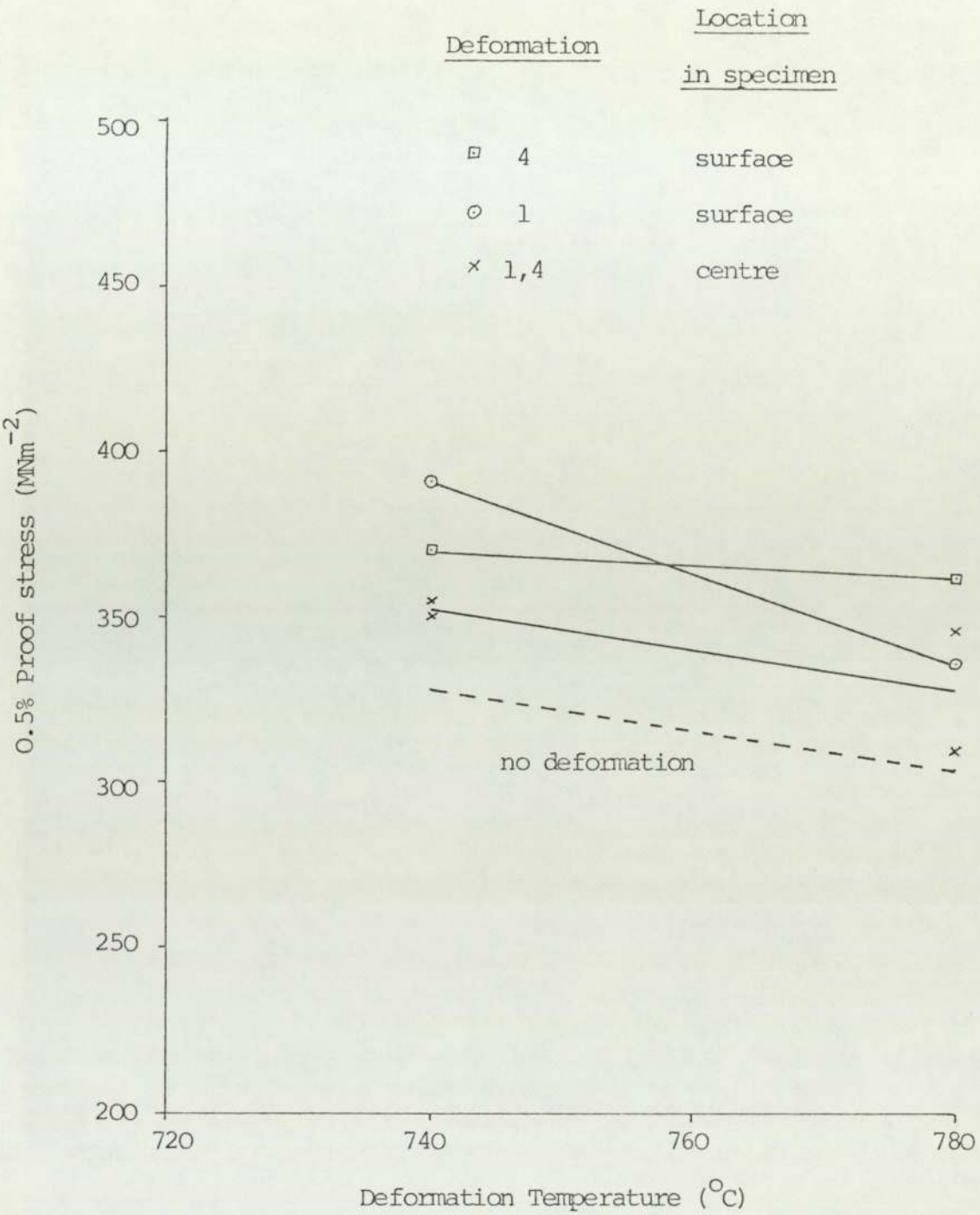

FIGURE 7.3 VARIATION IN PROOF STRESS WITH TEMPERATURE AND DEFORMATION FOR THE C-Mn-Nb STEEL TORSION SPECIMENS (AIR-COOLED AFTER DEFORMATION)

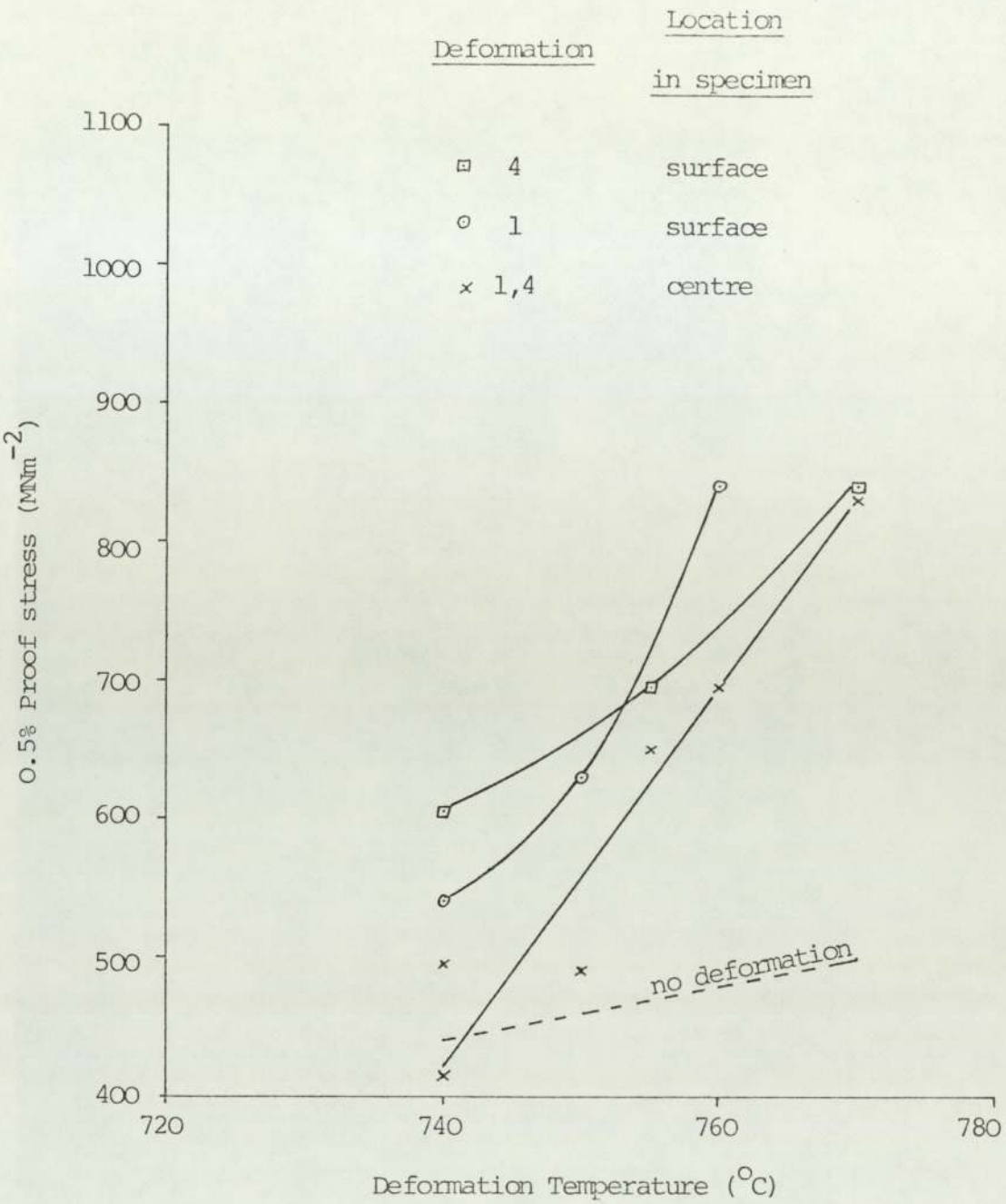

FIGURE 7.4 VARIATION IN PROOF STRESS WITH TEMPERATURE AND DEFORMATION FOR THE C-Mn STEEL TORSION SPECIMENS (WATER SPRAYED AFTER DEFORMATION)

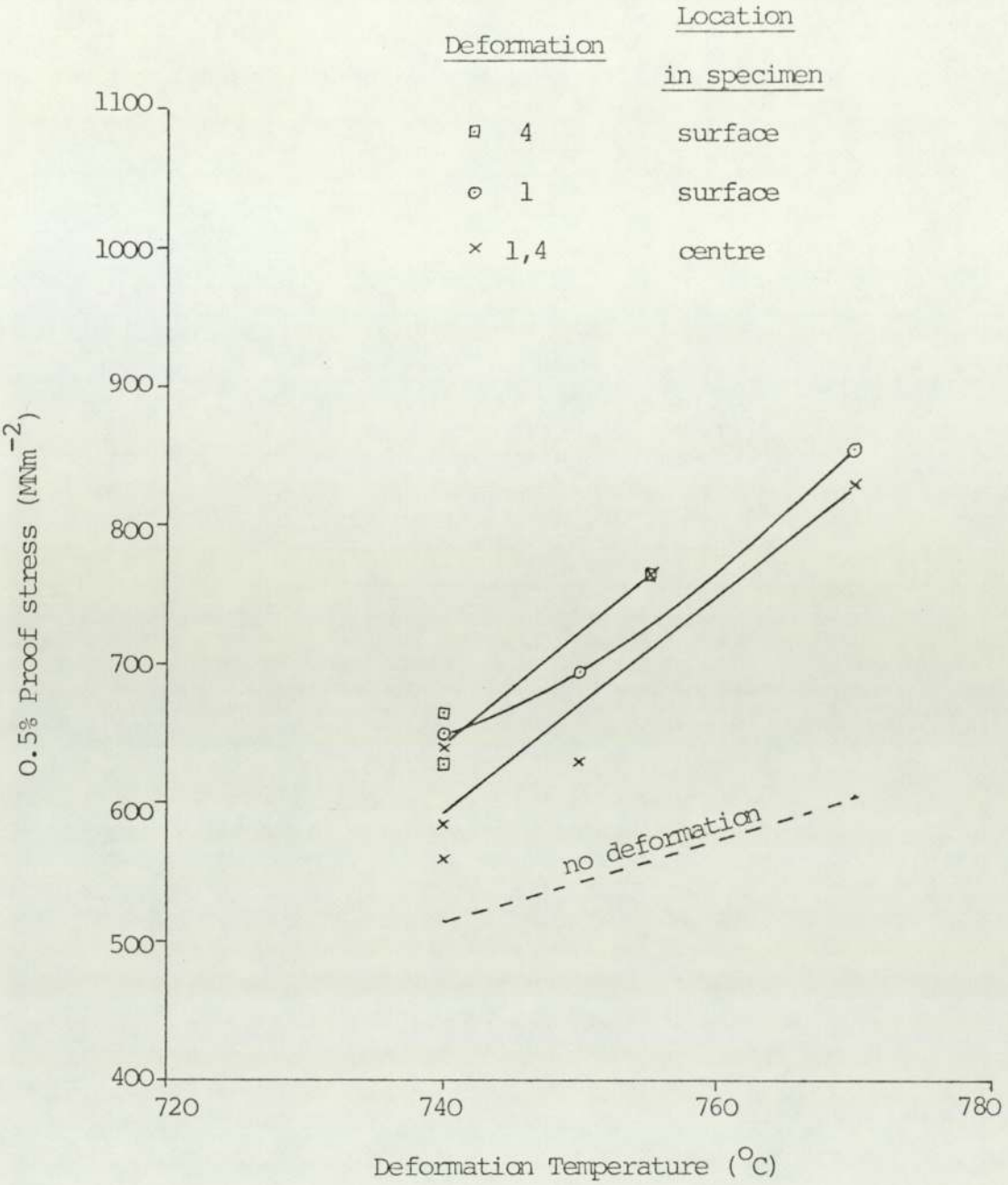

FIGURE 7.5 VARIATION IN PROOF STRESS WITH TEMPERATURE AND DEFORMATION FOR THE C-Mn-V STEEL TORSION SPECIMENS (WATER SPRAYED AFTER DEFORMATION)

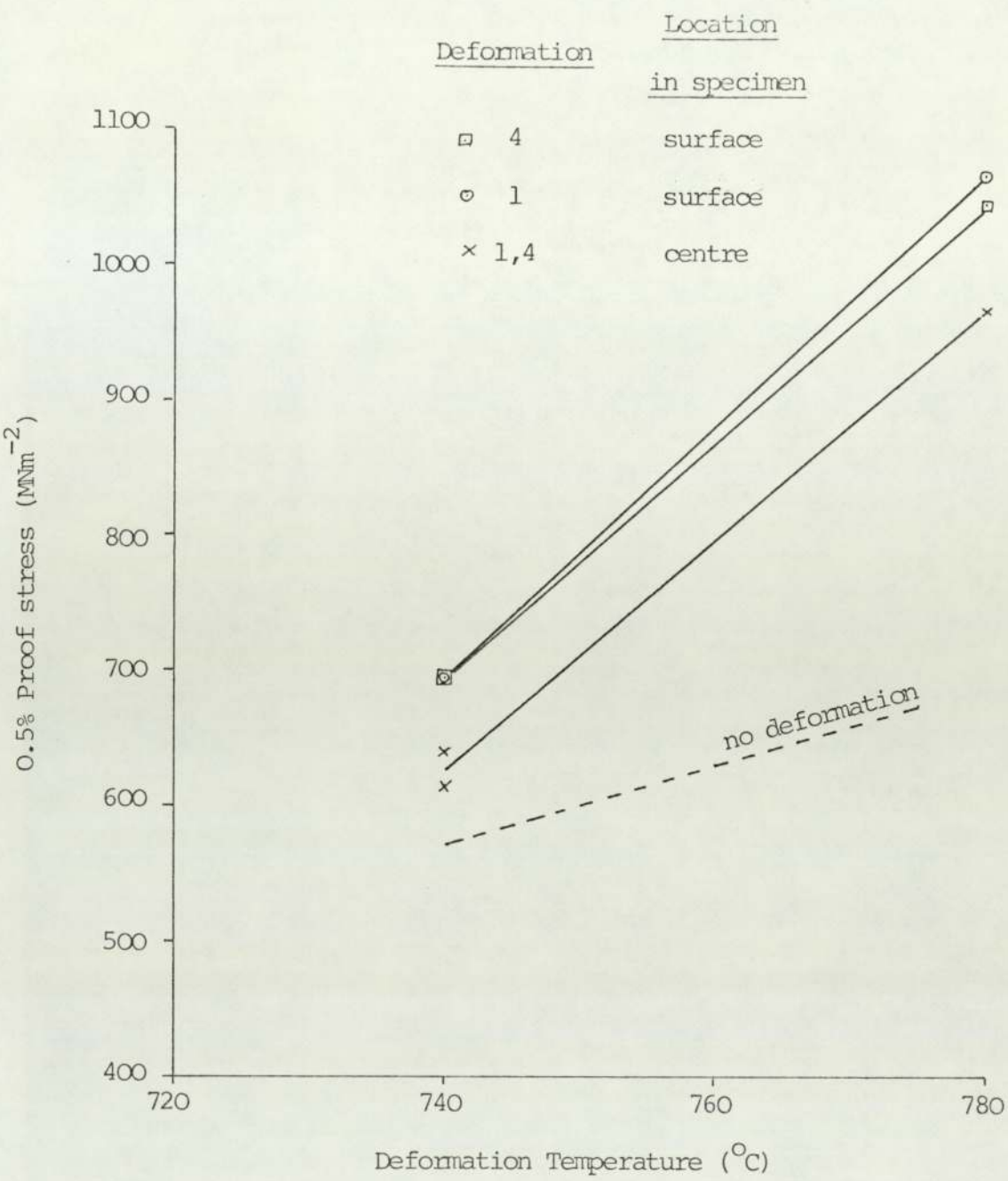

FIGURE 7.6 VARIATION IN PROOF STRESS WITH TEMPERATURE AND DEFORMATION FOR THE C-Mn-Nb STEEL TORSION SPECIMENS (WATER SPRAYED AFTER DEFORMATION)

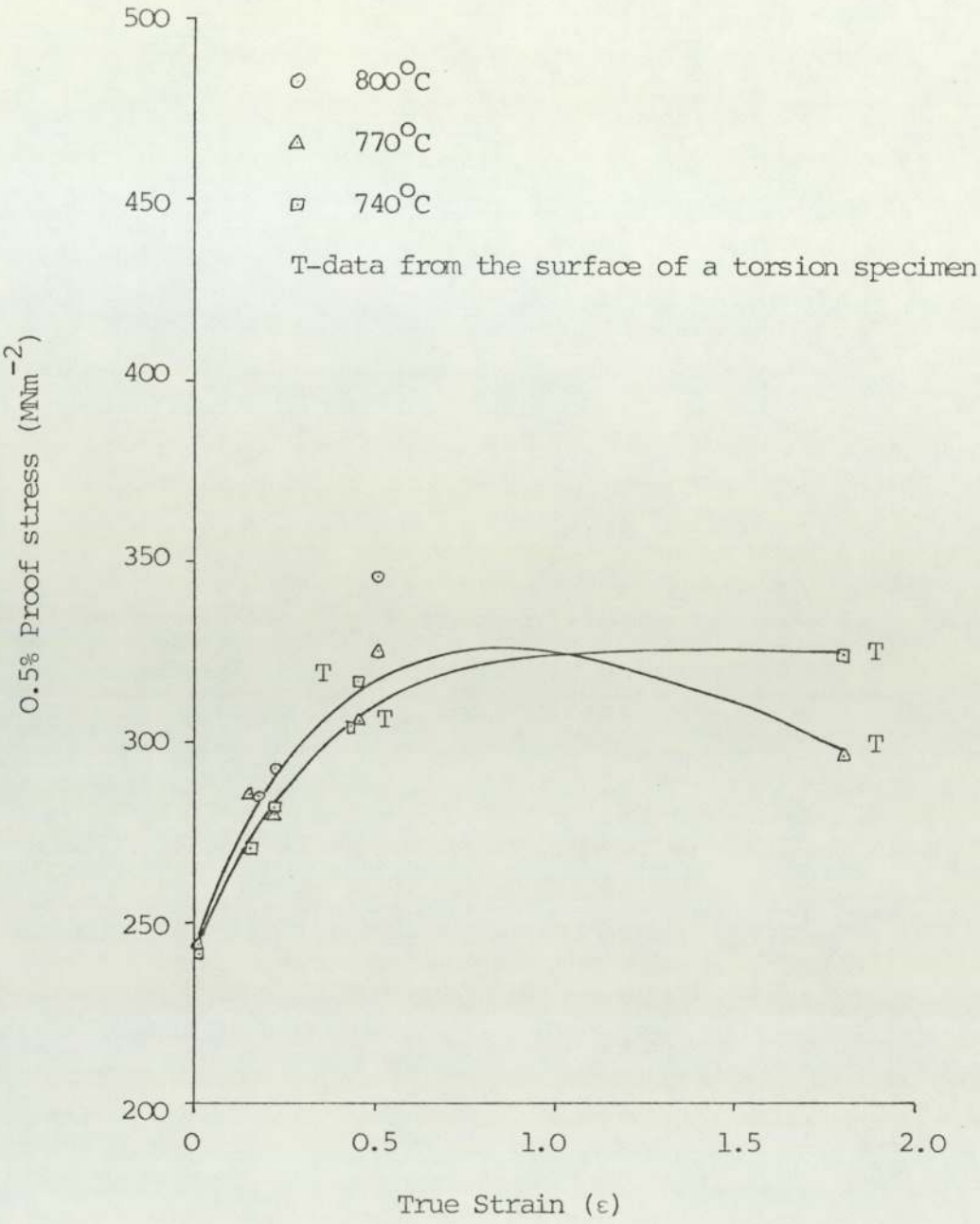

FIGURE 7.7 THE RELATIONSHIP BETWEEN STRAIN AT THE TEMPERATURES INDICATED AND ROOM TEMPERATURE PROOF STRESS FOR THE C-Mn STEEL. DATA POINTS ARE FROM ROLLING AND TORSION SPECIMENS, AIR-COOLED AFTER DEFORMATION

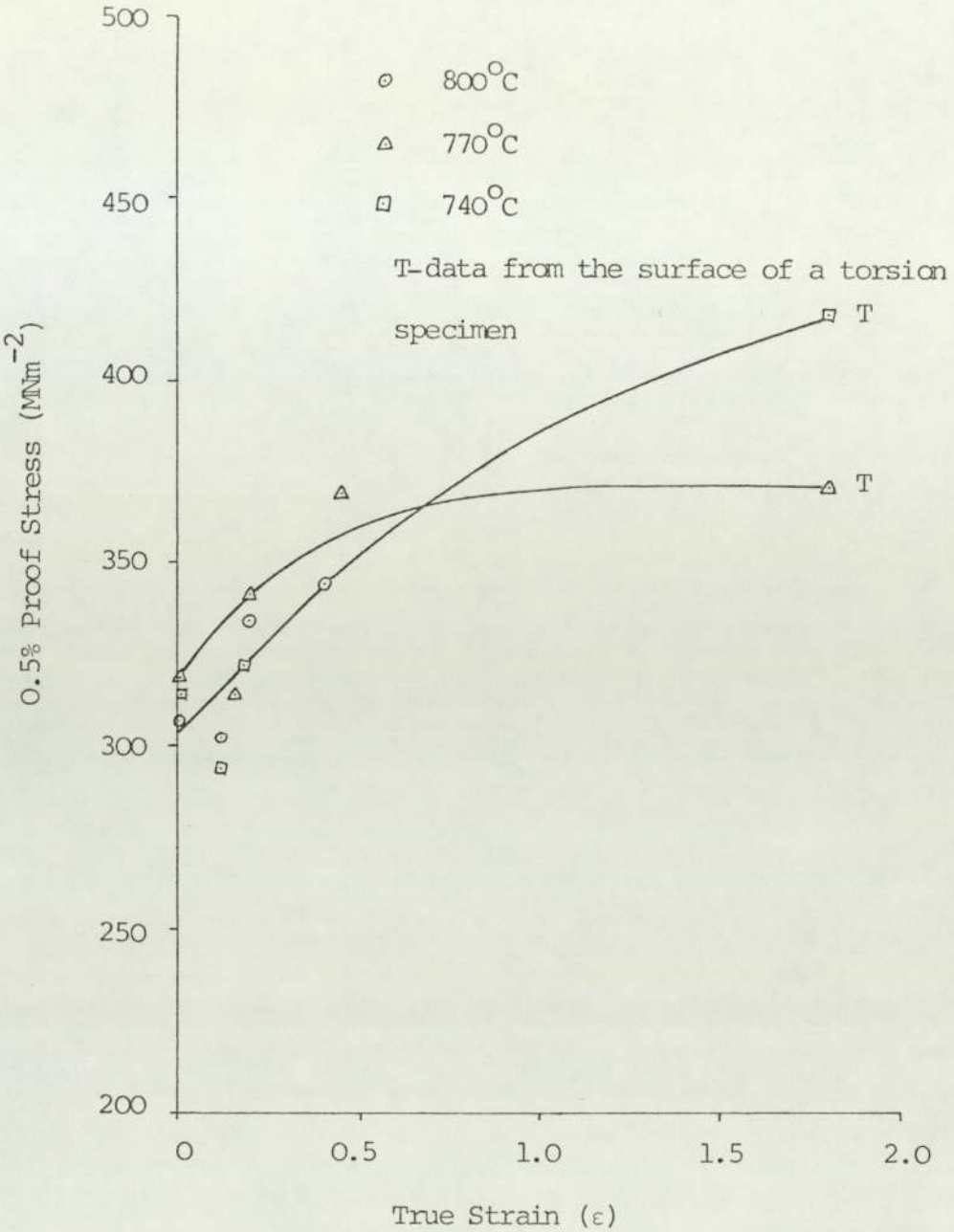

FIGURE 7.8 THE RELATIONSHIP BETWEEN STRAIN AT THE TEMPERATURES INDICATED AND ROOM TEMPERATURE PROOF STRESS FOR THE C-Mn-V STEEL. DATA POINTS ARE FROM ROLLING AND TORSION SPECIMENS, AIR-COOLED AFTER DEFORMATION

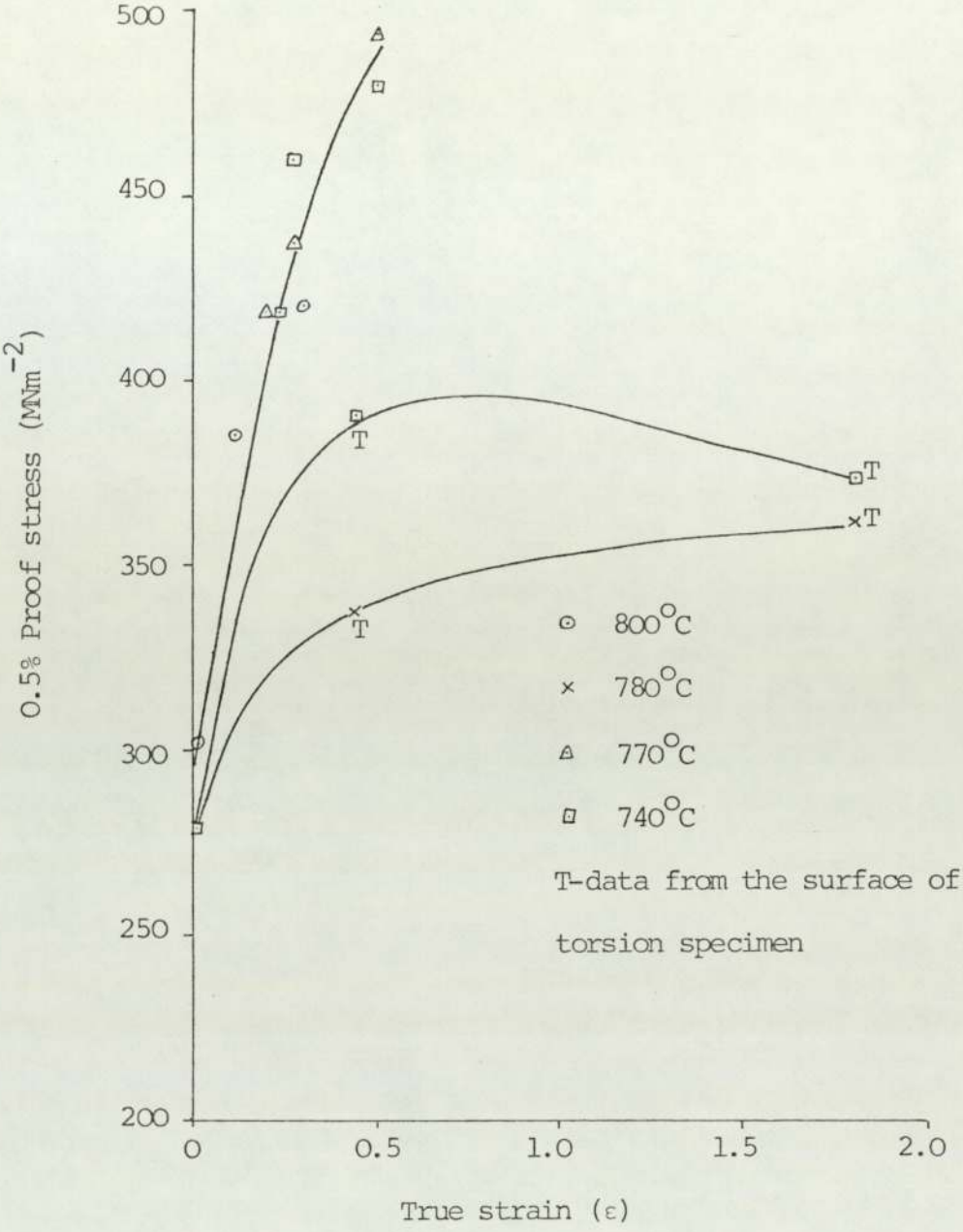

FIGURE 7.9 THE RELATIONSHIP BETWEEN STRAIN AT THE TEMPERATURES INDICATED AND ROOM TEMPERATURE PROOF STRESS FOR THE C-Mn-Nb STEEL. DATA POINTS ARE FROM ROLLING AND TORSION SPECIMENS, AIR-COOLED AFTER DEFORMATION

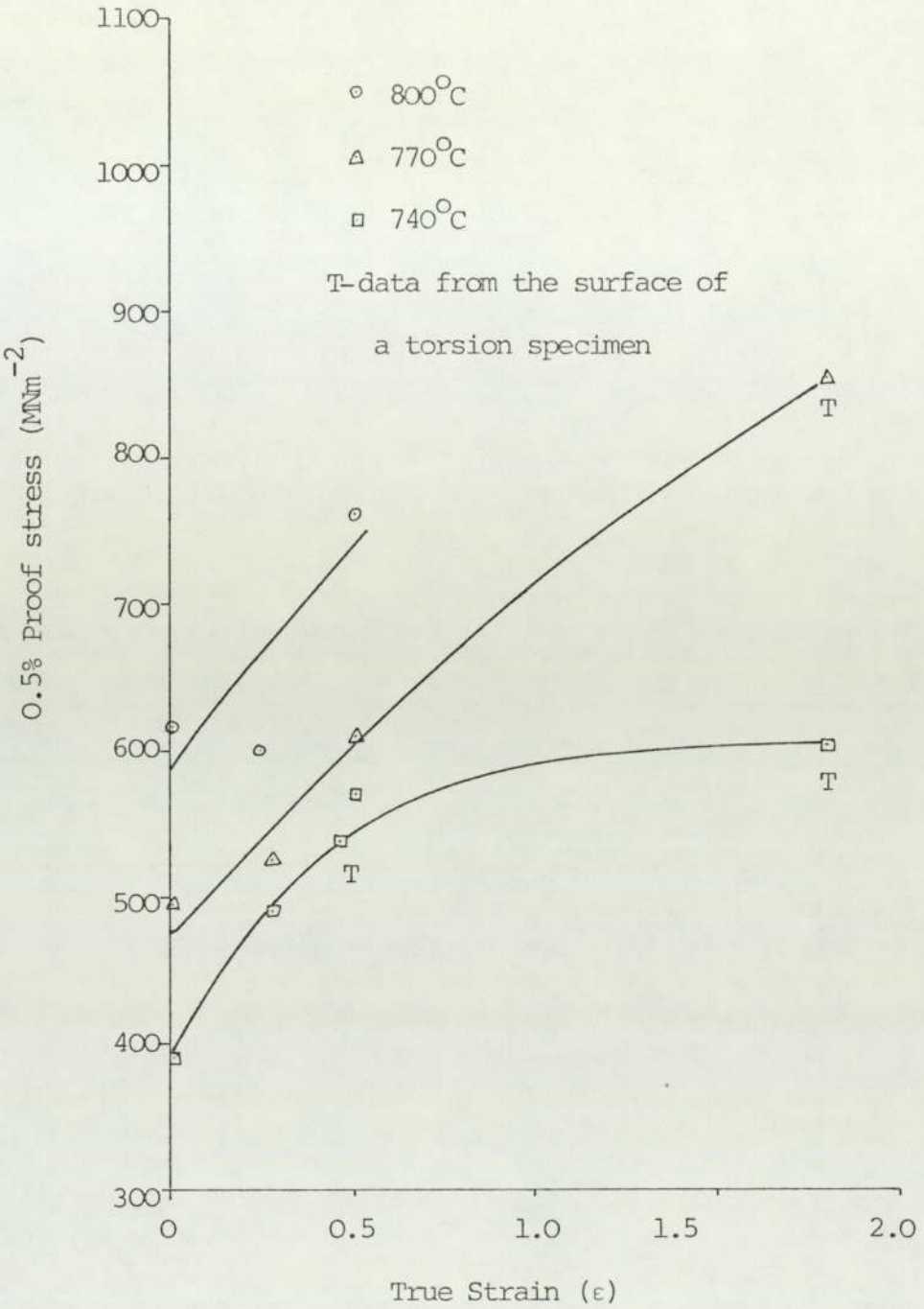

FIGURE 7.10 THE RELATIONSHIP BETWEEN STRAIN AT THE TEMPERATURES INDICATED AND ROOM TEMPERATURE PROOF STRESS FOR THE C-Mn STEEL. DATA POINTS ARE FROM ROLLING AND TORSION SPECIMENS, WATER SPRAYED AFTER DEFORMATION

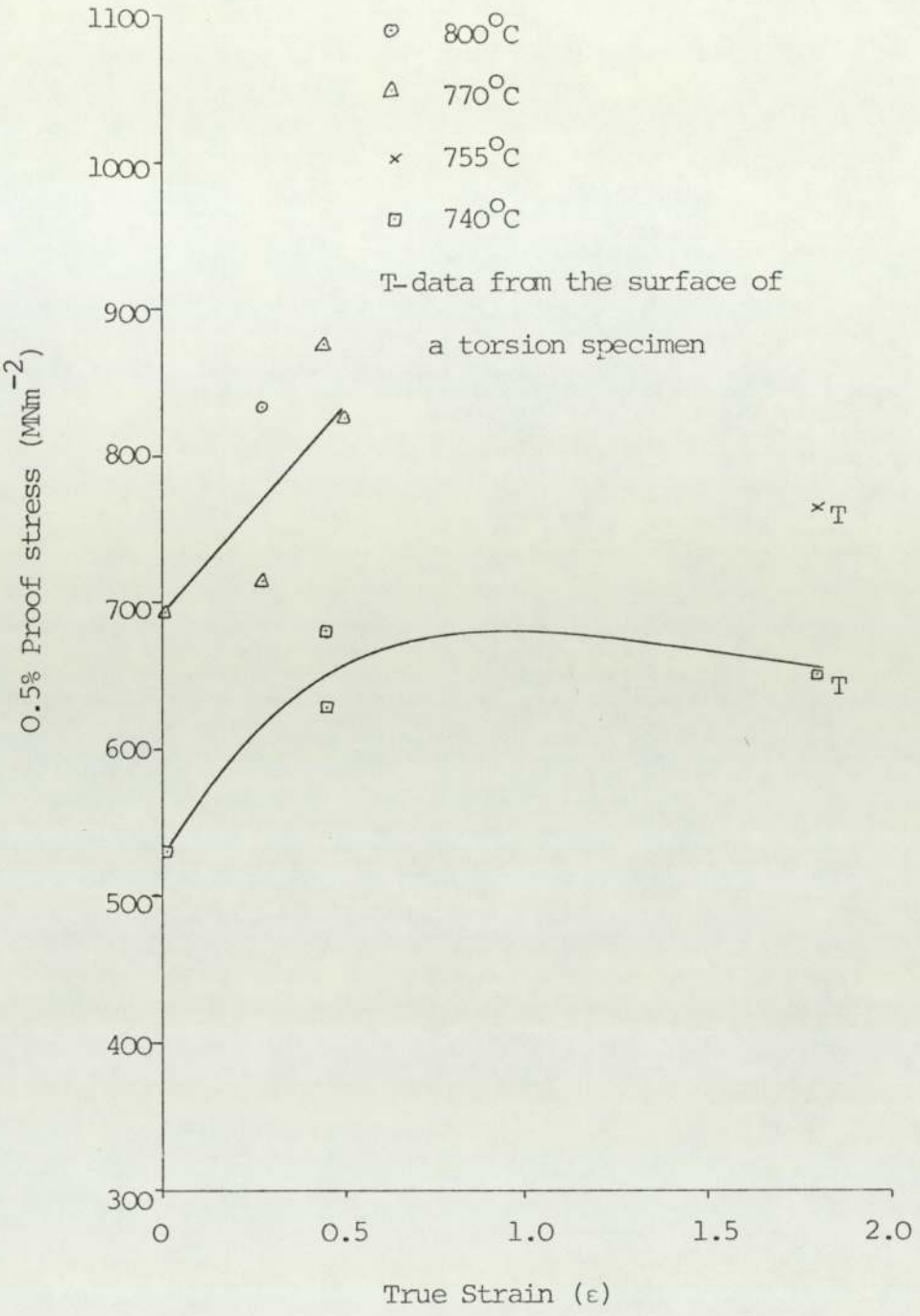

FIGURE 7.11 THE RELATIONSHIP BETWEEN STRAIN AT THE TEMPERATURES INDICATED AND ROOM TEMPERATURE PROOF STRESS FOR THE C-Mn-V STEEL. DATA POINTS ARE FROM ROLLING AND TORSION SPECIMENS, WATER SPRAYED AFTER DEFORMATION

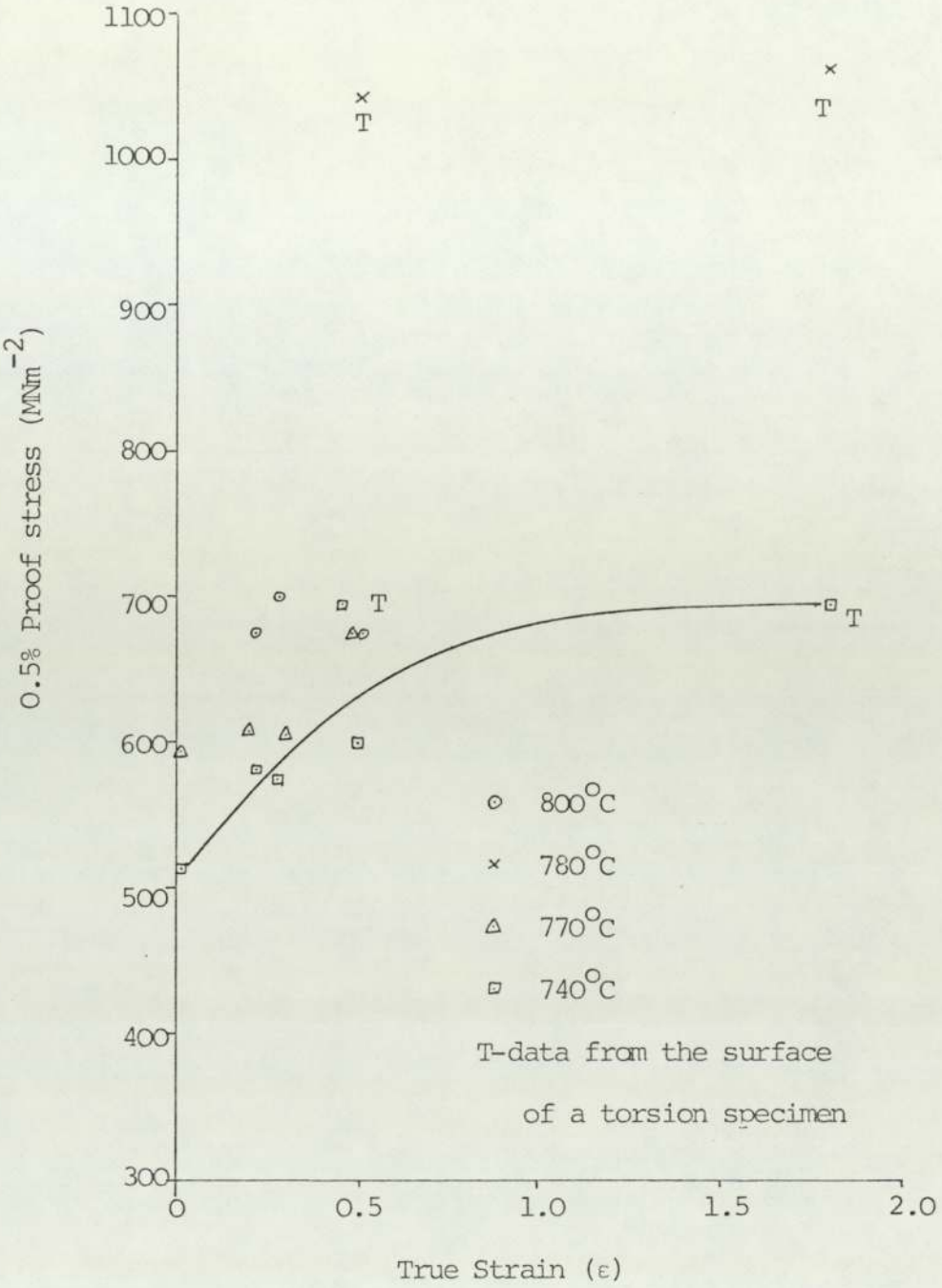

FIGURE 7.12 THE RELATIONSHIP BETWEEN STRAIN AT THE TEMPERATURES INDICATED AND THE ROOM TEMPERATURE PROOF STRESS FOR THE C-Mn-Nb STEEL. DATA POINTS ARE FROM ROLLING AND TORSION SPECIMENS, WATER SPRAYED AFTER DEFORMATION

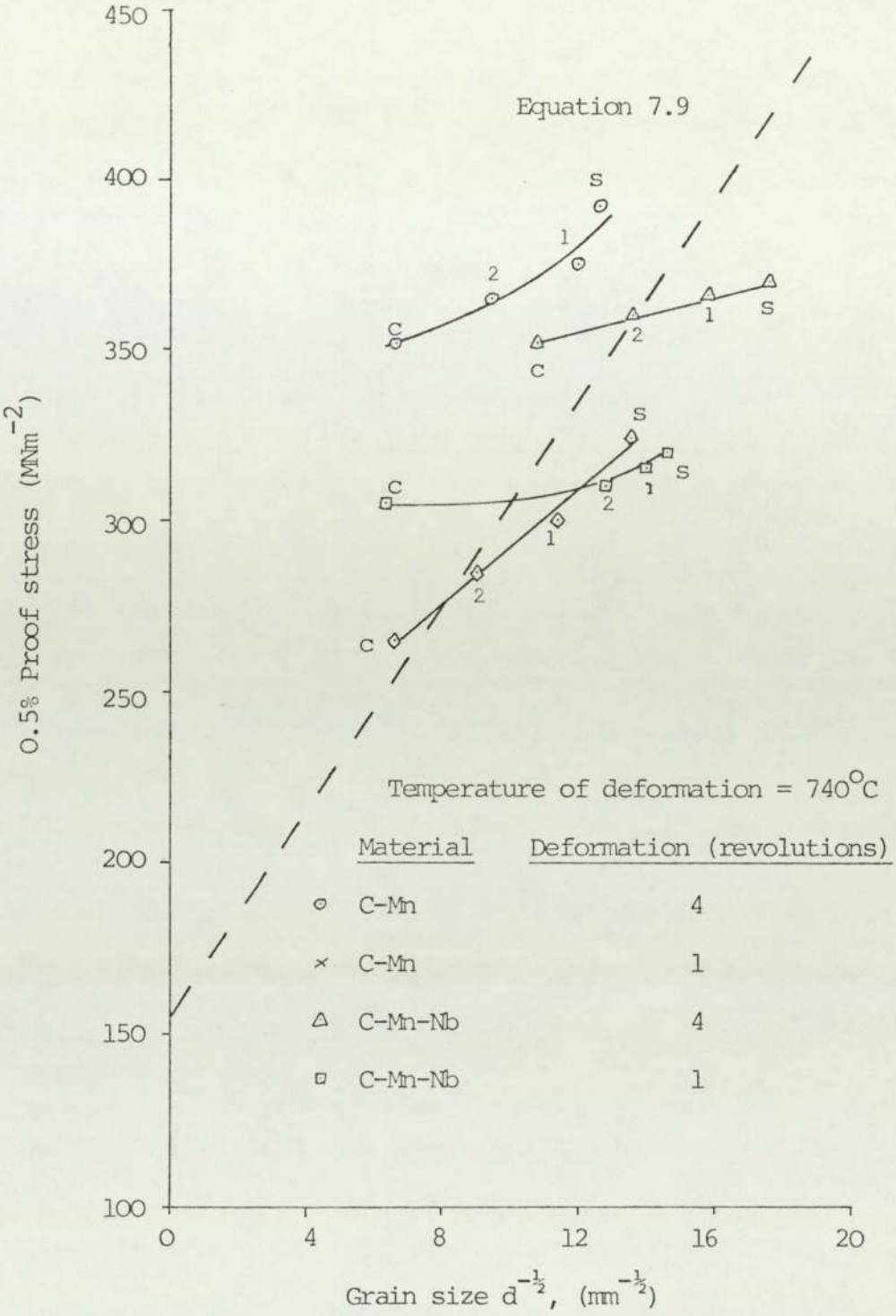

FIGURE 7.13 THE RELATIONSHIP BETWEEN PROOF STRESS AND GRAIN SIZE FOR EXPERIMENTAL TORSION DATA. THE RELATIONSHIP PREDICTED BY EQUATION 7.9 IS SHOWN DOTTED

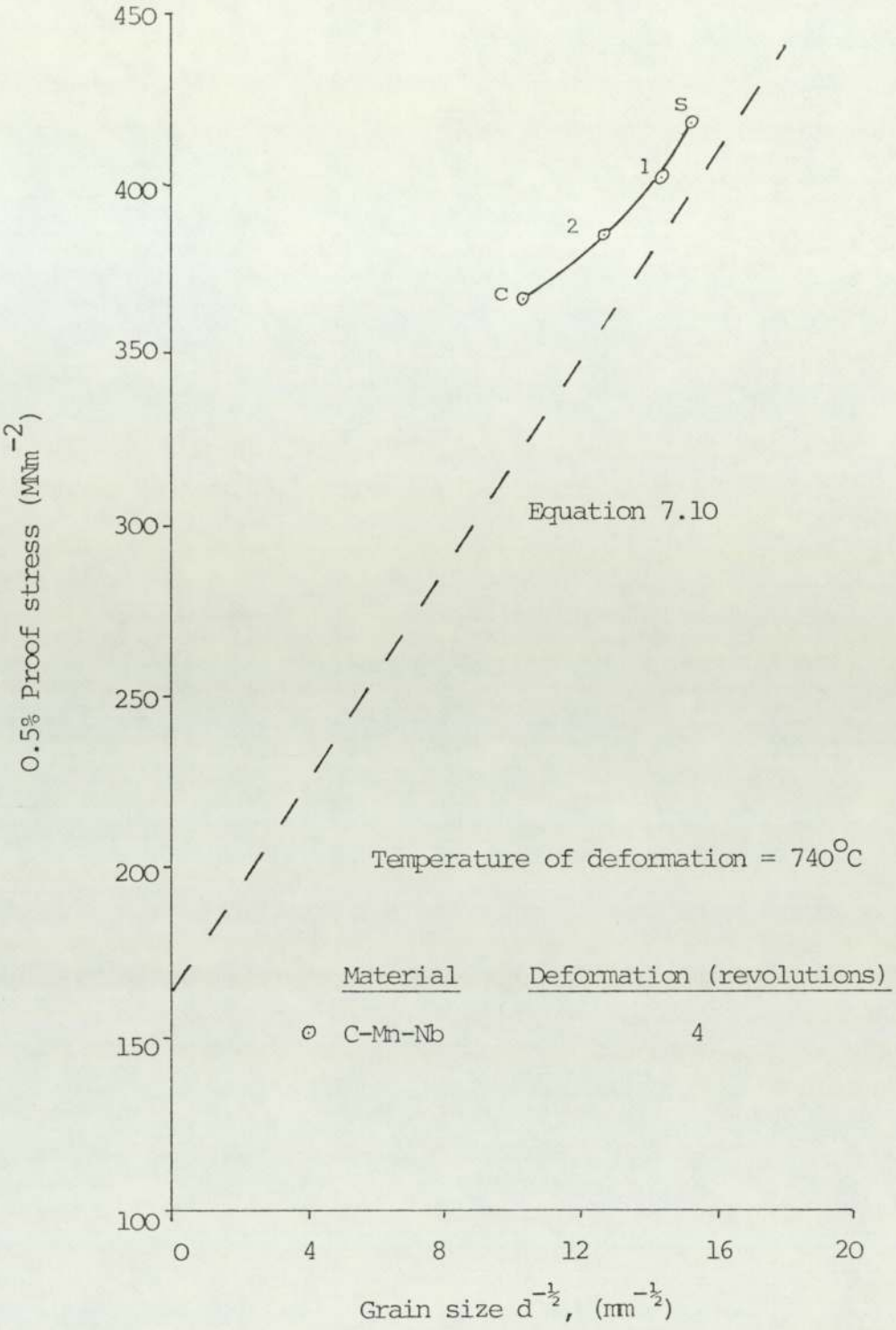

FIGURE 7.14 THE RELATIONSHIP BETWEEN PROOF STRESS AND GRAIN SIZE FOR EXPERIMENTAL TORSION DATA. THE RELATIONSHIP PREDICTED BY EQUATION 7.10 IS SHOWN DOTTED

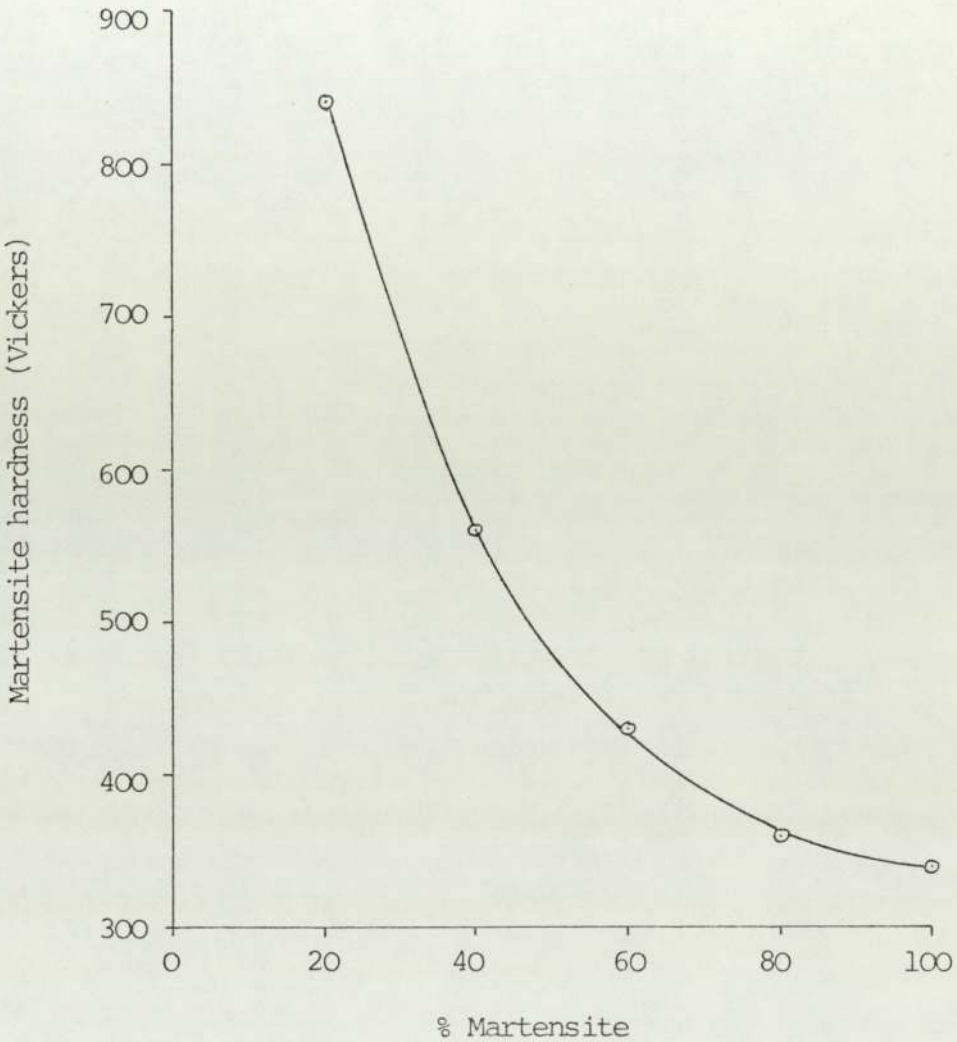

FIGURE 7.15 MARTENSITE HARDNESS AS A PERCENTAGE OF THE MARTENSITE CONTENT IN THE MICROSTRUCTURE (0.15% C STEEL)

8. CONCLUSIONS

Using the scanning electron microscope in the back-scattered electron mode enabled the structure of the ferrite in the microstructures to be observed. In the centre of the torsion specimens the initial grain structure of the ferrite can be observed. The variation in contrast within individual grains indicates that grains in this region have been strained to some extent. At the periphery of the torsion specimens the photomicrographs show clearly the development of a sub-grain structure in the ferrite. This can be clearly seen in all three steels after a deformation of 4 revolutions (true strain 1.81).

The results summarised in figures 7.7 - 7.9 for the air-cooled materials show that the proof stress increases with deformation. Up to a true strain of about 0.5 the proof stress for any one steel is very similar, thereafter some differences are apparent. At a true strain of 1.8, the proof stress increases as the temperature of deformation decreases in the two phase regime. This difference after a true strain of 1.8 is due to the smaller sub-grain size, increasing the sub-grain strengthening effect. The proof stress of the steel deformed by a true strain of 1.8 can be predicted with reference to the initial grain size, the sub-grain size of the deformed ferrite and precipitation effects. The effect that precipitation has requires closer investigation to determine more accurately the effect of precipitation.

The results for the water quenched specimens summarised in figures 7.10 - 7.12 are significantly dependent on the martensite content. This increase in proof stress with strain at constant temperature is due in part to the development of a sub-grain structure in the ferrite phase.

If components are to be used in the as-warm formed condition it is necessary to understand the composition, temperature and strain dependence of the resulting properties. Ideally a choice of composition which permits a desired strength level and toughness combination to be achieved would exhibit sensitivity of strain and temperature variations, such as to permit property control to be achieved in the warm working operation. If the working operation is not readily controlled the property sensitivity to these variables would preferably be slight.

The evidence of this study is that both vanadium and niobium reduce the sensitivity of the as warm-worked strength to strain at above a true strain of 0.5, but the temperature sensitivity is quite strong.

In the warm-worked and air-cooled condition the strength level in both the vanadium and niobium alloys was modest compared with those achieved in control-rolled line-pipe sheets. High strength could be obtained in the warm-worked and water quenched condition and although the toughness is not expected to be high, it may be that the duplex martensite/ ferrite structure may give reasonable toughness.

9. FUTURE WORK

The work contained in this study is only an introduction to the investigation of the effect that warm-forming has on the structure and properties of some simple steels. A major area for future work will be the study of the effect that warm-forming has on toughness, since this is a property of crucial importance, particularly where low temperature applications are involved.

It would not be possible to assess the toughness of a warm-formed steel using torsion as the mode of deformation. Although relationships have been suggested relating impact transition temperature to the grain size and to some extent composition, the effects of precipitates and sub-grains have not been analysed. The deformation would have to be done by rolling. This would require a significant reduction in a single pass in order to produce even sub-standard size specimens from the deformed material. (This was a major problem in this study and prevented experiments to determine toughness being carried out).

The production of component by warm-forming will inevitably result in differences in material flow within that component. It will be necessary therefore to study anisotropy of properties that may result from different material flows found in warm-formed components.

The contribution of precipitates to the properties of controlled rolled steels has been extensively studied. It will be important to study this aspect with respect to warm-forming in order to optimise the contribution that precipitation makes to warm-formed steels.

10. REFERENCES

1 F B Pickering : The Metallurgist and Materials Technologist, 9, pages 375-379, 1977

2 E O Hall : Proceedings, Physics Society, 64B, page 747, 1951

3 N J Petch : Journal of the Iron and Steel Institute, 174, page 25, 1953

4 T Gladman : Proceedings of Converence, "Micro-Alloying 1975" Washington DC, USA 1-3 October 1975, page 25

5 H J Kouwenhoven : Transactions of the American Society of Metals 62, page 437, 1969

6 N J Petch : Proceedings of Swampscott Conference, 1955, page 54 MIT Press

7 N J Petch : Proceedings of Swampscott Conference "Fracture" 1959

8 J J Irani : Iron and Steel Institute, Special Report No. 104, Page 110, 1967

9 T Gladman : Journal of the Iron and Steel Institute, 210, page 916, 1972

10 J S Hirselhorn and G S Ansell : Acta Metallurgica, 13, page 572, 1965

Contd/.....

11 M K Koul : Metals Engineering Quarterly, February 1976, page 1

12 J N Cordea and R E Hook : Metallurgical Transactions, 1, page 111, 1970

13 T Gladman : Proceedings of Conference, "Recrystallisation in the Control of Microstructure", London, 14-15th November 1973

14 T Greday and M Lamerigts : Proceedings of Conference "Micro-Alloying 1975", Washington DC, USA 1-3rd October 1975, page 145

15 A le Bon : Metals Science, 9, page 36, 1975

16 J J Jonas : Proceedings of Conference, "Recrystallisation in the Development of Microstructure", Leeds, UK, 1978

17 C S Smith : Transactions of the American Institute of Mining (Metallurgical) Engineers, 175, page 15, 1948

18 D McLean : Grain Boundaries in Metal, Oxford University Press, page 241, 1957

19 T Gladman : Proceedings of the Royal Society Series A, 294, page 298, 1966

20 C Zener : Private Communication to C S Smith, Transactions of the American Institute of Mining (Metallurgical) Engineering, 175, page 15, 1948

Contd/.....

21 M Hilbert : Acta Metallurgica, 13, page 227, 1965

22 K J Irvine et al : Journal of the Iron and Steel Institute, 205, page 161, 1967

23 I M Lifshitz and V V Slyozov : Journal of Physical Chemistry of Solids, 19, page 35, 1961

24 C Wagner : Z Electrochemie, 65, page 581, 1961

25 L Meyer, F Heisterkamp and W Mueschenborn : Proceedings of Conference "Micro-Alloying 1975", Washington DC, USA 1-3rd October 1975, page 130

26 J M Gray : Metallurgical Transactions, 3, page 1495, 1972

27 J J Jonas : AIME Symposium, "Precipitation Effects in HSLA Steels", Denver, USA, February 1978

28 P L Mangonan and W E Heitmann : Proceedings of Conference, "Micro-Alloying 1975", Washington DC, USA, 1-3rd October 1975

29 F B Pickering : Proceedings of Conference, "Micro-Alloying 1975", Washington DC, USA, 1-3rd October 1975, page 3

30 T Tanaka, N Tabata, T Hatamura and C Shiga : Proceedings of Conference "Micro-Alloying 1975", page 88

Contd/.....

31 T Gladman : Journal of the Iron and Steel Institute, 208, page 173, 1970

32 J M Arrowsmith : Metal Construction, 8, page 396, 1976

33 D Dulieu : BSC Conference "Inclusions and their Effect on Steel Properties", Leeds, UK, 1974

34 Discussion to ref. 33

35 K J Irvine : Iron and Steel Institute Report No. 104, "Strong Tough Structural Steels", 1967

36 T J Baker : Journal of the Iron and Steel Institute, 210, page 702, 1972

37 M Fakuda, T Hashimoto and K Kunishige : Proceedings of Conference "Micro-Alloying 1975"

38 B L Bramfitt and A R Marder : Proceedings of Conference "Processing and Properties of Low Carbon Steels", AIME, page 191, 1973

39 B Aaronson : Steel Strengthening Mechanisms, published by Climax Molybdenum Co, New York, page 77

40 M G Hall and W B Hutchinson : The Metallurgist and Materials Technologist, July 1980, page 371

Contd/.....

41 D N Hawkins : PhD Thesis, University of Sheffield, 1975

42 H O'Neill : Hardness Measurement of Metals and Alloys Second Edition. Published by Chapman and Hall, 1967 page 84

43 B Migand : Sheffield International Conference on Hot Working Processes 17 - 20th July 1979

44 F B Pickering : Physical Metallurgy and the Design of Steels, page 128